

### (12) United States Patent

Swanson et al.

### (54) AUTO-RANGING FOR TIME DOMAIN **INERTIAL SENSOR**

(75) Inventors: Paul D. Swanson, Santee, CA (US); Richard L. Waters, San Diego, CA

(73) Assignee: The United States of America as

represented by the Secretary of the Navy, Washington, DC (US)

(\*) Notice: Subject to any disclaimer, the term of this

patent is extended or adjusted under 35 U.S.C. 154(b) by 154 days.

Appl. No.: 13/282,062

(22)Filed: Oct. 26, 2011

**Prior Publication Data** (65)

> US 2013/0104622 A1 May 2, 2013

(51) Int. Cl. G01P 21/00 (2006.01)

U.S. Cl. 

(58) Field of Classification Search

None

See application file for complete search history.

# (10) Patent No.:

(45) Date of Patent:

US 8,490,462 B2

Jul. 23, 2013

#### (56)**References Cited**

### U.S. PATENT DOCUMENTS

5,023,503	Α	6/1991	Legge et al.
2006/0071578	A1*	4/2006	Drabe et al 310/309
2008/0236280	A1*	10/2008	Johnson et al 73/504.14
2010/0116630	A1	5/2010	Pinkerton
2010/0147073	A1*	6/2010	Johnson et al 73/504.16
OTHER PUBLICATIONS			

Unpublished U.S. Appl. No. 13/168,603, filed Jun. 24, 2011, Titled "Apparatus and Methods for Time Domain Measurement of Oscillation Perturbations," by Paul D. Swanson et al.

Unpublished U.S. Appl. No. 13/276,948, filed Oct. 19, 2011, Titled "Resonator with Reduced Acceleration Sensitivity and Phase Noise Using Time Domain Switch," by Paul D. Swanson et al.

### \* cited by examiner

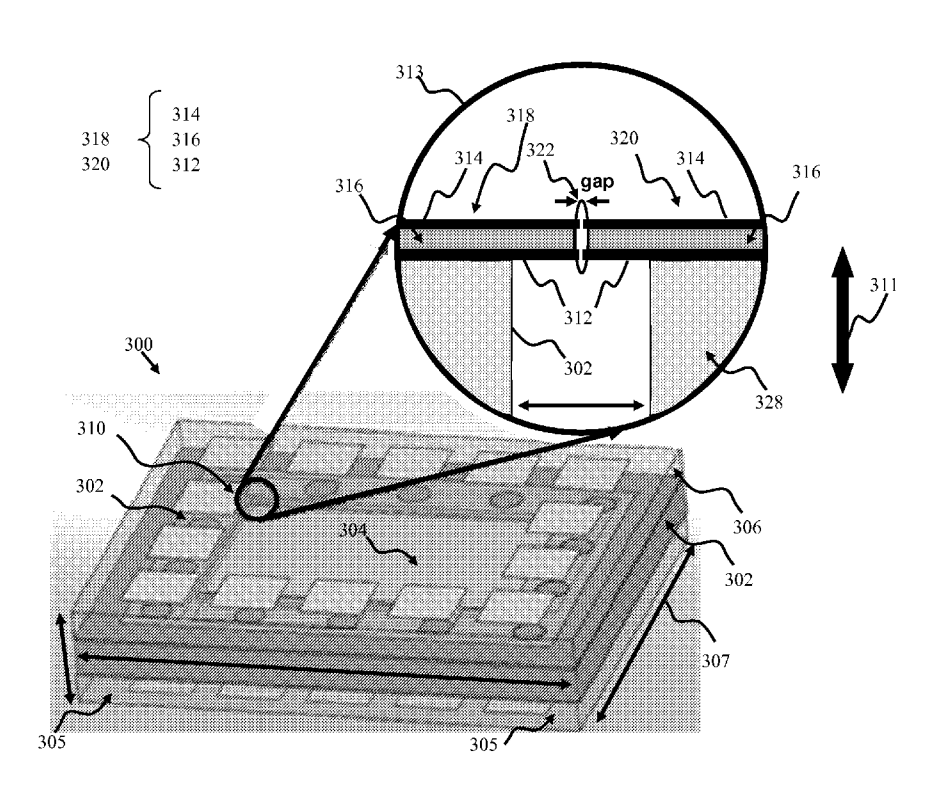
Primary Examiner — Robert R Raevis

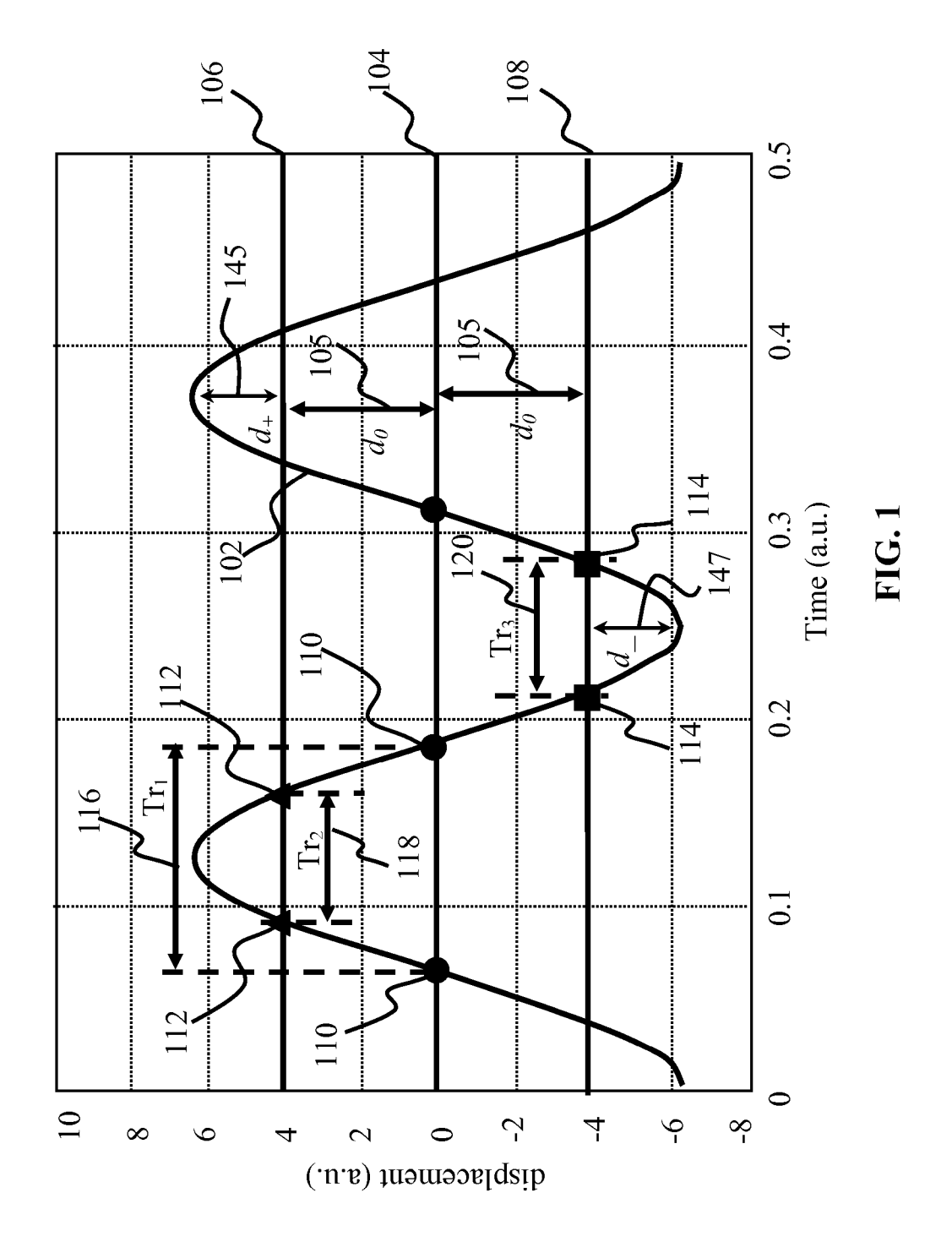
(74) Attorney, Agent, or Firm - Kyle Eppele; J. Eric Anderson

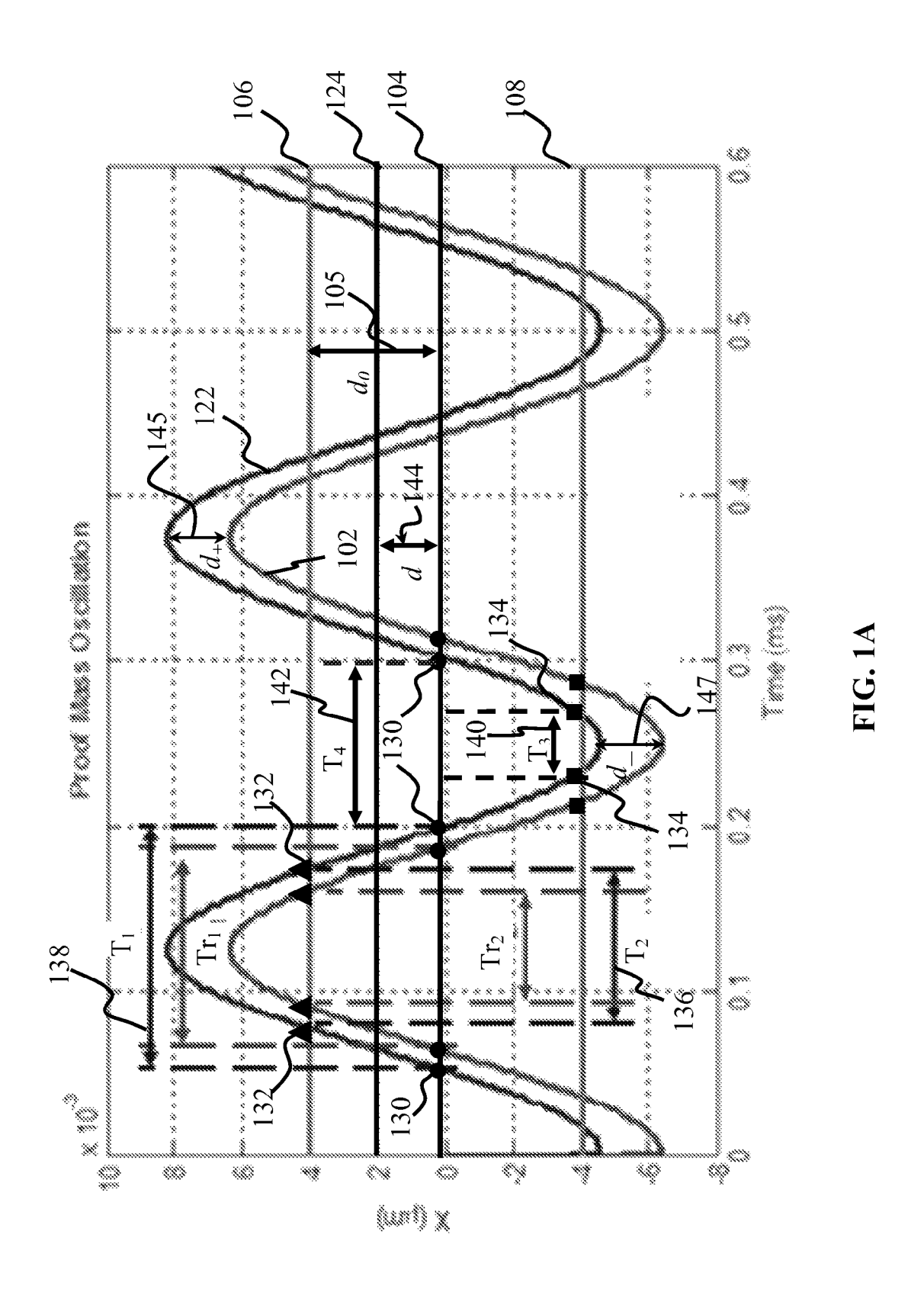
### ABSTRACT

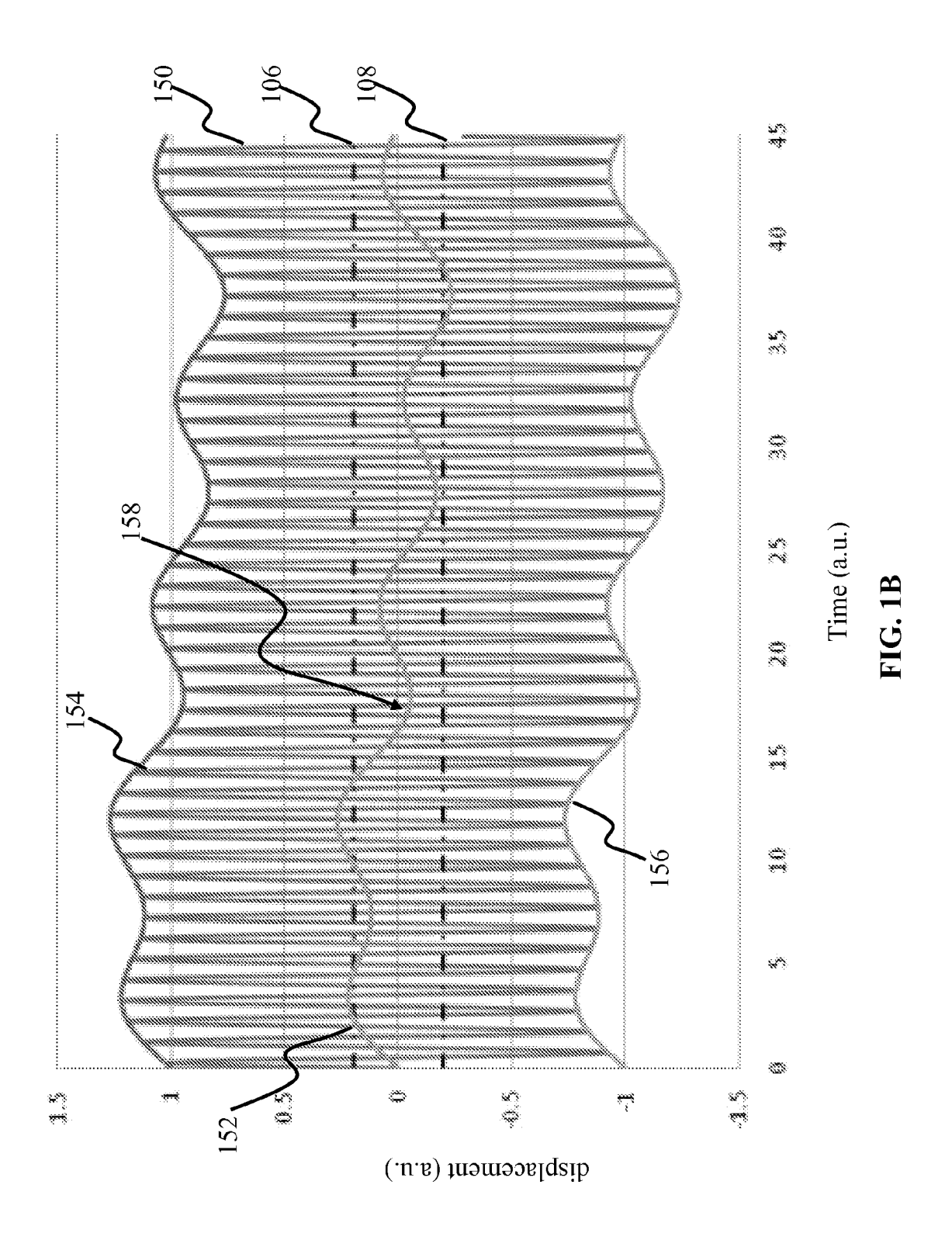
A method for adjusting the accuracy of a time-domain inertial sensor comprising the following steps: operatively positioning a harmonic oscillator of the time-domain inertial sensor between two capacitive plates; initiating harmonic oscillation of the oscillator in a first plane by creating with the capacitive plates a capacitively forced pulse; monitoring the harmonic oscillation of the oscillator; and electrostatically biasing both of the two capacitive plates such that a spring constant of the oscillator is effectively altered.

### 17 Claims, 34 Drawing Sheets









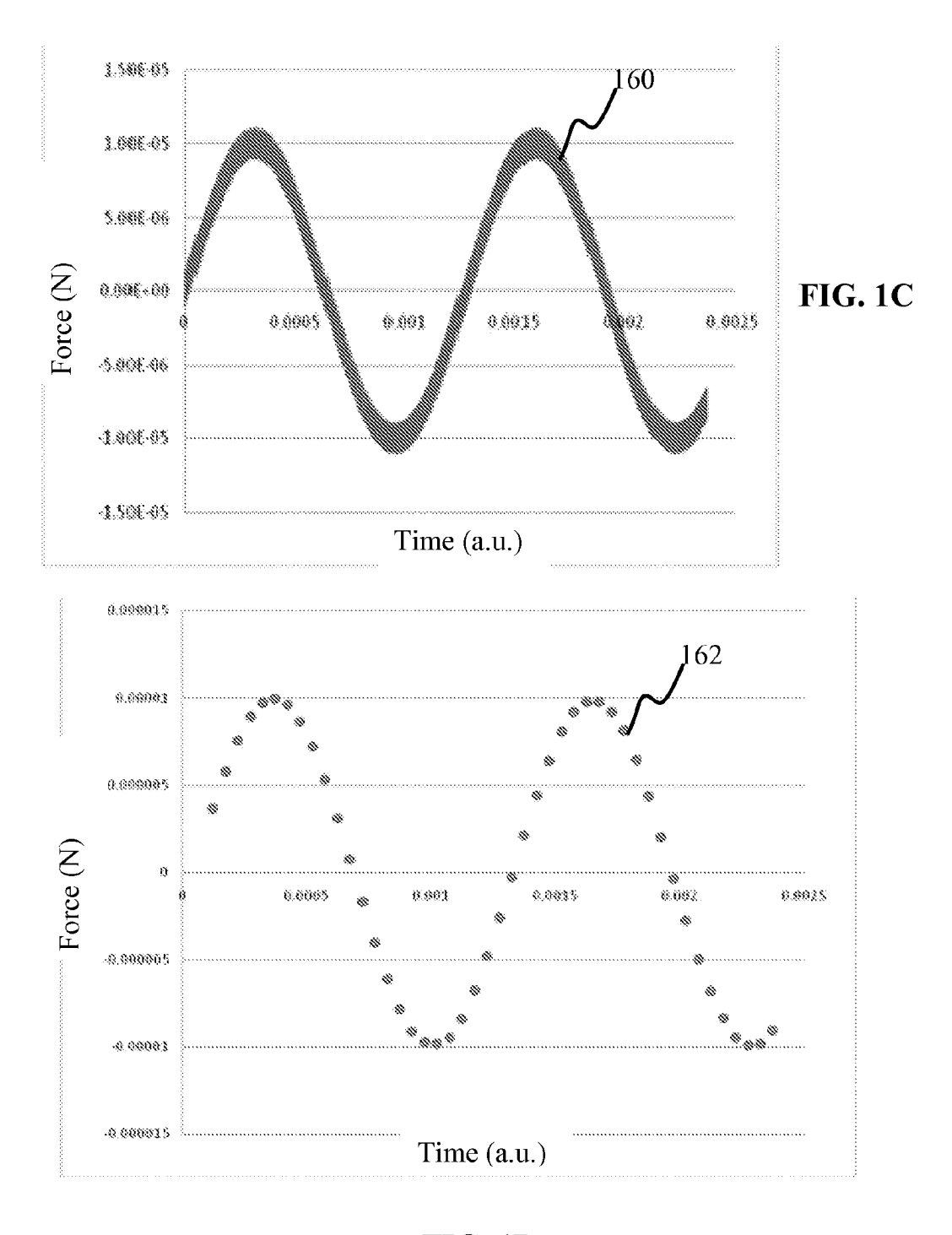
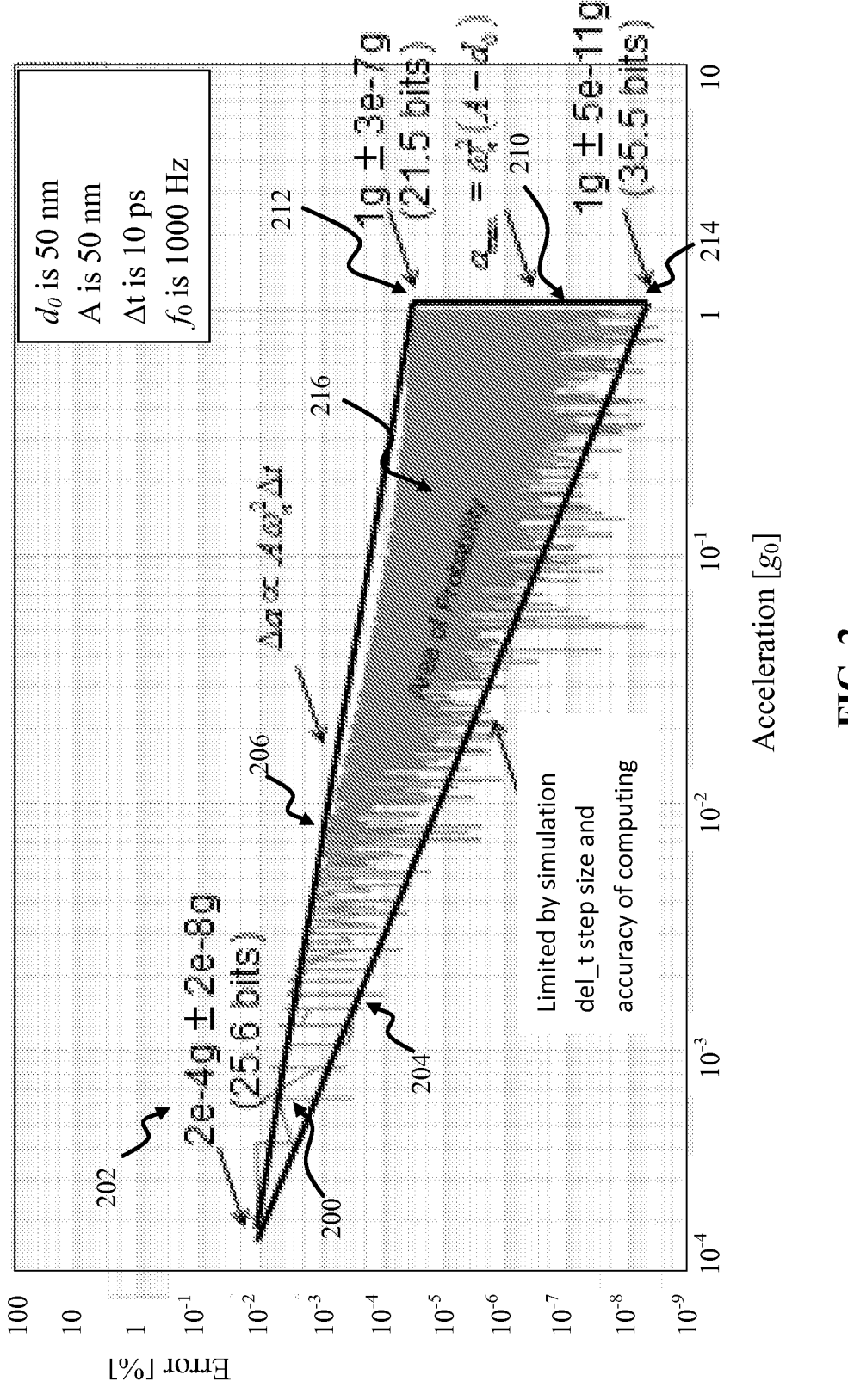


FIG. 1D



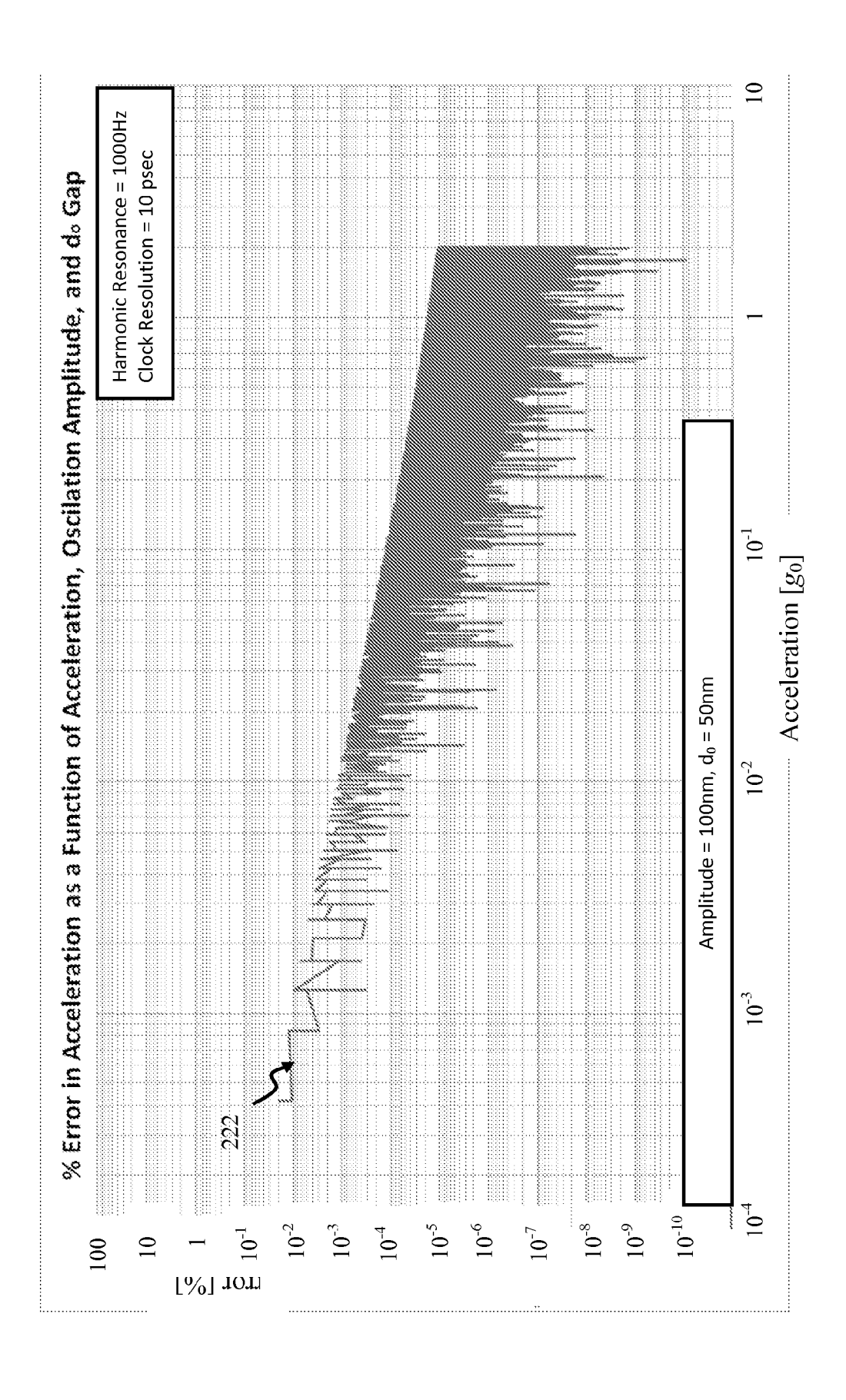


FIG. 2A-1

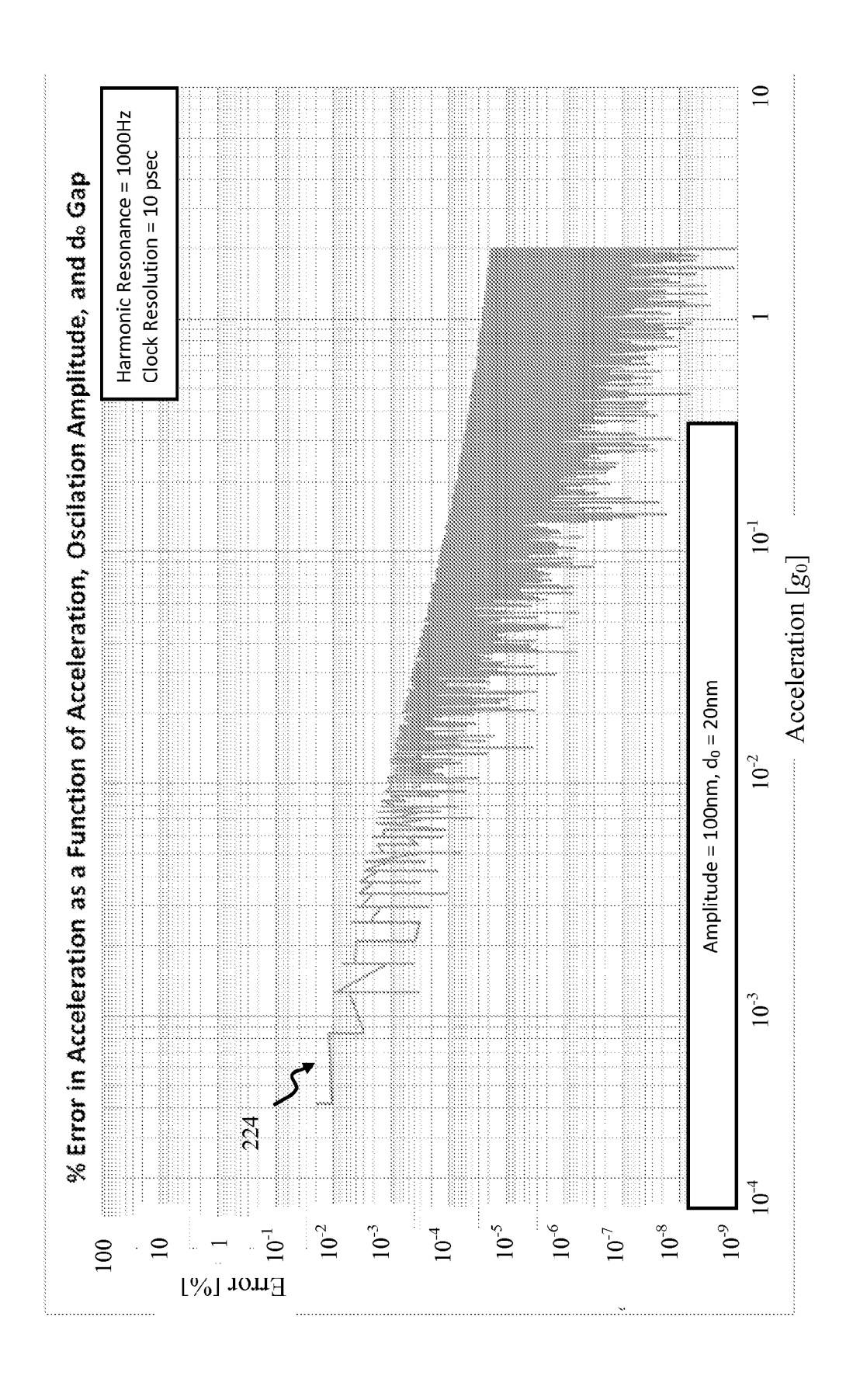


FIG. 2A-2

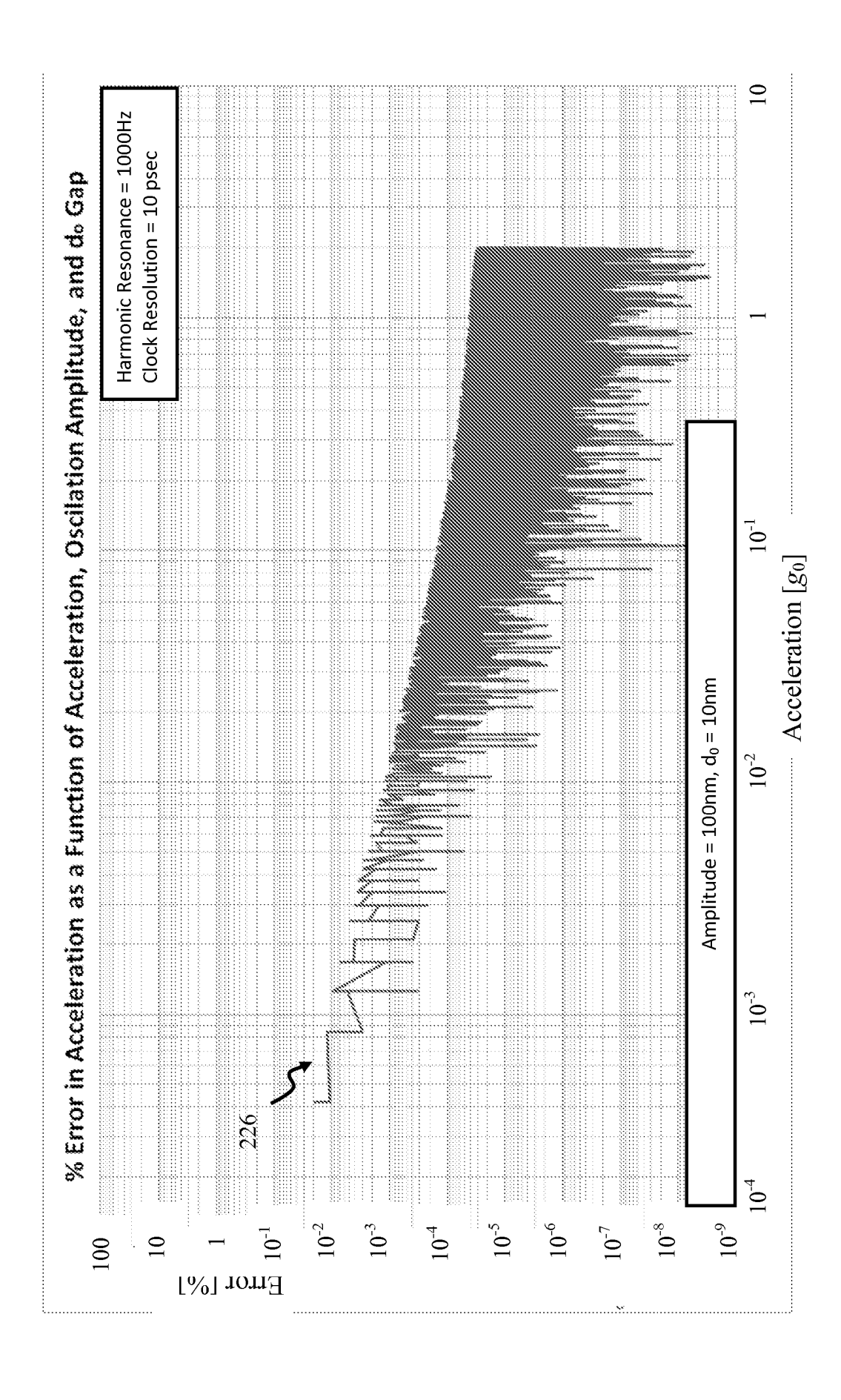


FIG. 2A-3

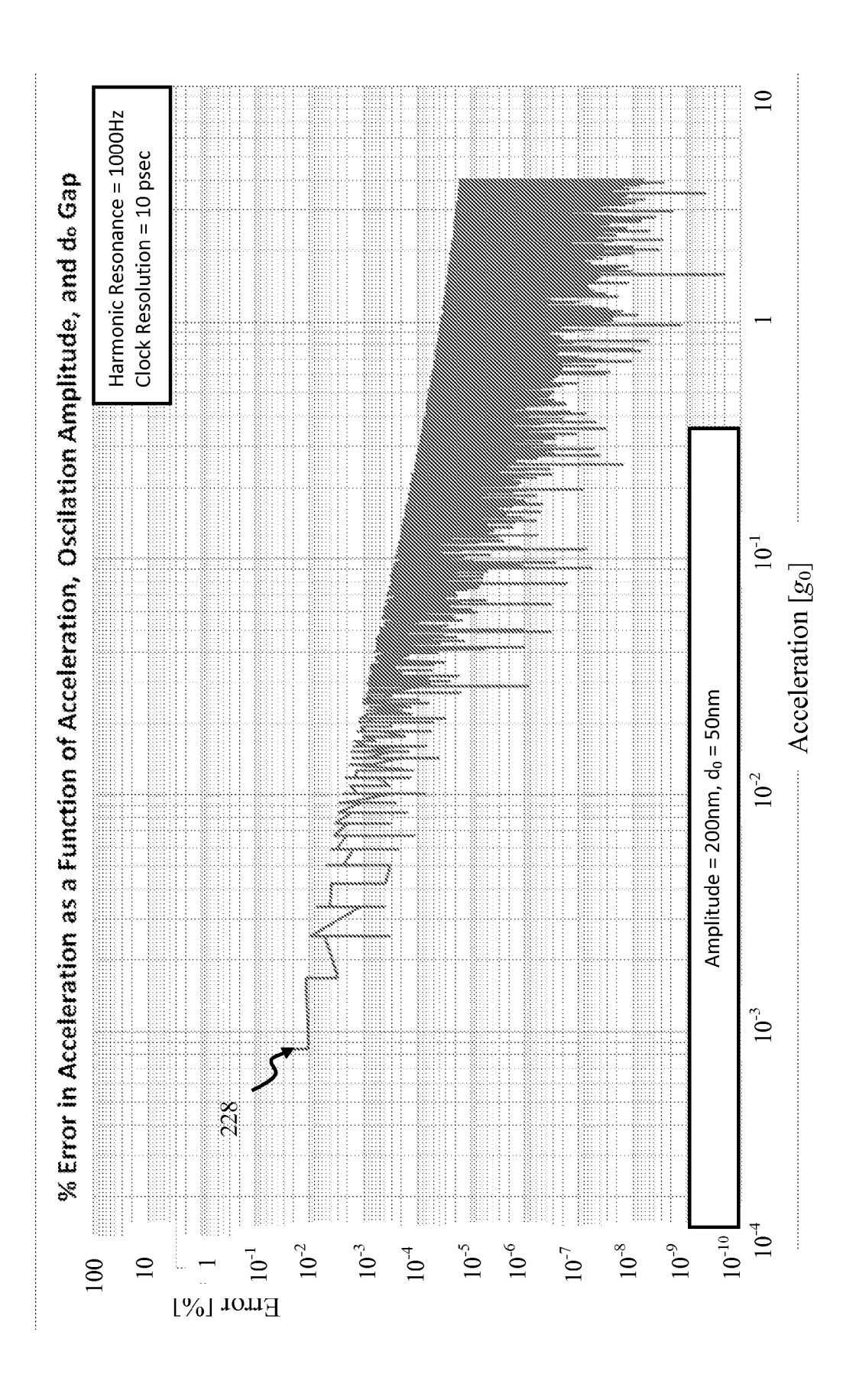


FIG. 2A-4

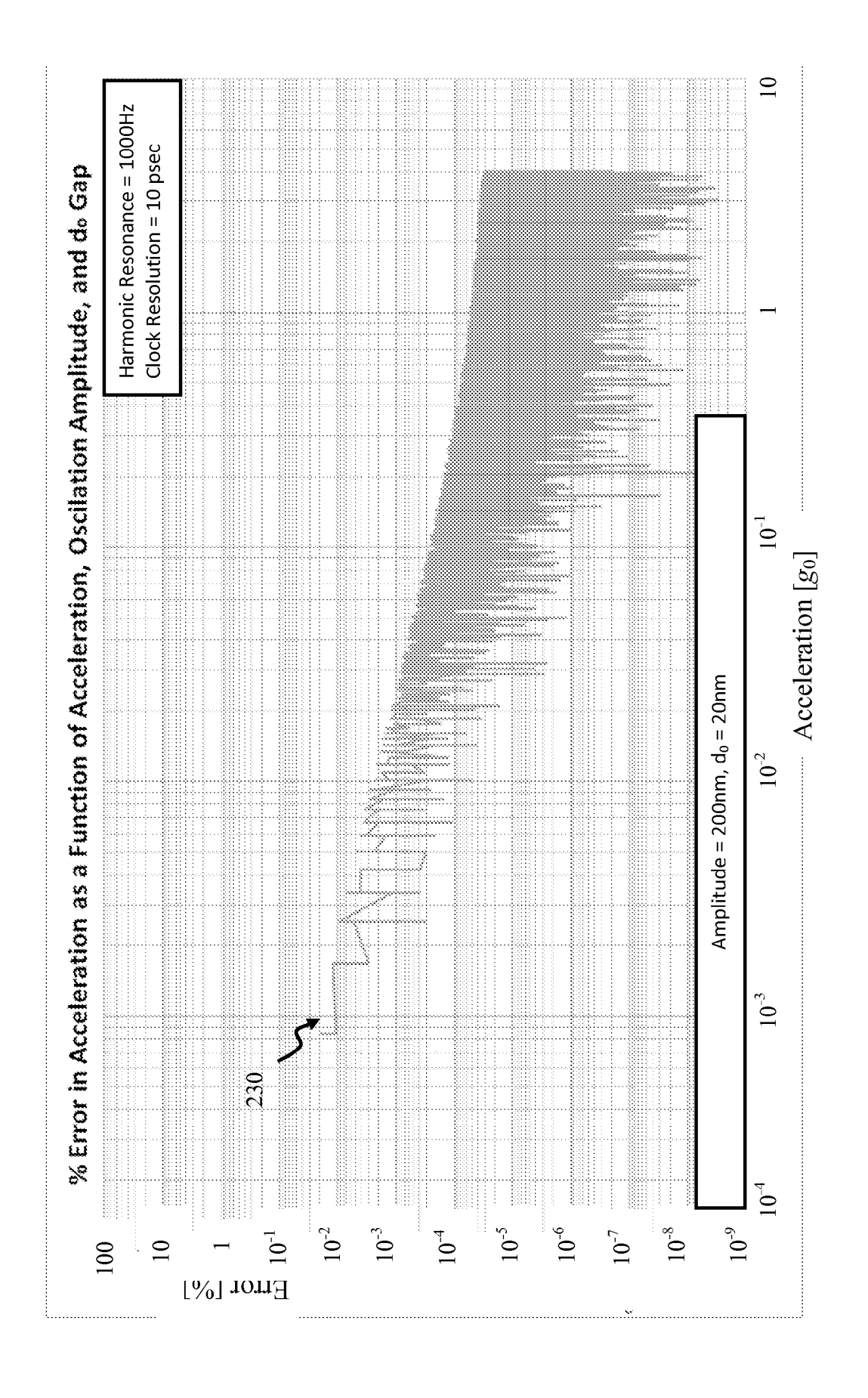


FIG. 2A-5

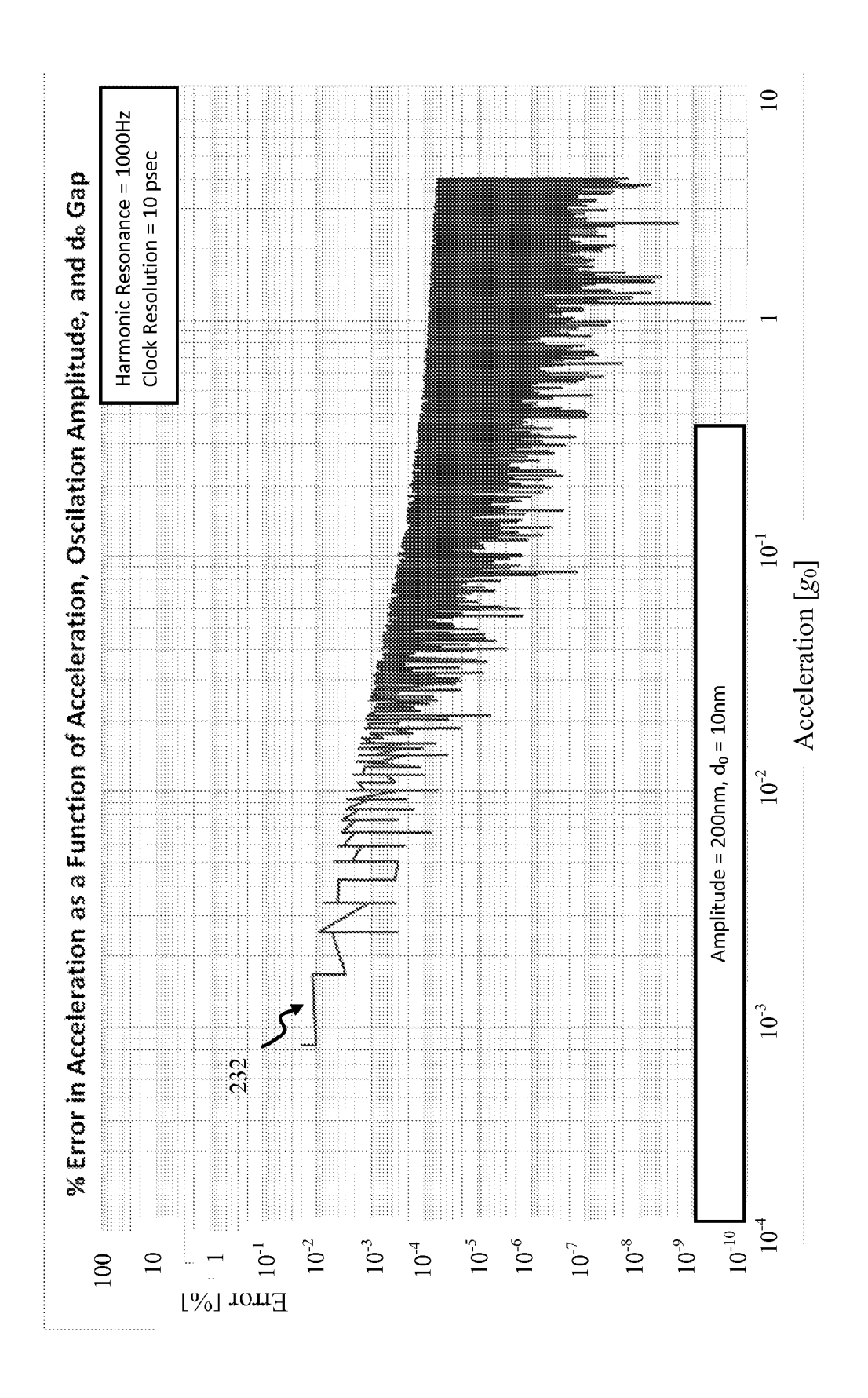


FIG. 2A-6

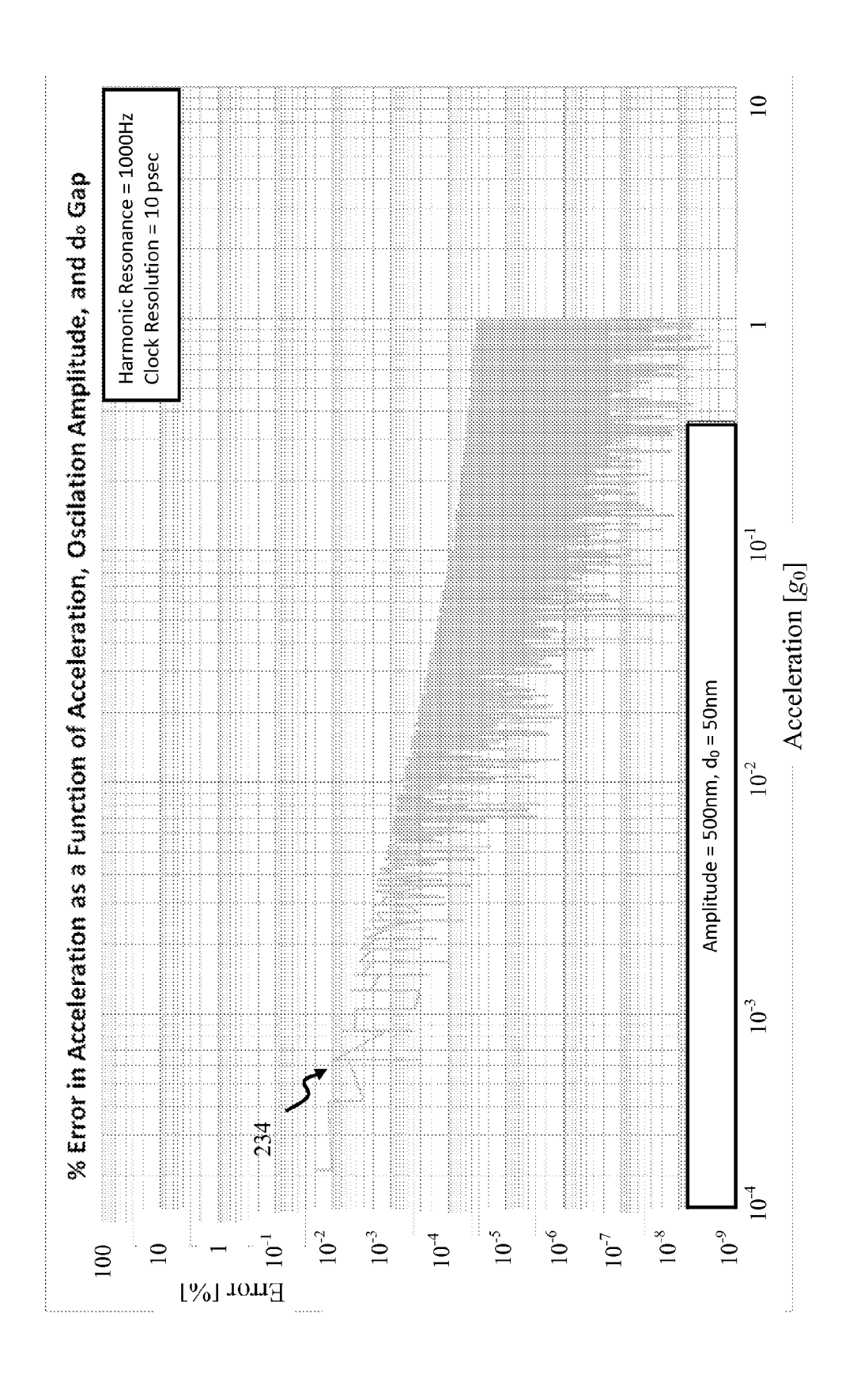


FIG. 2A-7

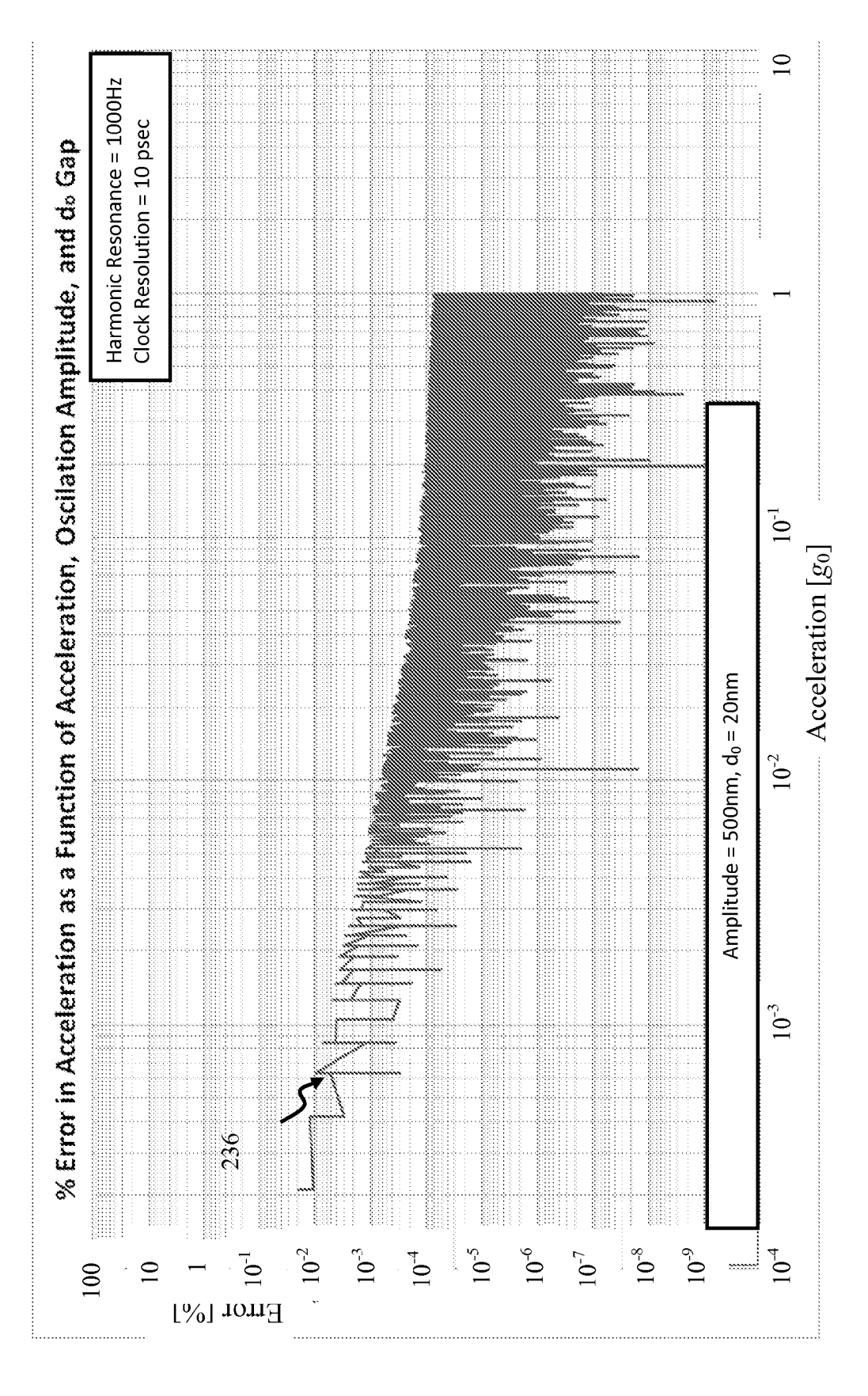


FIG. 2A-8

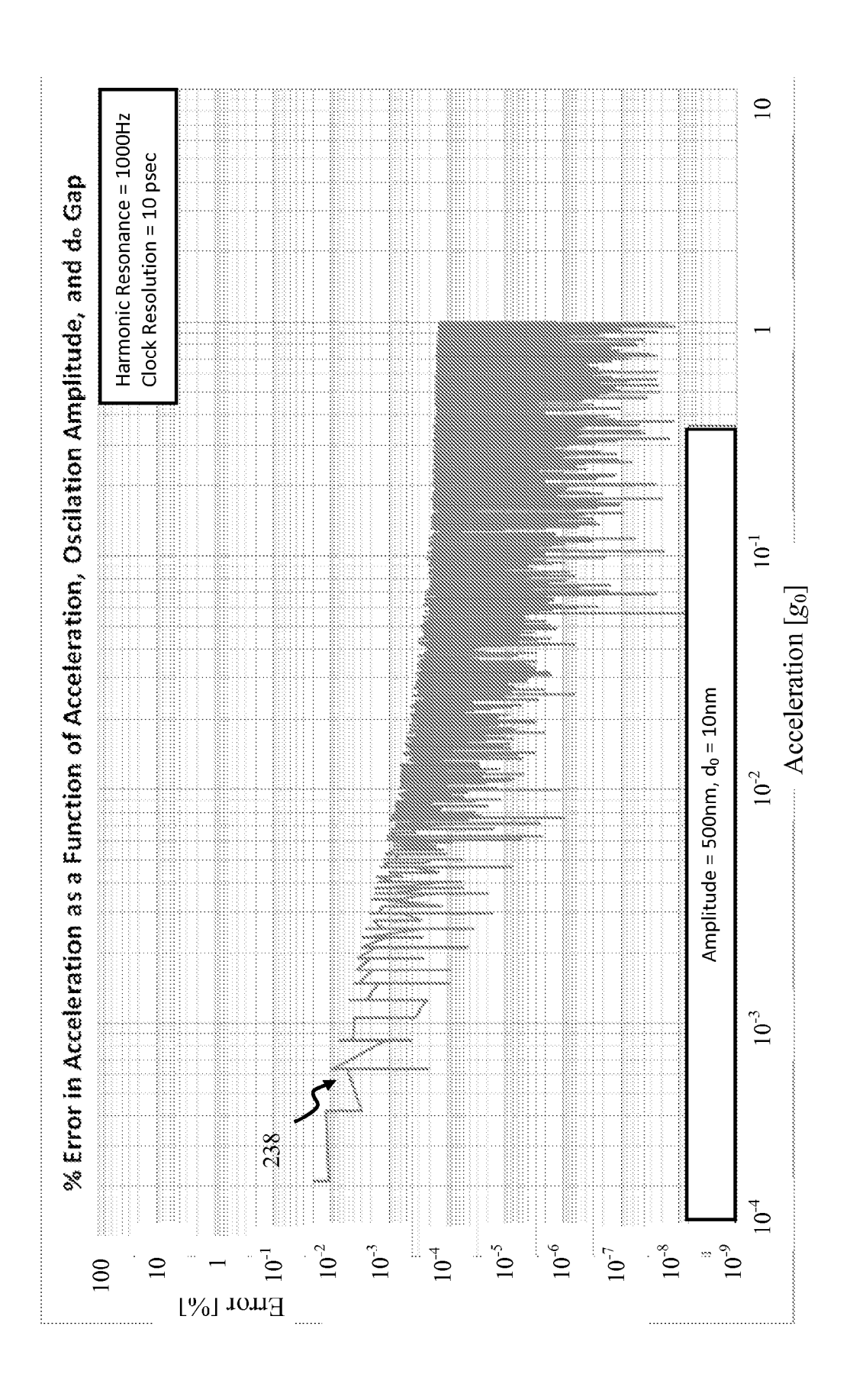


FIG. 2A-9

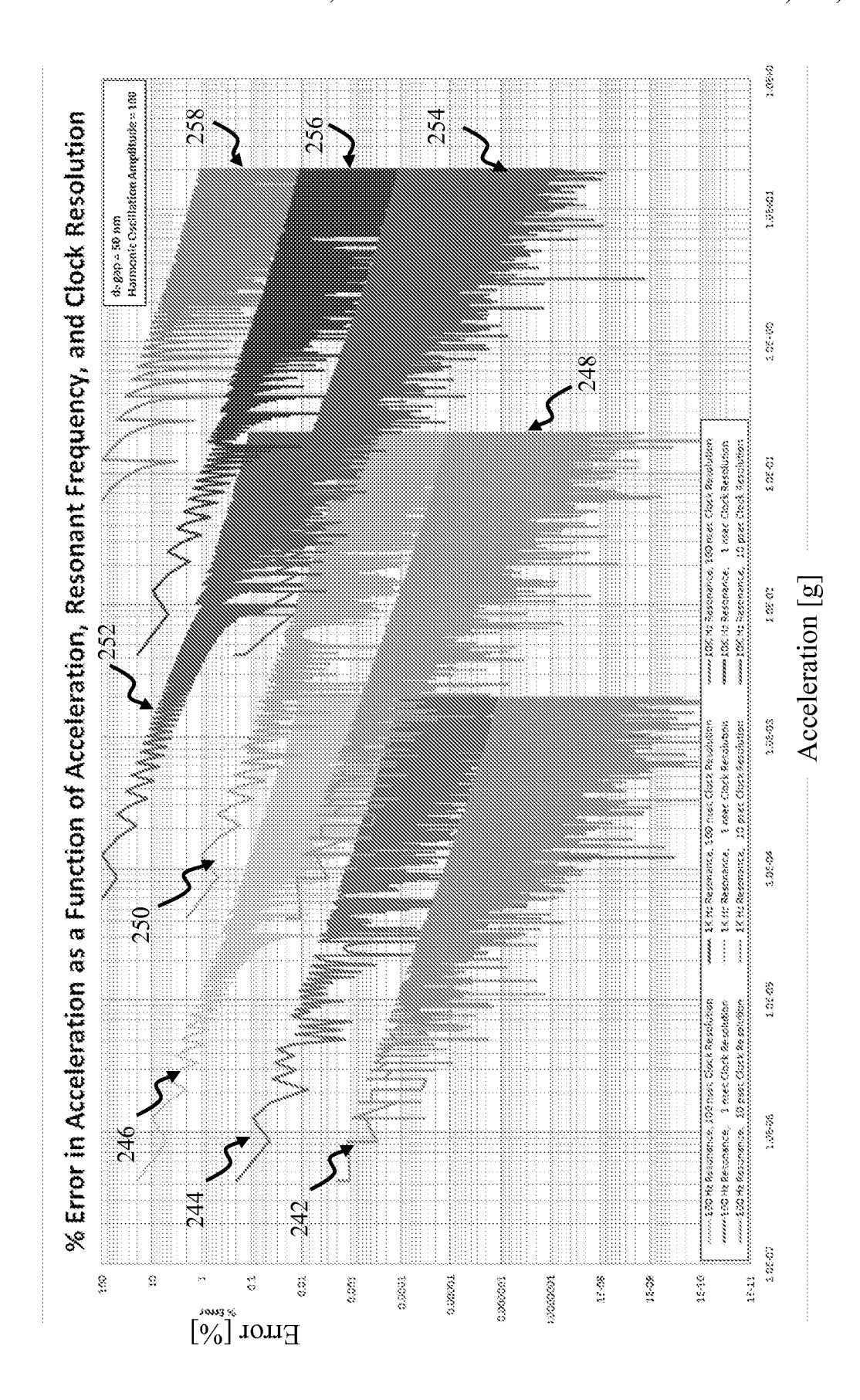
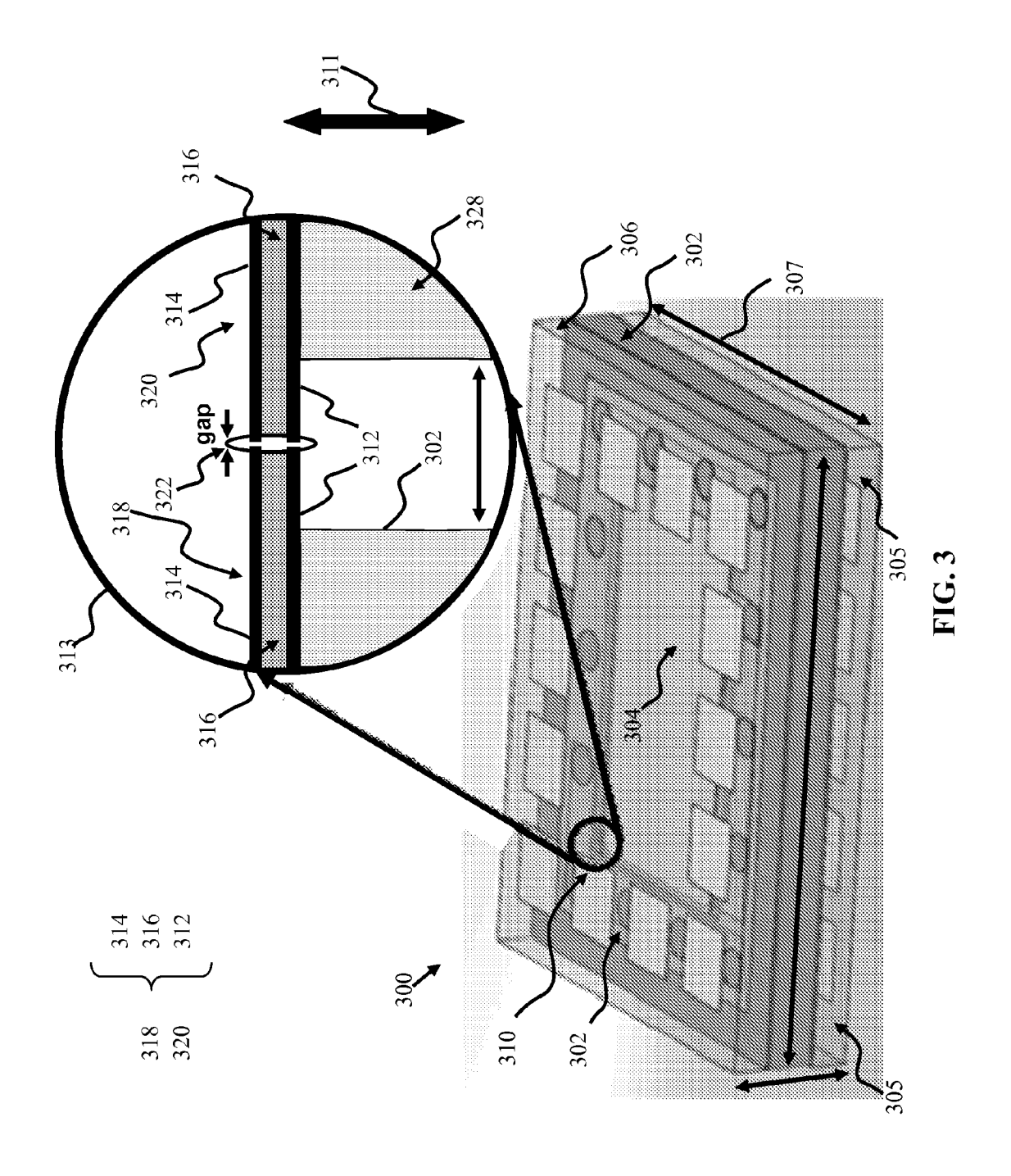
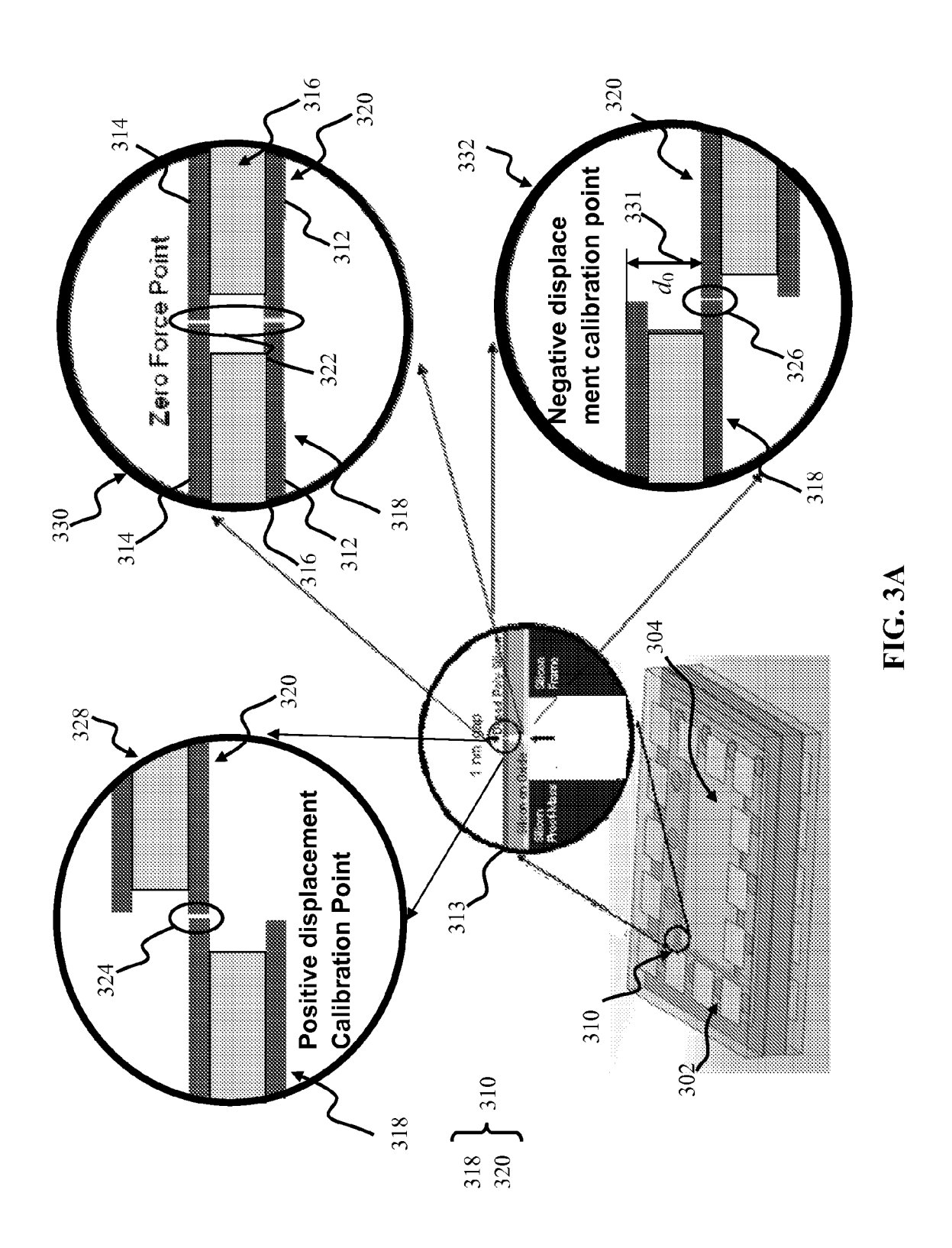
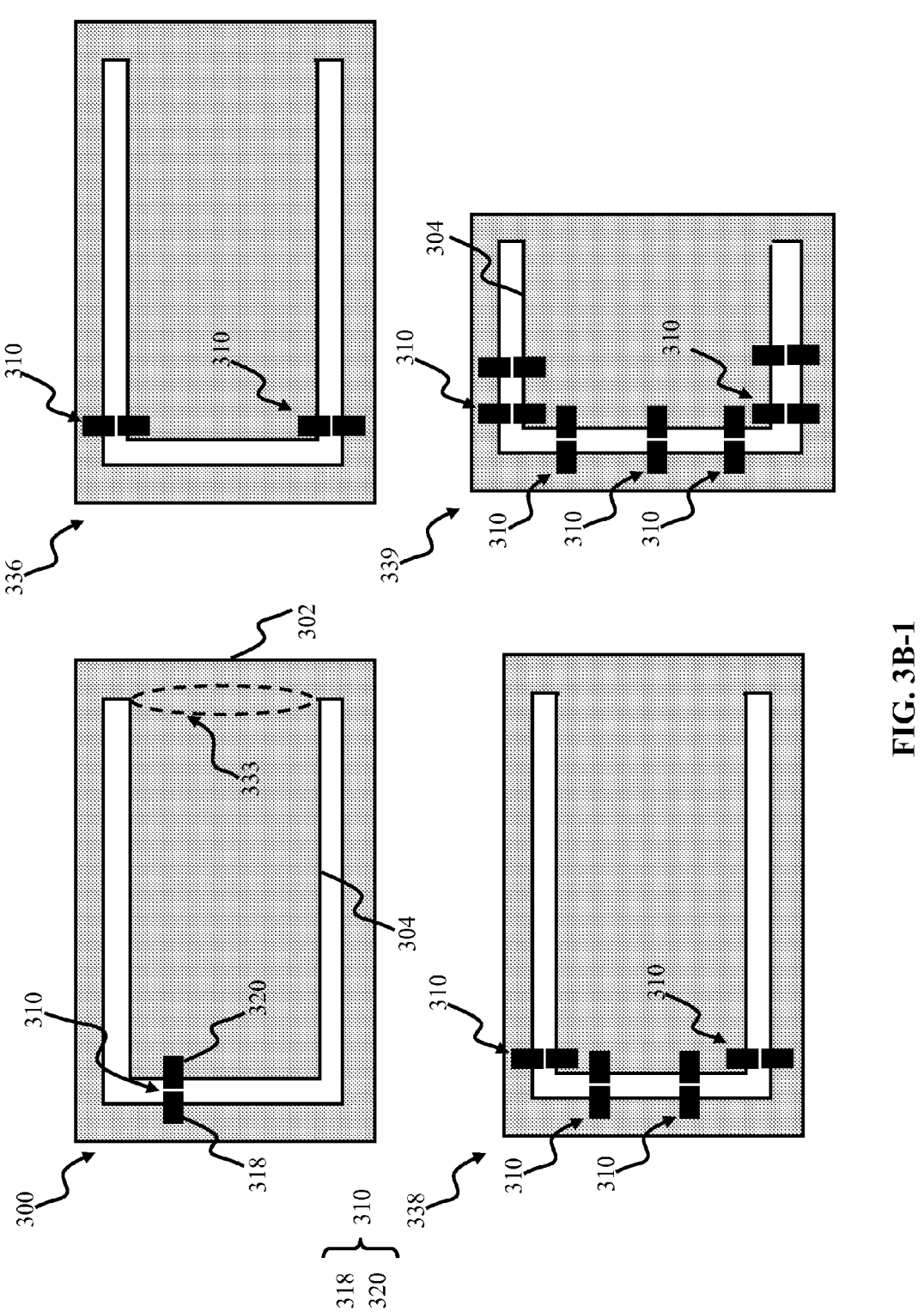
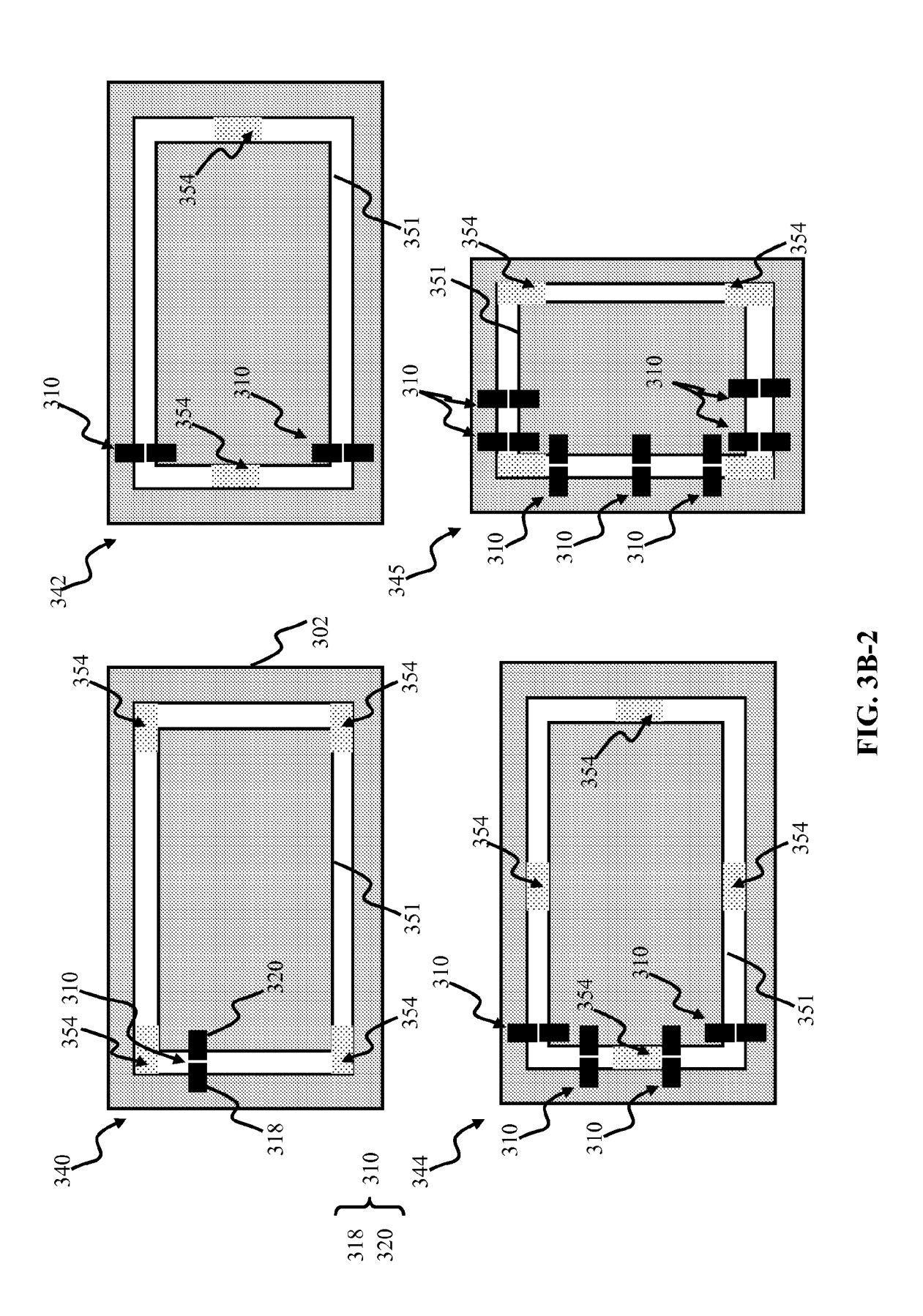


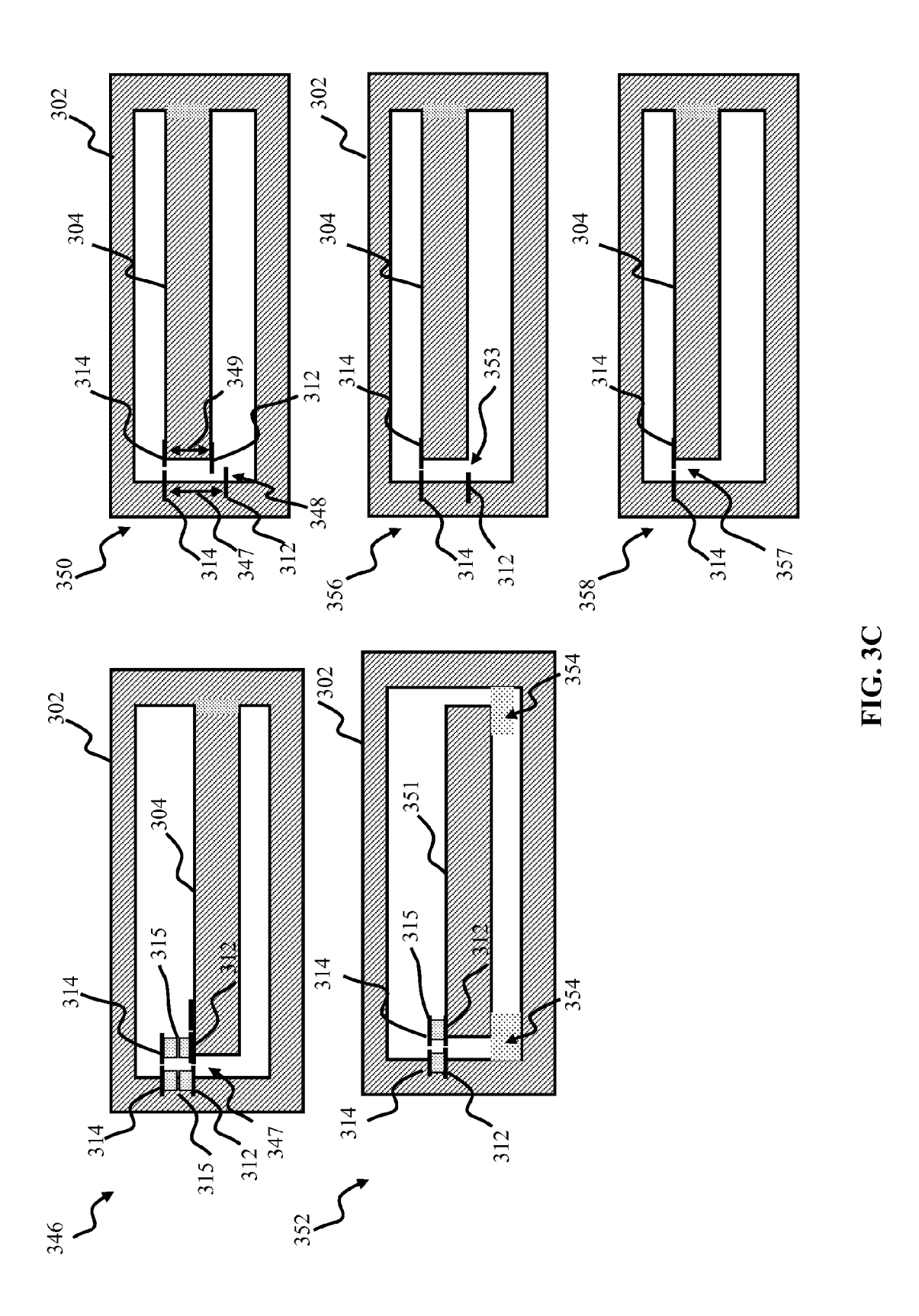
FIG. 2B

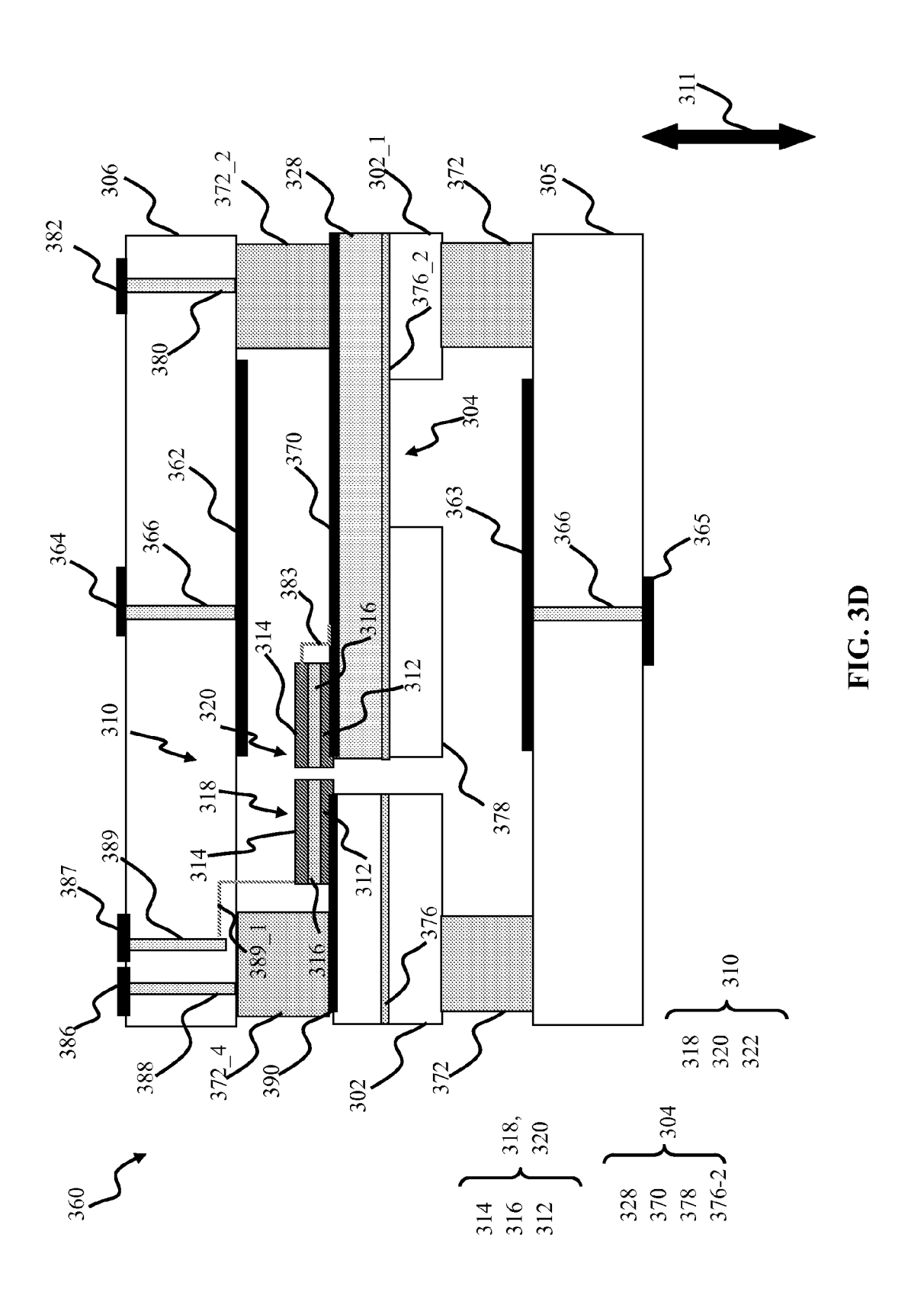


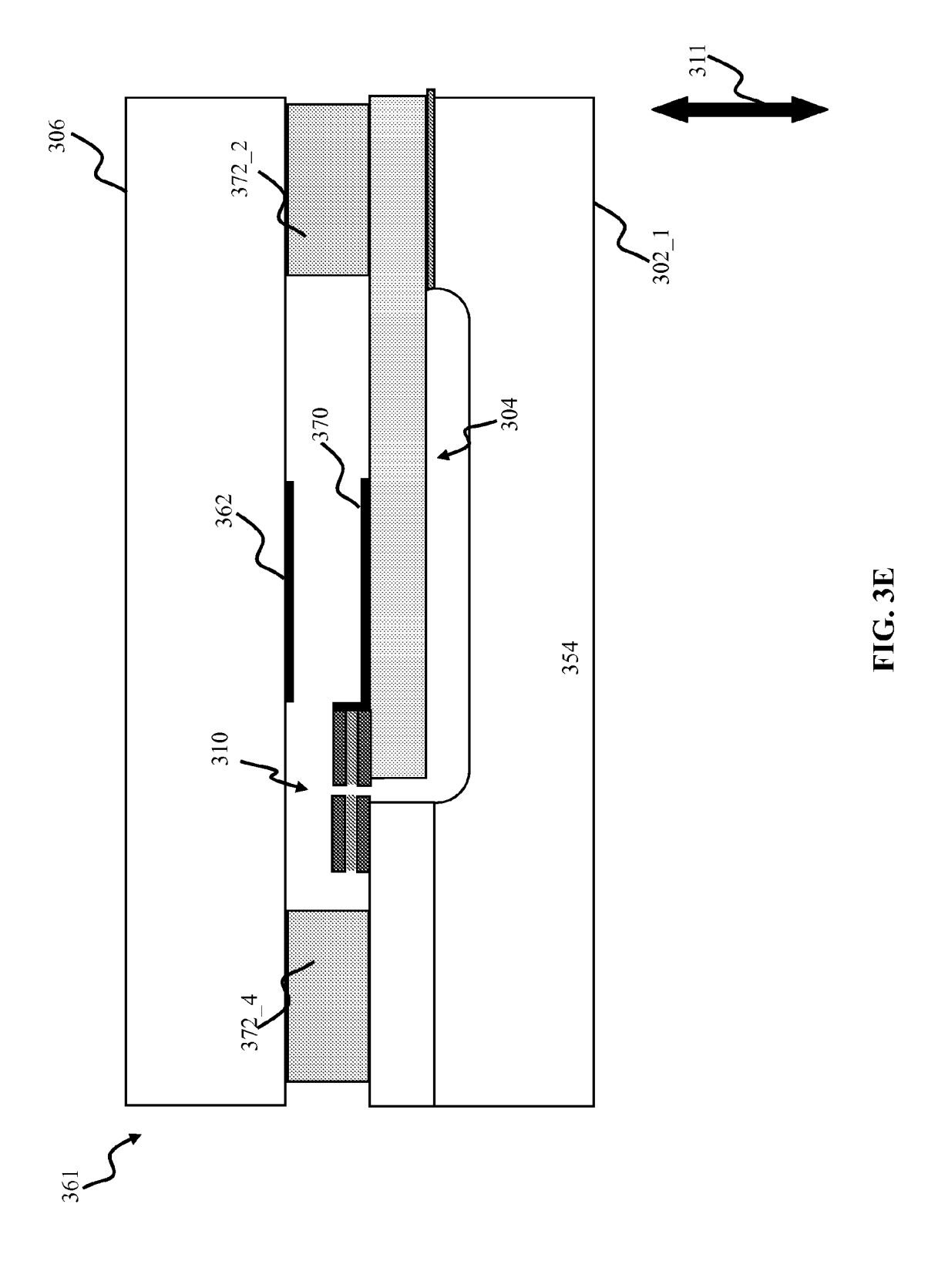


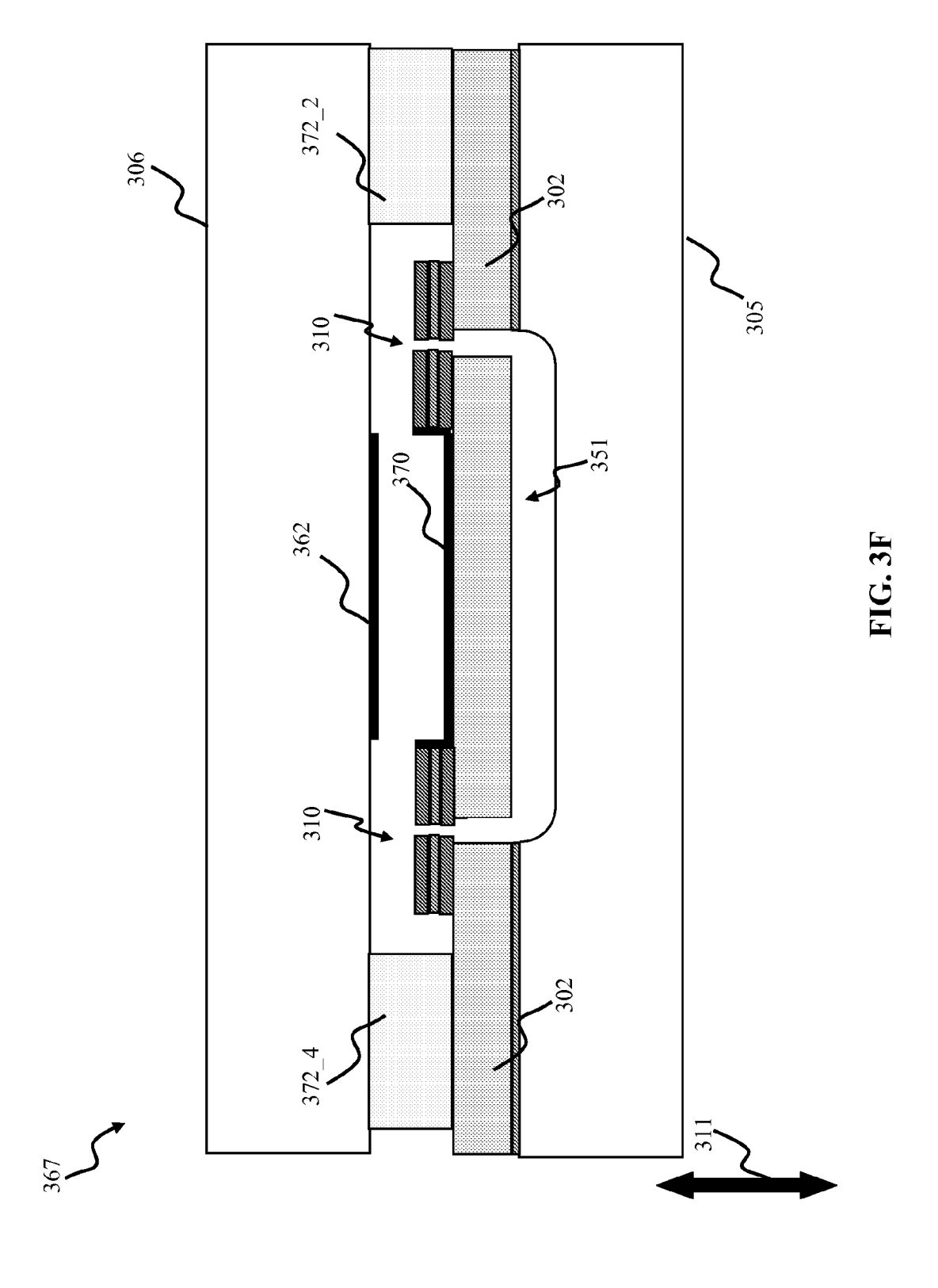


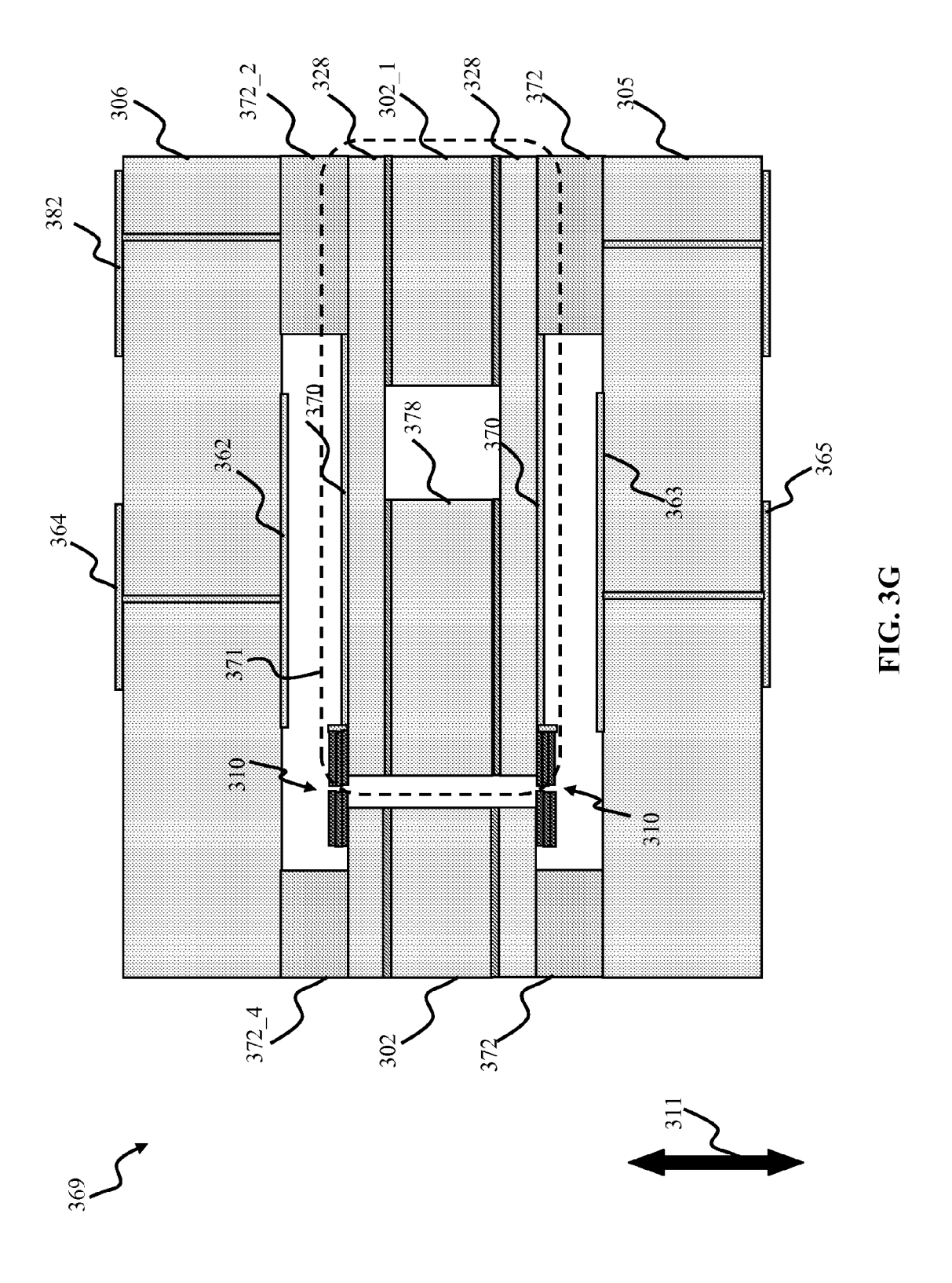


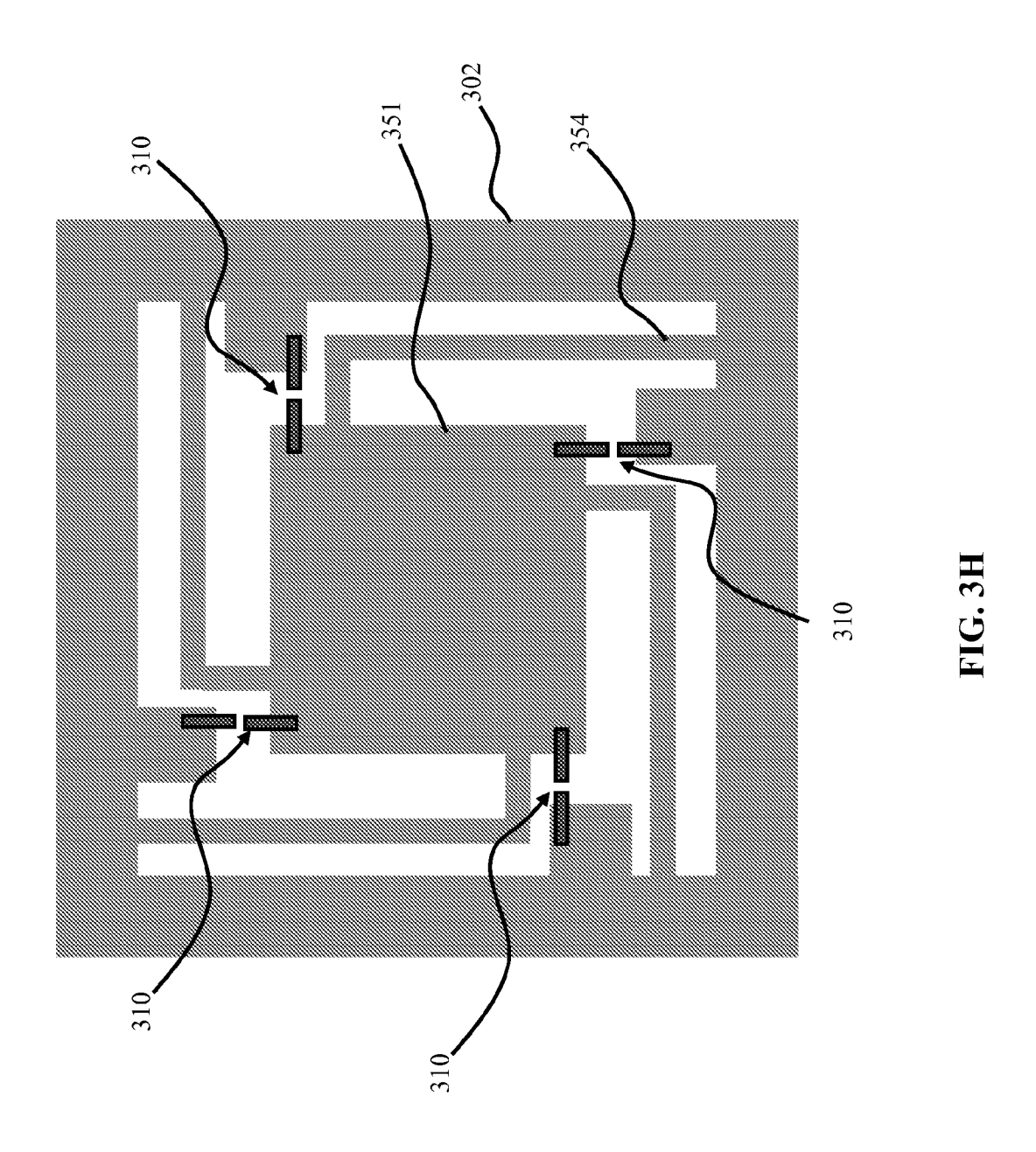














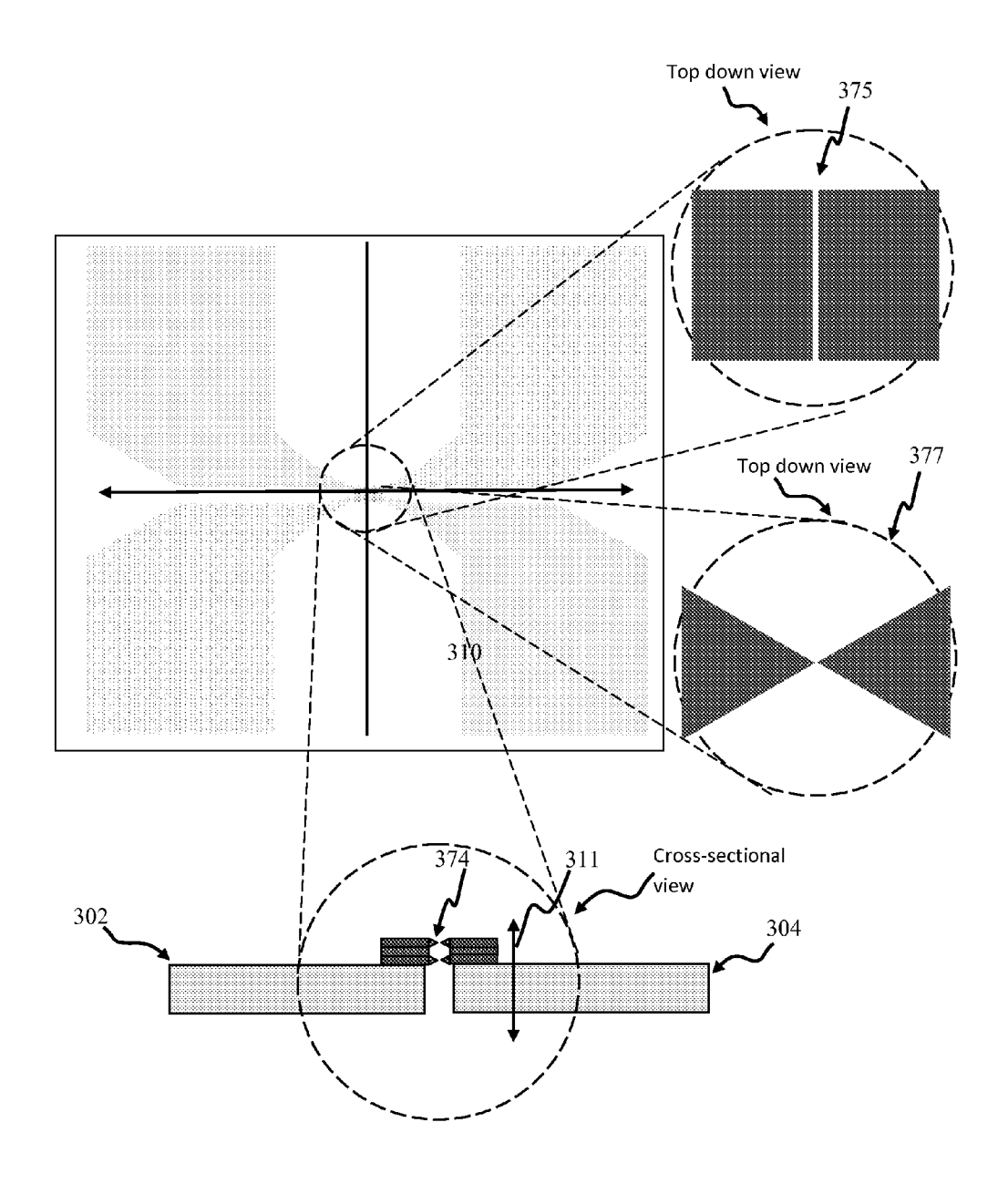
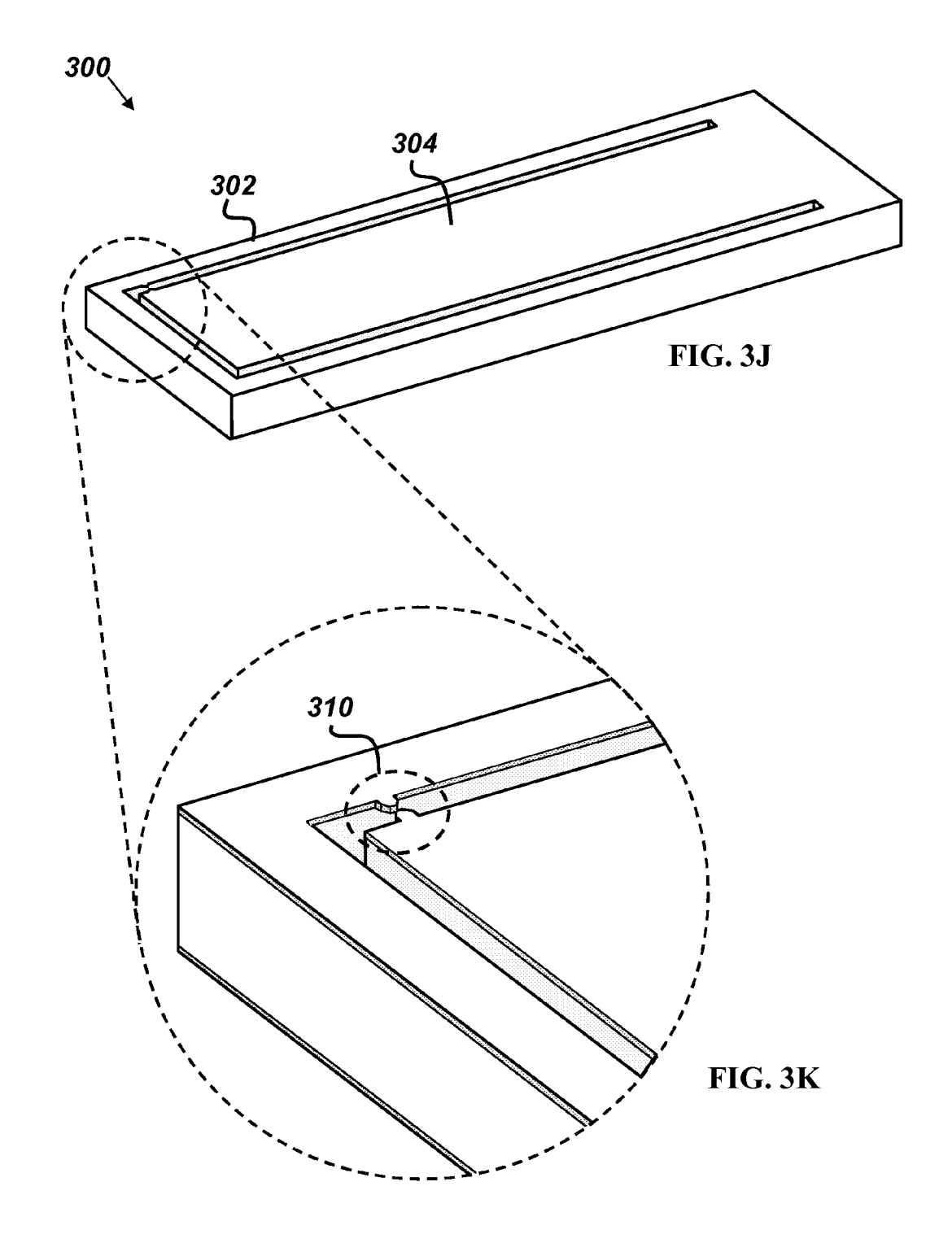
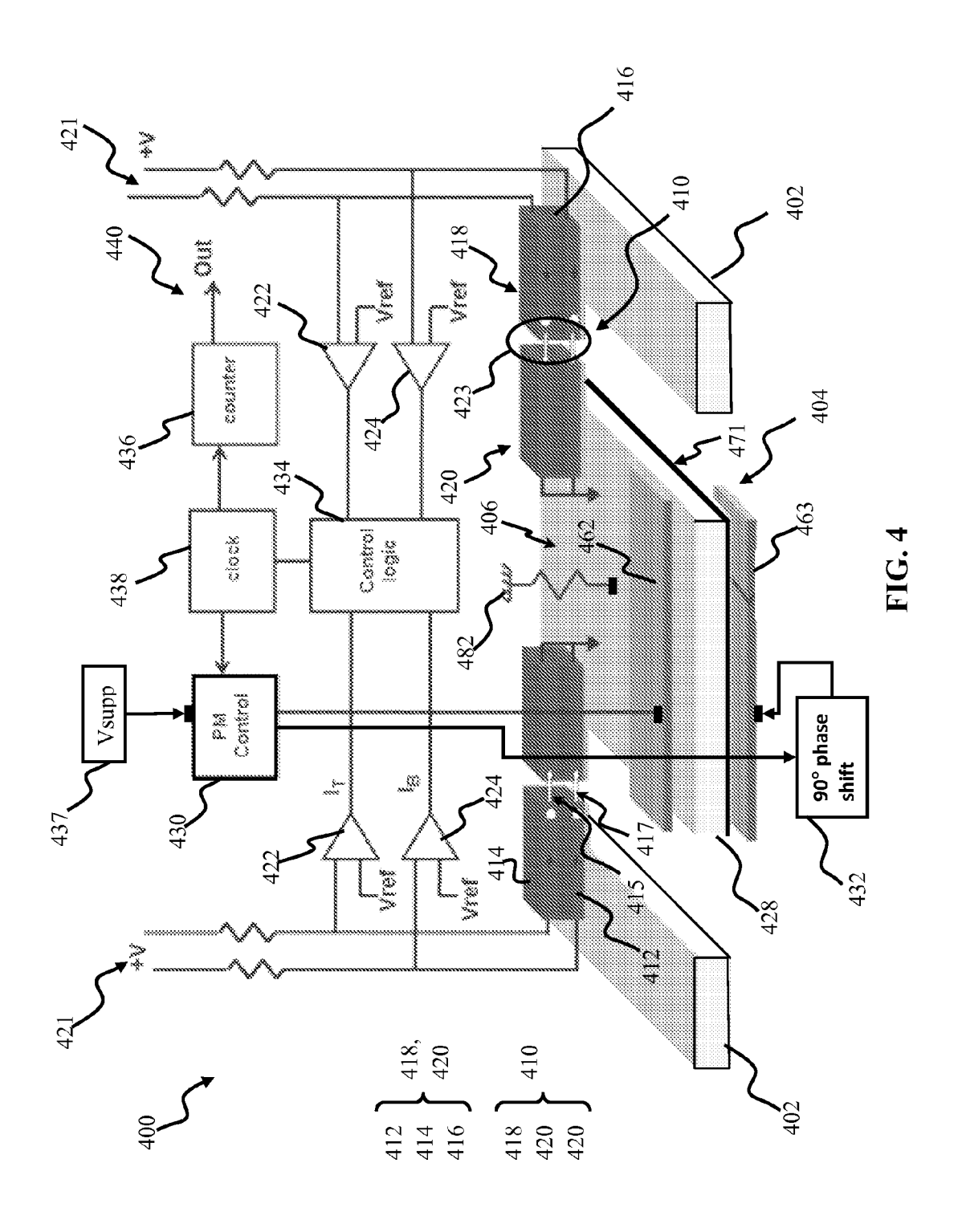
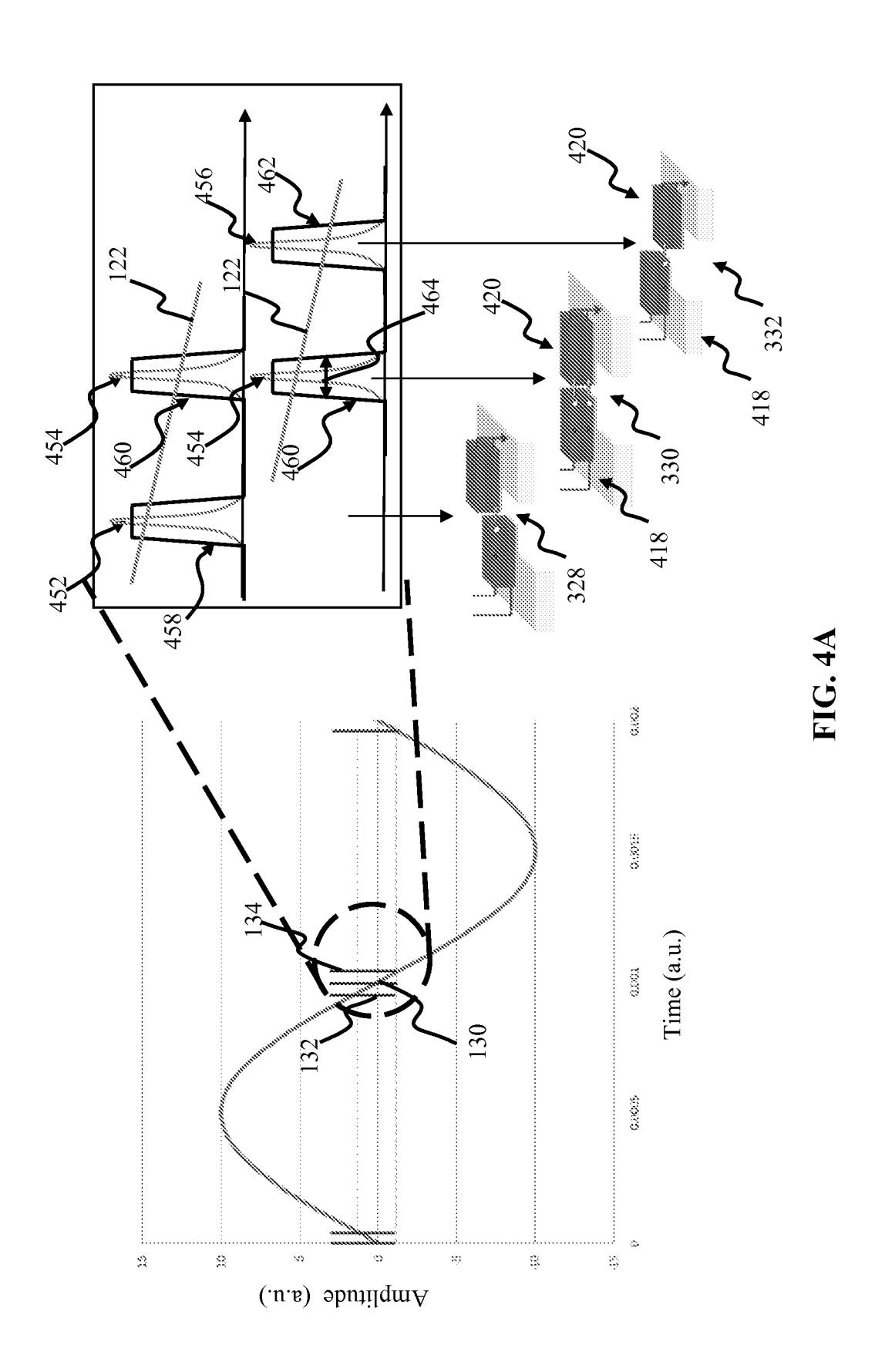
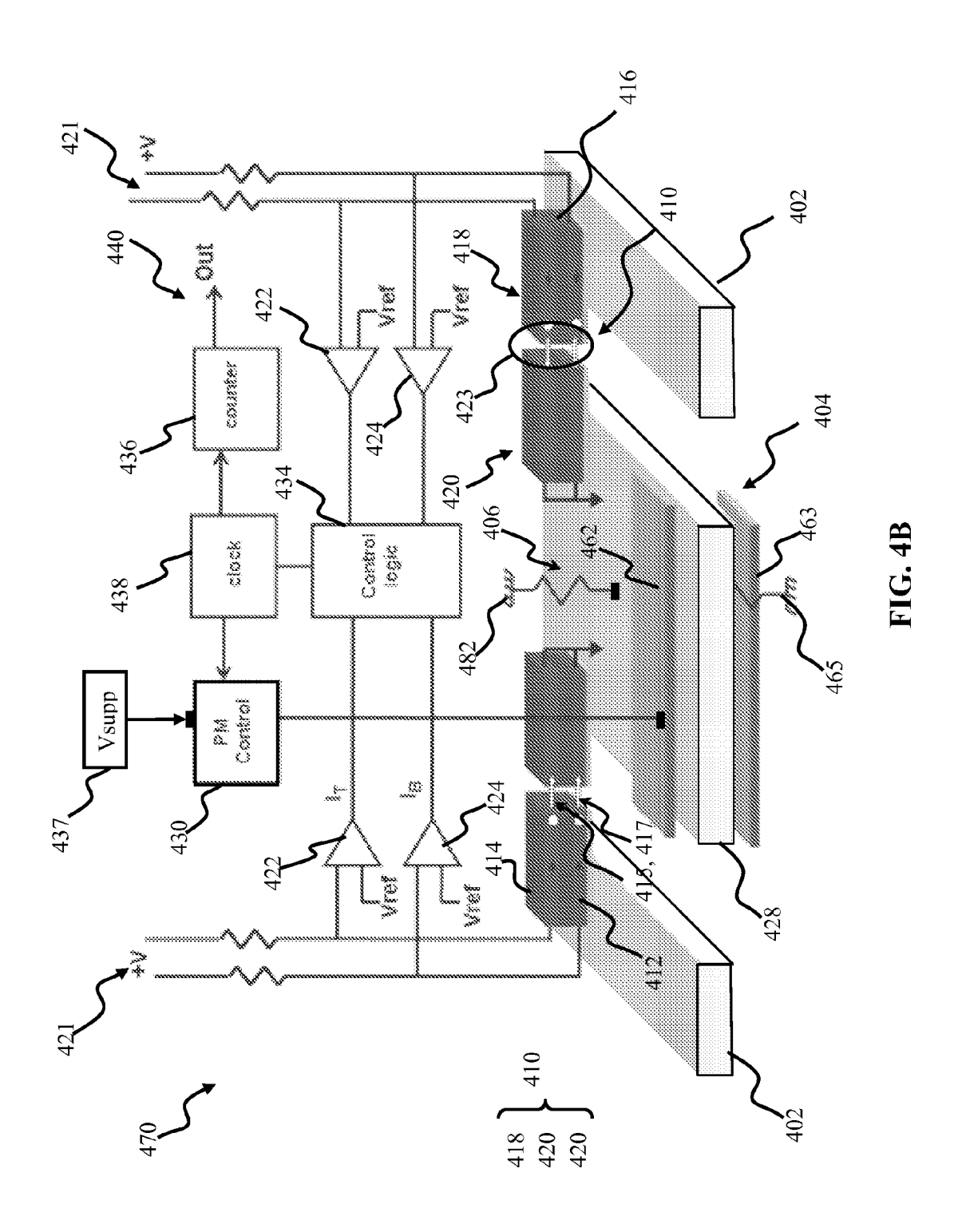


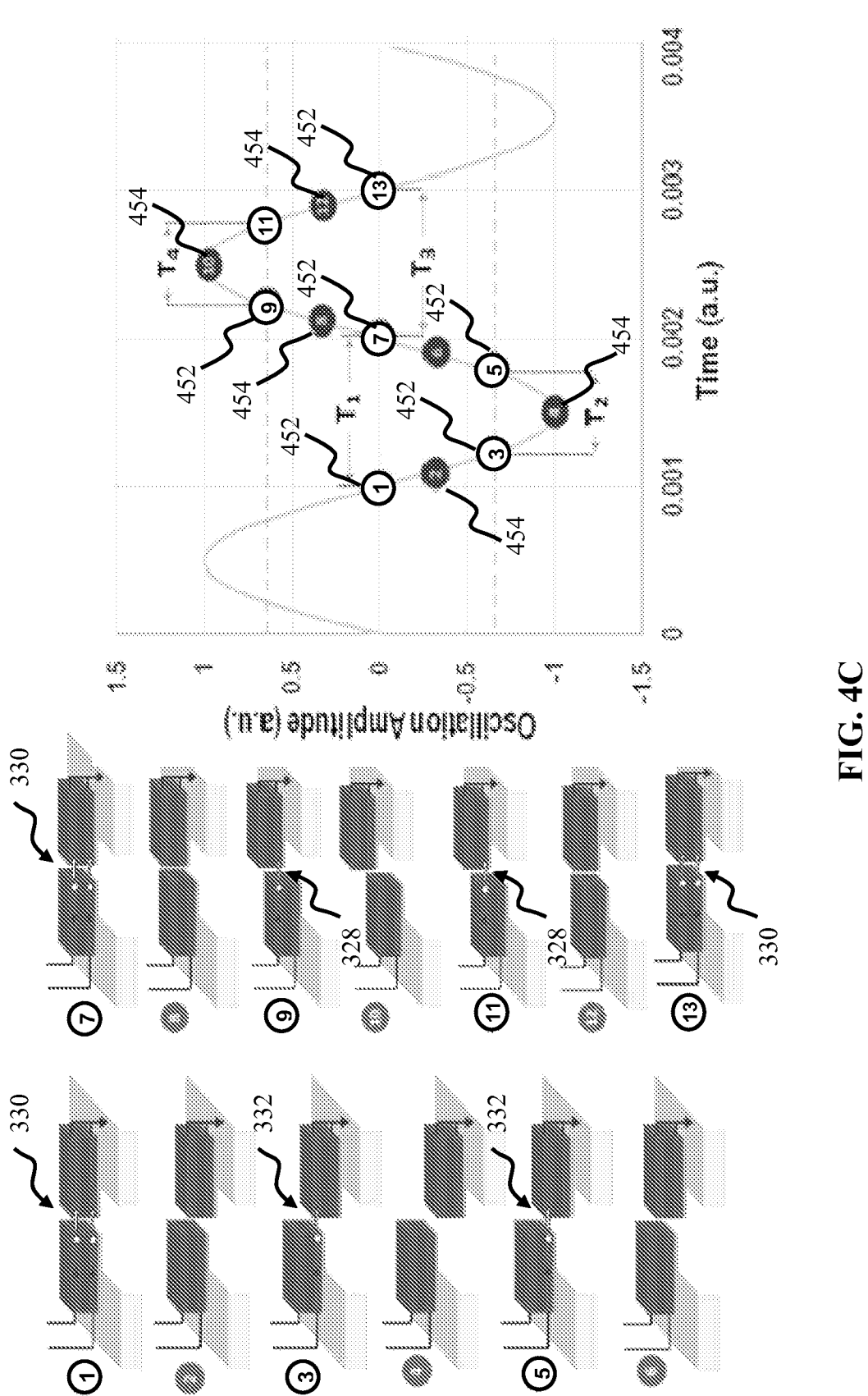
FIG. 31











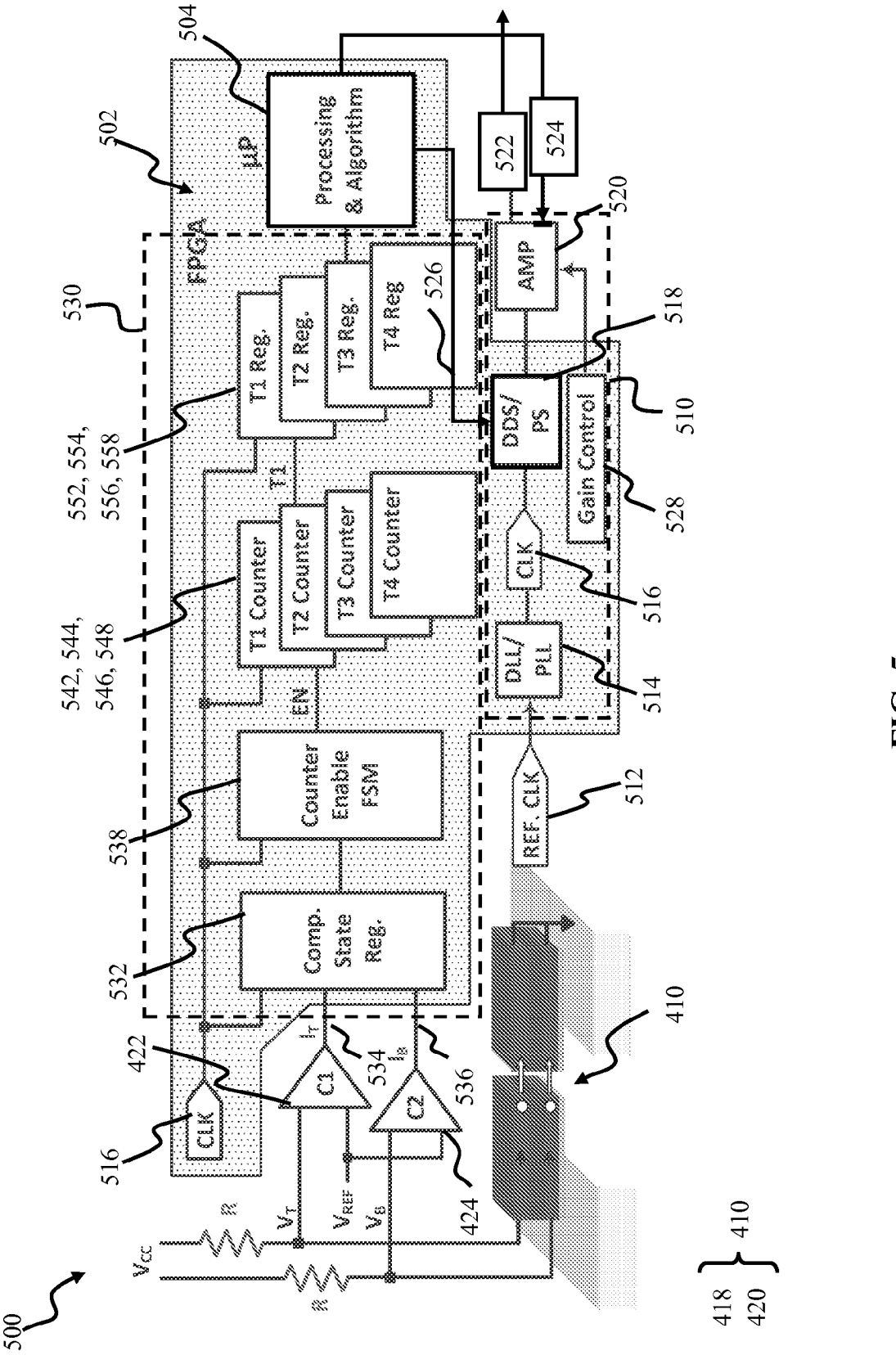
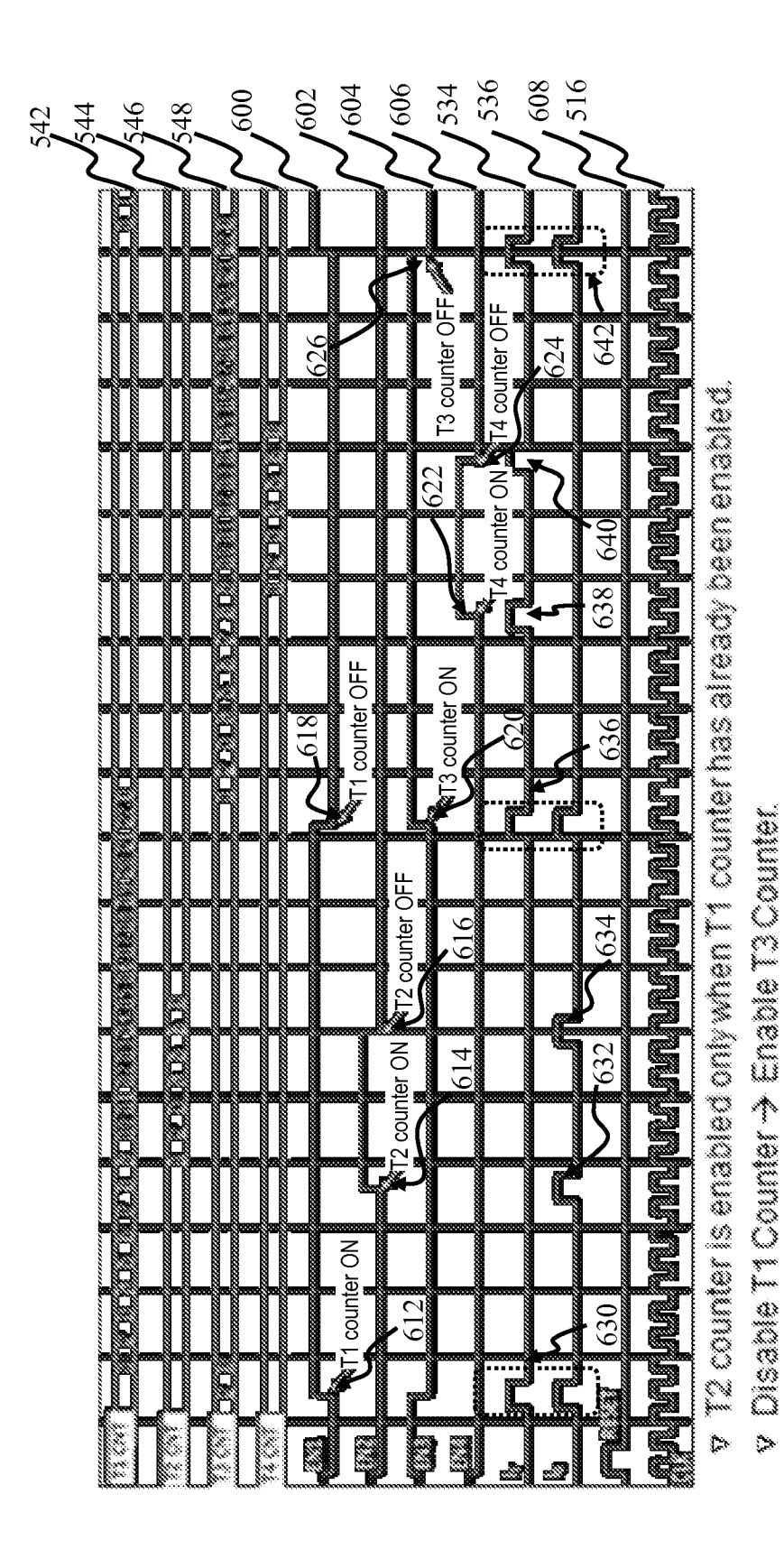
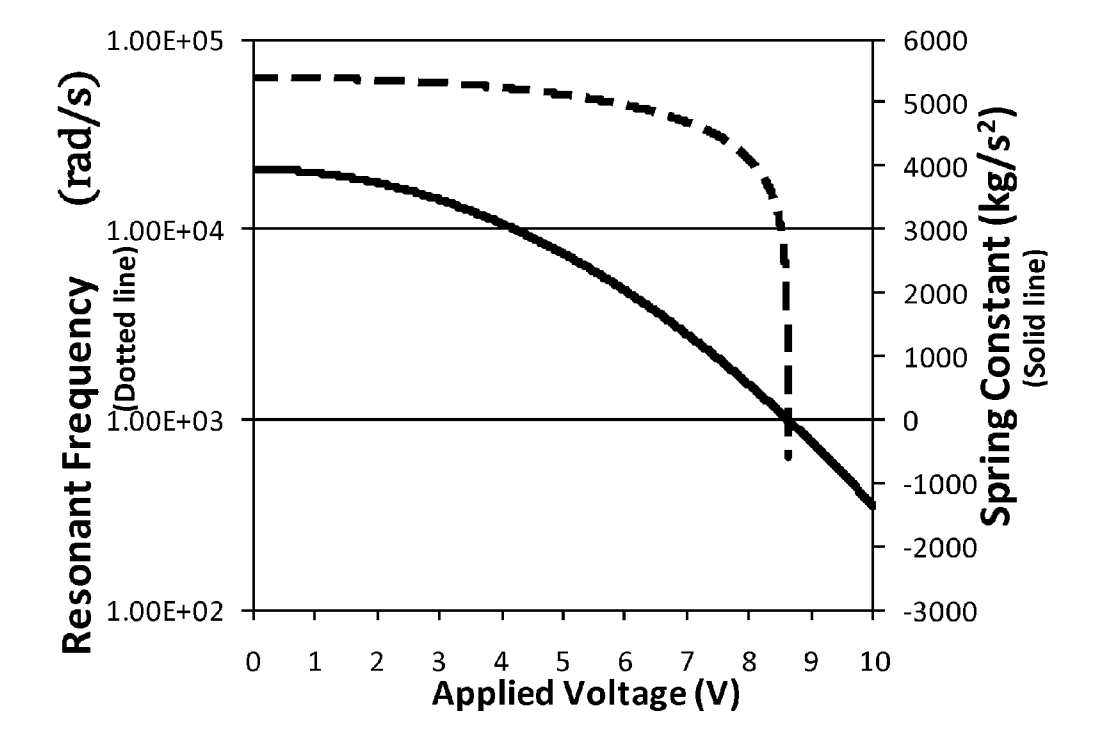


FIG. 5



14 Counter is enabled only when 13 counter has already been enabled.



**FIG.** 7

1

## AUTO-RANGING FOR TIME DOMAIN INERTIAL SENSOR

### FEDERALLY-SPONSORED RESEARCH AND DEVELOPMENT

This invention is assigned to the United States Government and is available for licensing for commercial purposes. Licensing and technical inquiries may be directed to the Office of Research and Technical Applications, Space and <sup>10</sup> Naval Warfare Systems Center, Pacific, Code 72120, San Diego, Calif., 92152; voice (619) 553-5118; ssc\_pac\_t2@navy.mil. Reference Navy Case Number 101298.

### BACKGROUND OF THE INVENTION

### 1. Field of the Invention

The present invention relates generally to oscillatory apparatus for use in sensing applications, and more particularly in 20 one exemplary aspect to an inertial time domain sensing apparatus, and methods of utilizing the same.

### 2. Description of Related Technology

Accurate measurements of parameters (such as for example force) are often required in a wide variety of appli- 25 cations. Micro-electromechanical sensors (MEMS) devices such as accelerometers have been extensively used in, e.g., dynamic distance and speed measurements, inclination, machine vibration, buildings and structural monitoring, component placement in manufacturing, process control systems 30 and safety installations. Angular rotation rate MEMS (also referred to as the gyroscope or the rate sensors) are useful in, inter alia, navigation, automotive (e.g., electronic stability control), entertainment (e.g., user motion detection for game consoles), photography (e.g., image stabilization), animal 35 behavior studies and many other applications. Pressure sensors are similarly widely used in applications such as weather, industrial monitoring and control, aircraft and automotive, oil and gas exploration, flow sensing, acoustics, etc. Many other parameter measurement applications exist (such as for 40 example, magnetic force measurements used in navigation and mineral exploration, or electrostatic force measurements used in microscopy, etc.).

However, most presently available inertial sensors of sufficient resolution for a given application are costly, thereby 45 limiting their use and widespread adoption. Conversely, more inexpensive inertial sensor solutions currently available do not provide sufficient accuracy and stability required for many applications, such as industrial measurement. Existing sensor solutions (whether of the more costly or more inexpensive variety) also require periodic recalibration and dedicated signal conditioning circuitry, and are generally susceptible to noise interference, thus limiting installation flexibility.

Yet another drawback of these prior art solutions relates to 55 their limited dynamic range; generally speaking, two or more separate sensors are required for sensing or measurement of parameter values of significantly different amplitude, thereby further increasing the cost and complexity of systems capable of measurement over wide dynamic ranges.

In the context of a force measurement, the typical prior art force sensor measures displacement (also often referred to as "deflection") of a spring-suspended proof mass in order to estimate a force acting on the proof mass. The methods of measuring such deflection vary in accuracy, variability, and 65 cost of implementation. Various measurement approaches may be used, such as for example capacitive, piezo-resistive,

2

electron tunneling sensing, and optical interferometry, in order to determine the proof mass deflection. In all of these approaches, the deflection (and thus the force) is inferred as a function of a measured voltage (or electric current), and therefore is inevitably subject to measurement errors due to, inter alia, thermal and electromagnetic noise. As a result, most existing force sensor solutions require very accurate signal conditioning circuitry (such as precision amplifiers, filters, voltage references, etc.), as well as periodic recalibrations to account for sensor aging (including e.g., changes in the physical properties or characteristics of the "spring" and/or proof mass with time), and electrical component drift. In the case of force sensors utilizing electron tunneling tips, tunneling can occur at several points along the motion of the tunneling tip—resulting in noise being added to the system.

Accordingly, there is a salient need for an improved high-accuracy and high-resolution force sensing apparatus having an increased dynamic range, that at the same time is both lower in cost and complexity as compared to existing solutions. Ideally, such improved sensing apparatus would also mitigate or completely obviate the need for calibration (i.e., be "self-calibrating"), and could be used in a wide variety of parametric sensing, measurement, or other applications.

#### **SUMMARY**

Disclosed herein is a method for adjusting the accuracy of a time-domain inertial sensor comprising the following steps: operatively positioning a harmonic oscillator of the time-domain inertial sensor between two capacitive plates; initiating harmonic oscillation of the oscillator in a first plane by creating with the capacitive plates a capacitively forced pulse; monitoring the harmonic oscillation of the oscillator; and electrostatically biasing both of the two capacitive plates such that a spring constant of the oscillator is effectively altered.

In addition, another embodiment of method for adjusting the accuracy of a time-domain inertial sensor in real time is disclosed, which comprises the following steps. The first step provides for initiating harmonic oscillation of an oscillator in a first plane with respect to a frame by creating a capacitively forced pulse with capacitive plates, which are operatively coupled above and below the oscillator. The next step provides for monitoring trigger event signals generated by a position switch. The position switch comprises: a first electrode disposed on the oscillator, a second electrode disposed above the first electrode in the first plane by a distance of  $d_0$ , a third electrode disposed on the frame, and a fourth electrode disposed above the third electrode in the first plane by a distance of  $d_0$ . The first, second, third, and fourth electrodes are arranged with respect to each other such that when the oscillator is at a zero force position first and second trigger event signals are generated by the first and third electrodes and by the second and fourth electrodes respectively. When the oscillator is displaced from the zero force position in the first plane by a distance of +d<sub>0</sub> a third trigger event signal is generated by the first and fourth electrodes. When the oscillator is displaced from the zero force position in the first plane by a distance of  $-d_0$  a fourth trigger event signal is generated by the second and third electrodes. Another step provides for 60 electrostatically biasing both of the two capacitive plates such that a spring constant of the oscillator is effectively altered.

#### BRIEF DESCRIPTION OF THE DRAWINGS

Throughout the several views, like elements are referenced using like references. The elements in the figures are not drawn to scale and some dimensions are exaggerated for

clarity. The features, objectives, and advantages of the invention will become more apparent from the detailed description set forth below when taken in conjunction with the drawings, wherein:

- FIG. 1 is a plot illustrating one embodiment of a method for 5 detecting oscillator position using trigger events in the absence of external forcing.
- FIG. 1A is a plot illustrating one embodiment of a method detecting oscillator position using trigger events in presence of external forcing.
- FIG. 1B is a plot illustrating one exemplary oscillator trajectory in the presence of time varying external forcing.
- FIGS. 1C and 1D are plots illustrating one embodiment of a method of detecting oscillator position using trigger events in presence of random noise.
- FIG. 2 is a plot depicting an exemplary simulation of acceleration measurement relative error as a function of acceleration according to one embodiment of the time-domain sensing method of the invention.
- FIG. **2A-1** through **2A-9** are a series of plots depicting the 20 simulation of acceleration measurement relative error as a function of acceleration for different values of oscillation amplitude and trigger position separation, according to one embodiment of the invention.
- FIG. 2B is a plot depicting the simulation of acceleration 25 measurement relative error as a function of acceleration for different values of resonant frequency and clock resolution, according to one embodiment of the invention.
- FIG. 3 is a top perspective view of one embodiment of a time-domain sensing apparatus comprising a tunneling position indicator switch according to the invention.
- FIG. 3A is an illustration depicting three (3) exemplary reference states of the tunneling position indicator switch of FIG. 3
- FIGS. **3B-1** and **3B-2** are top plan views illustrating various 35 embodiments of switch spatial configurations for use with the time-domain sensing apparatus of the invention.
- FIG. 3C is a side cross-section view illustrating various embodiments of trigger point configurations for use with the time-domain sensing apparatus of the invention.
- FIG. 3D is a side cross-section view illustrating one embodiment of a time-domain sensing apparatus comprising a dual-electrode switch according to the invention.
- FIG. 3E is a side cross-section view illustrating another embodiment of a time-domain sensing apparatus comprising 45 a dual-electrode switch according to the invention.
- FIG. 3F is a side cross-section view illustrating one embodiment of a time-domain sensing apparatus comprising a suspended proof mass assembly and two sets of dual-electrode switches according to the invention.
- FIG. 3G is a side cross-section view illustrating one embodiment of a time-domain sensing apparatus comprising a dual cantilever proof mass assembly and two sets of dual-electrode switches according to the invention.
- FIG. 3H is a top plan view illustrating another embodiment 55 of a time-domain sensing apparatus comprising a suspended proof mass assembly and multiple sets of dual-electrode switches according to the invention.
- FIG. 3I is a set of top plan and cross-sectional views illustrating multiple different electrode tip embodiments useful 60 with the various time-domain sensing apparatus embodiments described herein.
- FIG. 3J is a perspective view of another embodiment of a time-domain sensing apparatus comprising a tunneling position indicator switch.
- FIG. 3K is a cross-sectional view of an embodiment of a tunneling position indicator switch.

4

- FIG. 4 is a block diagram depicting one embodiment of a time-domain force sensing apparatus according to the invention, comprising two dual-electrode switches and a bipolar driver apparatus.
- FIG. 4A is a graphical illustration depicting amplification of tunnel current pulses generated by the sensing apparatus of the embodiment of FIG. 4.
- FIG. 4B is a block diagram depicting one embodiment of a time-domain sensing apparatus according to the invention, comprising two dual-electrode switches and a unipolar driver apparatus.
- FIG. 4C is a graphical illustration depicting exemplary trigger events and dual electrode switch positions for the time-domain sensing apparatus of FIGS. 4 and 4B.
- FIG. 5 is a functional block diagram depicting one embodiment of a system employing the time-domain sensing apparatus of the invention.
- FIG. 6 is a timing diagram illustrating an exemplary operational sequence for the time-domain force sensing system of FIG. 5.
- FIG. 7 is a plot showing an effective spring constant and a resulting tunable resonant frequency of an oscillator.

## DETAILED DESCRIPTION OF EMBODIMENTS

Disclosed herein is a method for adjusting the accuracy, or auto-ranging, of a time domain inertial sensor in real time so as to reduce measurement error of the time domain inertial sensor over a large dynamic range. First, an embodiment of a time domain inertial sensor and its manner of operation will be disclosed, followed by the method for auto-ranging.

As used herein, the terms "computer", "computing device", and "computerized device", include, but are not limited to, mainframe computers, workstations, servers, personal computers (PCs) and minicomputers, whether desktop, laptop, or otherwise, personal digital assistants (PDAs), handheld computers, embedded computers, programmable logic devices, digital signal processor systems, personal communicators, tablet computers, portable navigation aids, J2ME equipped devices, cellular telephones, smartphones, personal integrated communication or entertainment devices, or literally any other device capable of executing a set of instructions and processing an incoming data signal.

As used herein, the term "computer program" or "software" is meant to include any sequence or human or machine cognizable steps which perform a function. Such program may be rendered in virtually any programming language or environment including, for example, C/C++, C#, Fortran, COBOL, MATLABTM, PASCAL, Python, Verilog, VHDL, assembly language, markup languages (e.g., HTML, SGML, XML, VoXML), and the like, as well as object-oriented environments such as the Common Object Request Broker Architecture (CORBA), Java<sup>TM</sup> (including J2ME, Java Beans, etc.), Binary Runtime Environment (e.g., BREW), and the like. As used herein, the term "memory" includes any type of integrated circuit or other storage device adapted for storing digital data including, without limitation, ROM, PROM, EEPROM, DRAM, SDRAM, DDR/2 SDRAM, EDO/FPMS, RLDRAM, SRAM, "flash" memory (e.g., NAND/NOR), memristor memory, and PSRAM.

As used herein, the terms "microprocessor" and "digital processor" are meant generally to include all types of digital processing devices including, without limitation, digital signal processors (DSPs), reduced instruction set computers (RISC), general-purpose (CISC) processors, microprocessors, gate arrays (e.g., FPGAs), PLDs, reconfigurable compute fabrics (RCFs), array processors, secure microproces-

sors, and application-specific integrated circuits (ASICs). Such digital processors may be contained on a single unitary IC die, or distributed across multiple components.

As used herein, the term "proof mass" refers generally, and without limitation, to a sensor assembly configured for oscillatory motion due to an external influence (e.g., force), and subject to a restorative influence. As used herein, the terms "oscillator", and "oscillating mass" refer generally, and without limitation, to an assembly configured for periodic or aperiodic displacement with respect to a reference position. 10 As used herein, the terms "top", "bottom", "side", "up", "down", "left", "right", and the like merely connote a relative position or geometry of one component to another, and in no way connote an absolute frame of reference or any required orientation. For example, a "top" portion of a component may 15 actually reside below a "bottom" portion when the component is mounted to another device (e.g., to the underside of a PCB). As used herein, the term "spring" refers generally, and without limitation, to an element configured to provide a restorative force to an oscillator or oscillating mass.

A time domain inertial sensor provides, in one salient aspect, a robust, low-cost and high resolution oscillatory apparatus (such as might be used in sensing or measurement applications), and methods of implementing and using the same. In one exemplary embodiment, the oscillatory appara- 25 tus includes a controlled oscillator coupled to a switch apparatus (having at least one first element and at least one second element, which form one (or more) closed switch states), a driving circuit, and a sensing circuit. The driving circuit provides a driving signal configured to induce the oscillatory 30 motion, which, in turn, displaces the one (or more) first switch element with respect to the one (or more) second element.

In one approach, the driving signal includes a time-gated (or "pinged") signal that is turned on and off (e.g., periodically). In another approach, the oscillator is driven in a con- 35 tinuous fashion, such as via a time varying wave function. When the first element is aligned with the second element of the switch, a trigger signal is generated by the sensing circuit, indicating a closed switch state. In one exemplary implementation, two electron tunneling electrodes (one fixed and one 40 movable) are used as the switch and the signal includes a tunneling discharge pulse caused by the close proximity of electrode tips when the electrodes are aligned in the closed switch position. By measuring the time interval between successive trigger events (indicative of the oscillator passing 45 through a reference position) the period of oscillations is determined, and thereby the external force acting upon the apparatus can be derived.

In another implementation, additional tunneling electrodes are used in order to indicate when the oscillator passes 50 through additional trigger positions. By combining time periods corresponding to the oscillator passing through successive trigger positions, the period and the amplitude of oscillator motion is estimated, hence advantageously enabling parameter (e.g., force) measurements that are independent of 55 the oscillation amplitude.

The exemplary time-domain oscillatory apparatus is configured to provide digital (time-based) output, rather than an analog signal output. Such configuration ensures that the the triggering events, the nature of the oscillation (whether harmonic, or alternatively non-harmonic), and the accuracy of the time measurement of adjacent triggered events. Since the triggering events are based on the physical dimensions established during fabrication, the proposed design advantageously does not require continuing calibration; i.e., is "self calibrating".

6

Moreover, the exemplary device also advantageously can measure parameters varying over a wide dynamic range. In one variant, such wide dynamic range capability is achieved through variation of the driving signal (and resulting in variation of the amplitude of the oscillation); greater amplitude oscillations allow for measurement of greater external influences (e.g., forces). In this fashion, a single oscillatory sensor according to the invention can be used to measure a broad range of values, thereby obviating use of multiple sensors tuned to particular (more narrow) ranges as in the prior art. Methods and apparatus for using jitter to enhance device accuracy are also disclosed.

Detailed descriptions of the various embodiments and variants of the apparatus and methods of the invention are now provided. While primarily discussed in the context of an exemplary Micro-electro mechanical sensors (MEMS) device with electron tunneling sensing tip elements, it will be appreciated that the apparatus and methodologies discussed herein are not so limited. In fact, the oscillatory apparatus and methodologies described herein (MEMS or otherwise) may be used in any number of different contexts and applications, including but not limited to: sensing of optical, magnetic, piezoelectric, thermal, capacitive, chemical, and biological parameters, and signal domain conversion. Sensing Method

One embodiment of a method of sensing is described with respect to FIG. 1. The exemplary time domain-based method of FIG. 1 is in the context of sensing a force, and relies on measuring deflection (also referred to as the bias) of a proof mass/spring-based oscillator that is being driven at a frequency  $f_{dry}$ . In one configuration, the oscillations of the oscillator are substantially harmonic. Alternatively, the oscillations may be substantially non-harmonic or (e.g., not perfect sinusoids).

As a brief aside, in classical mechanics, a harmonic oscillator is a system that, when displaced from its equilibrium position, experiences a restoring force F that is proportional to the displacement x as:

$$F=-kx$$
. (Eqn. 1)

If the restoring force is the only force acting on the oscillator system, the system is referred to as a simple harmonic oscillator, and it undergoes simple harmonic motion, characterized by sinusoidal oscillations about the equilibrium point, with constant amplitude and constant frequency f<sub>0</sub> (which does not depend on the amplitude):

$$f_0 = \frac{1}{T_0} = \frac{1}{2\pi} \sqrt{\frac{k}{m}}$$
 (Eqn. 2)

where:

k is the spring constant;

m is the oscillator mass

 $f_0$  is the oscillator resonant frequency; and

 $T_0$  is the corresponding period of oscillations.

In the method of FIG. 1 ("harmonic" variant), the driving accuracy of the device is only dependent on the consistency of 60 frequency  $f_{dry}$  is configured to match the natural resonance frequency foof the proof mass/spring-based harmonic oscillator causing a sinusoidal motion of the proof mass, as shown by the trace 102 of FIG. 1. A system driven in-resonance typically requires a high-quality factor (Q) oscillating proofmass system. It will be appreciated, however, that for this embodiment, literally any driving signal that maintains the oscillator in resonance may be used.

is detected by measuring the time periods between successive triggering points (such as the points 130, 132, 134 in FIG. 1A), as described in detail below.

8

In another embodiment (not shown), the proof mass of the oscillator is driven "off-resonance", which provides, inter alia, precise control of the oscillation period and, hence, control of sensor accuracy. Off-resonance driven systems typically require a lower Q oscillator. In the absence of any external forcing, the proof mass trajectory is centered at a reference position 104, as shown in FIG. 1. The oscillatory motion of the proof mass is measured using "triggering" events that are generated when the mass passes through trigger points corresponding to predefined physical locations. In the embodiment of FIG. 1, these locations comprise: (i) a neutral (also referred to as a zero-force) point 104; (ii) a positive trigger point 106; and (iii) a negative trigger point 108. In the embodiment of FIG. 1, the trigger positions 106, 108 are configured at the same predetermined distance d<sub>0</sub> 105 (also referred to as the trigger gap or trigger spacing) away from the reference position 104. As will be appreciated by those skilled in the art, other trigger configurations are compatible with the invention, such as, for example, asymmetric 20 and/or multiple sets of positive and or negative trigger points 106, 108. In one specific variant, a single trigger position (such as the reference position 104 for example) is utilized.

Measured timing of the triggering events 130 is used to compute the period  $T_1$  (denoted by the arrow 138), which corresponds to the forced mass crossing of the reference trigger point 104 on the upswing of the mass oscillation. The period T<sub>2</sub> (denoted by the arrow 136) is determined by subtracting the times of the successive trigger events 132, and T2 corresponds to the mass crossing of the positive trigger point 106. The period  $T_3$  (denoted by the arrow 140) is determined by subtracting the times of the successive trigger events 134, and it corresponds to the mass crossing of the reference point 108. The period T<sub>4</sub> (denoted by the arrow 142) is determined by subtracting the times of the successive trigger events 130 and corresponds to the forced mass crossing of the reference trigger point 104 on the downswing of the mass oscillation, as illustrated in FIG. 1A.

In the embodiment of FIG. 1, the harmonic oscillations of the proof mass (as shown for example by the zero-force trace 25 102 of FIG. 1) causes each of the triggering points 104, 106,108 to generate a pair of triggering events marked by the circles 110, triangles 112, and squares 114, respectively, for each full cycle of mass oscillation.

In one exemplary approach, the measured periods between successive trigger events (i.e., T<sub>1</sub> through T<sub>4</sub>) are used to obtain an estimate of the proof mass deflection d (denoted by the arrow 144 in FIG. 1A) from the reference point. The proof mass deflection d<sub>+</sub> around the oscillation maximum (as depicted by the arrow 145 in FIG. 1A) is obtained by combining the upswing reference point crossing period  $T_1$  and the positive trigger point 106 crossing period T<sub>2</sub> as follows:

Timing of the triggering events 110, 112, 114 is measured using the same reference clock, and periods between successive crossings of the respective trigger points are computed. That is, the period Tr<sub>1</sub> (denoted by the arrow 116) is determined by subtracting the times of the successive trigger events 110 (which correspond to the mass crossing of the reference trigger point 104). The period Tr<sub>2</sub> (denoted by the arrow 118) is determined by subtracting the times of the successive trigger events 112 (which correspond to the mass crossing of the positive trigger point 106). The period Tr<sub>3 40</sub> (denoted by the arrow 120) is determined by subtracting the times of the successive trigger events 114 (which correspond to the mass crossing of the reference point 108).

$$d_{+} = A_{+}\cos\frac{\pi T1}{P}, A_{+} = \frac{d_{0}}{\cos\frac{\pi T2}{P} - \cos\frac{\pi T1}{P}},$$
 (Eqn. 3)

When the proof mass is subjected to an external force  $F_{ext}$ of a frequency  $f_{ext} < f_{dry}$ , the equilibrium point of the proof 45 mass harmonic oscillations is shifted from the reference zeroforce position. That is, a low frequency forces acting on the proof mass results in a low frequency shift (also referred to as the deflection) of the equilibrium point. Because applied inertial forces impact the DC bias of the simple harmonic oscil- 50 lator, it is by definition immune to other zero-mean frequencies that may be coupled into the harmonic oscillator; that is, any high frequency oscillation centered around mean value (e.g., zero) will average to that mean value.

where:  $d_0$  is the distance between the reference trigger point 35 and the positive trigger point (the trigger gap); A<sub>+</sub> is the amplitude of the oscillations at the oscillation

P is the period of oscillations defined as  $P=T_1+T_3$ ; d+ is the proof mass deflection estimate around the oscillation maxima;  $T_1$  is the upswing reference point crossing period; and

 $T_2$  is the positive trigger point crossing period.

Similarly, the proof mass deflection d\_ around the oscillation minimum is (as depicted by the arrow 147 in FIG. 1A) obtained by combining the upswing reference point crossing period  $T_3$  and the negative trigger point crossing period  $T_4$  as follows:

 $d_{-} = A_{-0} \cos \frac{\pi T3}{P}, A_{-} = \frac{d_{0}}{\cos \frac{\pi T4}{P} - \cos \frac{\pi T3}{P}},$ (Eqn. 4)

As indicated by the trace 122 in FIG. 1A, the oscillations of 55 the proof mass in the presence of external forcing are shifted from the zero-force oscillations trajectory. As a result, the forced oscillation trace 122 is centered around a level (indicated by the line 124) that is deflected from the reference point 104.

where:  $d_0$  is the trigger gap; A\_ is the amplitude of the oscillations at the oscillation

P is the period of oscillations defined as  $P=T_1+T_3$ ;

d\_ is the proof mass deflection estimate around the oscillation minima;

T<sub>3</sub> is the downswing reference point crossing period; and  $T_4$  is the negative trigger point crossing period.

Similar to the mass motion described with respect to FIG. 1, harmonic oscillations of the proof mass in the presence of external forcing (e.g., the trace 122 in FIG. 1A) cause each of the triggering points 104-108 to generate a pair of triggering events marked by circles 130, triangles 132, and squares 134, respectively, for each full cycle of mass oscillation. The external force acts to create an offset (bias) in the oscillator, which

In one variant, two independent estimates, d<sub>+</sub> and d<sub>-</sub>, are used to provide deflection measurements twice in each cycle (which may or may not be every half cycle) of oscillations, hence improving sensor frequency response. In another variant, the independent estimates d<sub>+</sub>, d<sub>-</sub> are combined to produce an averaged deflection d thereby reducing measurement short

term error. In yet another variant, an averaging window of variable length is used to further improve measurement precision.

In the deflection estimations according to Eqns. 3 and 4, the period of oscillation P is measured every oscillation cycle and the periods  $T_1$  through  $T_4$  are defined in FIG. 1A. Note that the calculated deflection is independent of the amplitude of oscillation. In one embodiment useful for acceleration force measurements, the accelerations corresponding to the deflection derived from the Eqns. 3 and 4 are obtained as follows:

$$a_{+} = d_{0} \left(\frac{2\pi}{P}\right)^{2} \frac{\cos \frac{\pi T 1}{P}}{\cos \frac{\pi T 1}{P} - \cos \frac{\pi T 2}{P}},$$
 (Eqn. 5)

$$a_{-} = d_0 \left(\frac{2\pi}{P}\right)^2 \frac{\cos \frac{\pi T3}{P}}{\cos \frac{\pi T4}{P} - \cos \frac{\pi T3}{P}}$$
 (Eqn. 6)

The derivation of Eqns. 3 and 4 assumes that the external force is constant throughout the measurements of  $T_1$  through  $T_4$ , which places a limit on the highest frequency of the external force that can be accurately resolved using these equations. Therefore, in the case of a continuous driving signal, it is necessary to select a driving frequency  $f_{drv}$  that is higher than the maximum expected forcing frequency: i.e.  $f_{rev} < f_{drv}$ .

As is seen from Eqns. 3 and 4, the deflection estimates utilize ratios of measured period between reference events  $T_1$  through  $T_4$  and the period of forced oscillations P. Provided that all of these time intervals are obtained using the same reference clock, the final deflection (and, therefore, force) 35 estimate advantageously becomes insensitive to clock systematic errors, such as, for example, drift due to aging, temperature, or other environmental changes. The calculation method of Eqns. 3 and 4 is also insensitive to changes in resonant frequency with temperature or other environmental 40 effects.

In another embodiment of the invention, a clock jitter or variation (e.g., on the order of no more than a half clock cycle in one implementation) is purposely introduced into the reference clock such that low frequency inertial forces applied to 45 the sensor can be averaged over time. As is well known, quantization noise or error cannot be averaged; introduction of such jitter advantageously mitigates or eliminates such quantization error, thereby allowing for effective averaging (and hence increasing the accuracy of the device).

FIG. 1B illustrates one exemplary case of oscillations (harmonic in this instance) in the presence of external forcing. The trace 152 in FIG. 1B depicts the time-varying external forcing, and the trace 150 depicts the oscillator trajectory, which is a superposition of the oscillator high frequency 55 constant amplitude oscillations and the variable amplitude forcing. The traces 154, 156 depict the upper and the lower extent of the oscillator motion, respectively. Note that by selecting the proof mass driving amplitude to exceed the span between the upper and the lower trigger points 106, 108, 60 measurements of proof mass deflections due to external forcing are possible even when the deflection magnitude is smaller than the spacing between the trigger points (as depicted by the arrow 158).

FIGS. 1C and 1D illustrate proof mass deflection measure-65 ments in the presence of high frequency white additive noise according to an embodiment of the invention. The trace **160** in

10

FIG. 1C depicts exemplary input comprising a random noise signal that is superimposed on a sinusoidal input (acceleration) force signal. As previously noted, the driving force for the oscillator can be anything that keeps the device in resonance. The trace 162 shows the output of the measurement algorithm based on the change in timing between successive "triggering" events. Note that the original input force is reconstructed accurately (as indicated by the output 162) even when the input 160 has significant random variations.

In another approach, a generalized regression technique is applied to the equation of sinusoidal oscillations of a time varying amplitude A(t) and a period P. The fit equation in one exemplary implementation is defined as:

$$x_i = d + A(t)\cos\left(\frac{2\pi t_i}{P} + \varphi\right), \tag{Eqn. 7}$$

where:

d is the deflection from the reference trigger point;

A(t) is the time-varying oscillation amplitude;

P is the period of oscillations;

 $x_i$  are the positions of the oscillator at time  $t_i$ , and

 $\phi$  is a phase shift.

Equation 7 is a generic equation from which Equations 3-6 herein may be derived.

It will be appreciated by those skilled in the art that many specific "curve fitting" models, describing amplitude changes with time A(t), may be used consistent with the invention, including but not limited to exponential, trigonometric, polynomial, or any combinations thereof. These may be used to, inter alia, take into account the effects of e.g., "jerk" (rapid non-linear acceleration events) or damping of the oscillator.

Furthermore, although Equations 1-7 describe a linear harmonic oscillator, the methodology described above is extendable to non-harmonic oscillators. For example, one such non-harmonic oscillator might be governed by a non-linear equation of motion, such as:

$$Fn(k)=-kG(x)$$
. (Eqn. 8)

where:

x is the oscillator displacement; and

G(x) is a non-linear function of displacement.

Similarly to the methodology of Equations 3-4, the non-linear equation of motion (Eqn. 8) is approximated using a polynomial (or another function) and the oscillator deflection as a function of period is obtained.

FIGS. 2-2B present simulation data related to the accuracy of the time-domain acceleration force sensing illustrating one embodiment of the proof mass deflection measurement method of Eqns. 3-4. FIG. 2 presents simulated relative error as a function of acceleration computed using the time-domain acceleration measurement method of Equations 5-6 and the following model parameters of the time-domain oscillator: the trigger gap  $d_0$  of 50 nm and the driving frequency of 1000 Hz, drive amplitude of 500 nm, and clock resolution of 10 ps. The acceleration in FIG. 2 is expressed in the units of standard gravity  $g_0$ =9.8 m/s² and it ranges from  $10^{-4}$   $g_0$  to about 1  $g_0$ . The trace 200 shows the relative measurement error of  $2\times10^{-8}$  for an input signal of magnitude  $2\times10^{-4}$   $g_0$  (denoted with the arrow 202), to about  $3\times10^{-7}$  for a 1  $g_0$  input signal (or 21.5 bits) at the upper acceleration range (denoted with the arrow 214).

The error roll-off of is approximated with the following equation:

$$\Delta a \propto A \omega^2 \Delta t$$
 (Eqn. 9)

as shown by the line 206, where:

A is the oscillator amplitude;

 $\omega$  is the oscillator resonant frequency  $2\pi f_0$ ; and

 $\Delta t$  is the clock resolution.

As seen from the Eqn. 9, larger oscillation amplitude A allows measurement of larger accelerations, and hence larger force.

The resolution of the method used in FIG. 2 simulations is estimated at 25.6 bits at the lower acceleration range (denoted by the arrow 202); it ranges between 21.5 bits and 35.5 bits at higher accelerations, as denoted by the arrows 212, 214, 10 respectively. The area 216 within the triangle formed by the lines 204, 206, 210 is referred to the probability area, and denotes how closely a measured time period is an integer multiple of clock cycles. In general, the trigger condition can occur anywhere within a given clock cycle, implying that the 15 measured time period can be off by a maximum of one clock cycle. For the case where the trigger event coincides with the clock cycle, the error is limited by the ability to accurately compute the cosine function as given in Eqns 3-6. In general, any given measured time period will result in an error 20 between zero (0) and one (1) clock cycle, and will therefore lie somewhere within the triangle **216**.

FIG. 2A-1 through 2A-9 present data related to the relative error sensitivity to the oscillation amplitude A and the trigger gap  $d_0$ . The data in FIG. 2A are obtained for a fixed oscillation 25 frequency of 1000 Hz and sampling clock resolution of 10 picoseconds (ps). The lines in FIGS. 2A-1 through 2A-9 marked with the arrows 222, 224, 226, 228, 230, 232, 234, 236, and 238 respectively are computed as follows:

FIGS. 2A-1 through 2A-3 correspond to the oscillation 30 amplitude of 100 nm and the trigger gap of 50 nm, 20 nm, and 10 nm, respectively;

FIGS. 2A-4 through 2A-6 correspond to the oscillation amplitude of 200 nm, and the trigger gap of 50 nm, 20 nm, and 10 nm, respectively; and

FIGS. 2A-7 through 2A-9 correspond to the oscillation amplitude of 500 nm, and the trigger gap of 50 nm, 20 nm, and 10 nm, respectively.

As seen from the data presented in FIGS. 2A-1 through higher relative error (as, for example, illustrated by the curve 238 in FIG. 2A-9 being shifted upward relative to the curve 236 in FIG. 2A-8), while smaller oscillation amplitude corresponds to a lower relative error and lower acceleration range, (as, for example, illustrated by the curve 222 in FIG. 45 2A-1 being shifted downward and to the left relative to the curve 238 of FIG. 2A-9).

FIG. 2B presents exemplary simulation data related to the relative error sensitivity to the oscillation frequency  $f_{drv}$  and the reference clock resolution. The data in FIG. 2B are 50 obtained for a fixed trigger spacing of 50 nm and fixed oscillation amplitude of 100 nm. The different lines in FIG. 2B (marked with the arrows 242-258) are computed as follows:

the lines marked with the arrows 242, 244, 246 correspond to the oscillation frequency of 100 Hz and the clock 55 resolution of 10 ps, 1 ns, and 100 ns, respectively;

the lines marked with the arrows 248, 250, 252 correspond to the oscillation frequency of 1 kHz and the clock resolution of 10 ps, 1 ns, and 100 ns, respectively; and the lines marked with the arrows 254, 256, 258 correspond 60 to the oscillation frequency of 10 kHz and the clock resolution of 10 ps, 1 ns, and 100 ns, respectively

As seen from the data presented in FIG. 2B, higher clock resolution generally corresponds to lower relative errors (as, for example, illustrated by the curve 254 being shifted down- 65 ward relative to the curve 258), while lower oscillation frequency corresponds to lower relative errors and lower accel12

eration range, (as, for example, illustrated by the curve 252 being shifter downward and to the left relative to the curve

Using Equations 5-6, acceleration dependence on the oscillator amplitude A and period can be expressed as fol-

$$a = d_0 \left(\frac{2\pi}{P}\right)^2 \frac{\cos\frac{\pi T1}{P}}{\cos\frac{\pi T2}{P} - \cos\frac{\pi T1}{P}} \propto A\omega^2$$
 (Eqn. 10)

where:

a is the acceleration;

A is the oscillator amplitude;

P is the period of oscillations;

d<sub>0</sub> is the trigger gap;

 $\omega$  is the radial frequency of oscillations expressed as  $2\pi/P$ ;  $T_1$  is the upswing reference point crossing period; and  $T_2$  is the positive trigger point crossing period.

As seen from Equation 10, higher oscillation amplitude produces higher acceleration (for the same frequency). Lower oscillator frequency implies that a smaller force and, hence, lower acceleration is required to produce a given displacement of the oscillator. The maximum force measured by the sensor is based on the difference between the oscillator ampli-

tude and the trigger spacing. Therefore the maximum allowed acceleration range changes with the oscillator frequency, when the other model parameters are kept fixed.

It is noted that the exemplary time-domain sensing apparatus describes by Equations 3-6 and 10 advantageously provides for a dynamically adjustable measurement system. Spe-35 cifically, the sensor dynamic range (e.g., the range of measurable accelerations in Eqn. (10)) can be dynamically adjusted by changing the amplitude of the oscillator motion; e.g., by adjusting the driving signal.

It is further noted that although, the illustrated embodi-2A-9, smaller electrode spacing d<sub>0</sub> generally corresponds to a 40 ments described above with respect to FIGS. 1 and 1A use three different trigger positions (e.g., 104, 106, 108 in FIG. 1A) in order to obtain force estimates (via Eqns. 3-6), any number of known trigger points may be used consistent with the principles of the invention. For example, in one approach, a single trigger point is used, and oscillation amplitude is assumed constant and is estimated from the magnitude of the harmonic driving force  $F_{drv}$ . Provided that the oscillator has low losses (high Q-factor), such implementation is capable of providing accuracy well in excess the presently available sensors of similar size, bandwidth, and power consumption. In one implementation, a width of the amplified tunneling pulse is used to further improve accuracy of the single trigger point approach. The width of the amplified tunneling pulse serves generally the same purpose as the fixed spacing between tunneling tip pairs, thereby enabling the single tunneling tip configuration to provide measurements that are independent of the oscillation amplitude. Furthermore, various other techniques of determining the deflection of a driven proof mass (that comprise, for example, multiple sets of trigger points) may be used with the time-domain force sensing methods of the invention.

Sensing Apparatus

Referring now to FIG. 3, one embodiment of the time domain inertial force sensing apparatus of the invention is shown and described. The exemplary sensing apparatus 300 of FIG. 3 comprises a frame 302 and a cantilevered proof mass assembly 304 sealed between a base 305 and a capping

wafer 306 using, in one variant, a gold thermo-compression wafer bonding technique. As will be appreciated by those skilled in the arts, many other fabrication methods may be used, including but not limited to gold-tin eutectics or other eutectics, glass-frit bonding, fusion bonding, electrostatic 5 bonding, etc.

The frame and the proof mass each comprise an electron tunneling electrode assembly, which together form a digital switch structure 310 shown in the inset (magnified view) 313 in FIG. 3. The switch structure is in this embodiment formed 10 by one or more pairs of opposing electron tunneling electrodes, such as the reference electrode assembly 318 disposed on the frame 302 and the sensing electrode assembly 320, disposed on the proof mass assembly 304. In the absence of external forcing (zero force state), the top electrode 314 of the 15 assembly 318 is configured so as to be aligned with the top electrode 314 of the assembly 320. The bottom electrode 312 of the assembly 318 is configured so as to be aligned with the bottom electrode 312 of the assembly 320, as shown in the inset 313 in FIG. 3.

The electrodes 312, 314 comprise a layer of conductive material (such as e.g., doped polysilicon, or a thin metallization such as platinum, chromium, aluminum, tungsten, etc.) separated by an insulating layer 316 (such as e.g., silicon oxide, or silicon on insulator) disposed in-between, as shown 25 in FIG. 3. The reference electrode assembly 318 is disposed on the bulk silicon element of the silicon frame 302, and the sensing electrode assembly 320 is disposed on the bulk silicon element 328 of the proof mass assembly 304.

As will be appreciated by those skilled in the arts given the 30 present disclosure, a wide variety of other electrode assembly configurations exist which may be used consistent with the invention, including for example electrodes 312, 314 of different thickness, material, position, and/or shape. For example, atomic layer deposition may be used to form the 35 electrodes 312 and 314. In another embodiment, the electrodes 312 and 314 may be comprised of one or more layers of graphene. A source of noise in the sensing apparatus 300 is the repeatability of the tunneling event. In embodiments of the sensing apparatus 300 where the electrodes 312 and 314 40 are made of material that is several atoms thick, tunneling can occur at several points along the vertical motion of the electrodes 312 and 314—resulting in noise being added to the sensing apparatus 300. The use of graphene or other singleatom-thick conductive material layers for the electrodes 312 45 and 314 helps ensure that the tunneling event occurs consistently, thus minimizing the noise.

At the zero force position, the electrode pairs **312**, **314** are aligned horizontally and separated by a narrow gap. In the embodiment of FIG. **3**, the gap **322** is on the order of 1 50 nanometer (nm) in width. In one variant, the gap is selected to fall in the range from about 1 nm to about 50 nm. Yet other values may be substituted.

The close proximity of the electrodes within each electrode pair 312, 314 causes an electron tunneling discharge across 55 the gap. As a brief aside, electron tunneling was originally developed for use in Scanning Tunneling Microscope (STM). In the STM, a sharp metallic tip is positioned about 10 Angstroms above a metallic surface. Electron tunneling has been previously applied to inertial measurements. Tunneling based accelerometers typically comprise a fixed cantilever scanning tunneling microscope (STM), with the cantilever acting as a proof mass. Tunneling devices take advantage of the relationship between tunneling current and tip-to-surface distance in order to measure the proof mass deflection. When a DC 65 voltage bias is applied between tip and surface, a tunneling current of about 1 nano-ampere (nA) can be measured. Small

14

variations (1 Angstrom) in the tip-surface separation appear as large variations (e.g., 10-80%) in the tunneling current.

Returning now to the embodiment of FIG. 3, in order to create a tunneling switch, the tunneling electrodes of the opposing switch sides are subjected to different electric potentials. That is, the tunneling electrodes 314, 312 of the reference electrode assembly 318 are subjected to a DC potential (DC charge) that is different from the DC potential of the respective electrodes 314, 312 of the sensing electrode assembly 320. In one variant, the electrodes 312, 314 of the sensing electrode assembly 320 are grounded (zero potential), and the electrodes of the reference assembly are charged to a specific positive voltage, for example 30 V. Typically, voltage difference across the electrodes 312, 314 is less that 50 V, which is sufficient to produce a pulse of current across the gap in the range between 1 nm and 50 nm.

It is appreciated by those skilled in the art given the present disclosure that other charge configurations are compatible with the invention, such as for example: (i) grounded reference electrodes and charged sensing electrodes, or (ii) one positively charged and one negatively charged electrode, etc. Furthermore, it is noted that gap width and electrode material selection will generally affect working range of the charge voltage, with wider gaps requiring a higher difference in voltage potentials.

In one implementation, the sensor cavity (the volume between the base and the capping wafers) is at least partly evacuated, thus creating at least a partial vacuum. Vacuum reduces damping of the proof mass, thereby increasing the Q-factor of the oscillator, although this is by no means a requirement of practicing the invention. In alternate implementations, the sensor cavity may be backfilled with an inert gas such as nitrogen or argon.

The aforementioned difference in the electrode potentials forms a charged electrode tip pair. Whenever these charged tips pass through the reference position (such as, the zero force point), a high electric field region is temporarily formed between the charged tips, causing an electric discharge across the tunneling gap 322. The corresponding tunneling currents induced in the electrodes 312, 314 act as precise indicators of the electrode tip alignment, thus serving as the mechanism for measuring external forcing. The magnitude of external forcing can be estimated using a variety of methods, including but not limited to, the methods described with respect to FIGS. 1-2A. For instance, in one embodiment, the force is computed by dividing the resonant frequency period of the proof mass by the measured time between the pulses, corresponding to the zero force point.

It is noted that in the embodiment of the inertial sensing apparatus shown in FIG. 3, the tunneling effect is only used as the trigger mechanism (generating a tunneling current when the electrode pairs 312, 314 are aligned) in order to indicate when the oscillating proof mass passes through the trigger points. Other approaches may be used as well, however.

The proof mass (and therefore, the sensing electrode assembly 320) are configured to oscillate in a direction (as indicated with the arrow 311 in FIG. 3) that is substantially perpendicular to the plane of the sensor 300. The illustrated electrode configuration of FIG. 3 advantageously allows for much a wider separation between the electrode tips (1 nm vs. 1-10 Angstrom), as the device does not need to measure the actual distance between the electrode tips. A wider gap further prevents accidental tip-to-tip contact, thereby increasing robustness and longevity of the device. Moreover, such an electrode configuration does not limit electrode displacement to the Angstrom-level, thereby greatly increasing the

dynamic range (and utility) of the inertial sensing device as compared to, inter alia, prior art tunneling sensors.

Furthermore, no feedback loop closures of any kind are required for proper operation of the device. The larger surface area of the electrodes 312, 314, which is primarily due to a larger lateral extent of the conductive layers (such as, in the dimension indicated by the arrow 307 in FIG. 3), advantageously results in a larger tunneling current as compared to typical STMs; e.g., those that use a needle-type sensing electrode. Because the tunneling mechanism is used as a switch in the sensing apparatus of FIG. 3, it is also impervious to tunneling tip degradation, provided that the tunneling current remains above the noise floor of the front-end amplifier, which is  $3 \times 10^{-15}$  A in one exemplary variant.

Depending on the specific sensor application requirements of the sensing application, the forcing frequency is in the range from about 100 Hz to about 200 kHz. The corresponding maximum amplitude of the proof mass oscillations is between about 10 nm and about 50 µm. The size of the 20 exemplary sensing device 300 is selected based on various specification or operational parameters including, but not limited to, resonant frequency, thermal noise floor, sensor dynamic range, power consumption, configuration (e.g., one axis, two axes), and cost. In one embodiment, the proof mass 25 assembly is between 50 µm and 500 µm in width, and between 100 μm and 9 mm in length. The sensor frame is constructed to be sufficiently large to house the proof mass while allowing for wafer level bonding and electrical interconnects (typically requiring additional 100-500 µm around the perimeter of the 30 proof mass).

The foregoing exemplary dimensions underscore yet another advantage of the present invention; i.e., extremely high performance within a very spatially conservative form factor. This enables not only host devices to be made smaller 35 and less costly, but also the use of many sensors collectively (e.g., in an array) in a space efficient manner. Notwithstanding, it will be appreciated by those skilled in the arts that the above dimensions are merely exemplary, and the sensing device could be made larger or smaller as required by the 40 application or other considerations.

Referring now to FIG. 3A, one embodiment of the electrode trigger configuration of the sensing apparatus 300 of FIG. 3 is shown and described. As discussed with respect to FIG. 3, the force sensing apparatus comprises: (i) an oscillator (the proof mass assembly 304) and (ii) the dual-tip switch 310, formed by the dual-tip reference electrode assembly 318 (disposed on the frame 302) and the dual-tip sensing electrode assembly 320 (disposed on the proof mass assembly).

Switch assemblies of the type described herein can be 50 positioned within the force sensing apparatus in a variety of configurations. The sensor 300 comprises a single dual-tip switch 310 (comprised of the electrode pairs 312, 314) disposed along a transverse edge of the proof mass that is opposite from the mass attachment point 333 to the frame, as 55 shown in greater detail in FIG. 3B-1. Such switch placement advantageously maximizes the displacement of the sensing electrode assembly 320 during operation.

In other embodiments, the sensing apparatus 336, 338, 339 comprise multiple sets of switches 310, disposed in various 60 configurations as shown in FIGS. 3B-1 and 3B-2. In one such alternate embodiment, the force sensor 339 comprises an arrays of switches disposed along the perimeter of the proof mass cantilever 304. Each switch within the array can be composed of multiple tunneling tips stacked on one another 65 and separated by a dielectric of spacing  $d_0$ , as shown in the sensor embodiment 346 of FIG. 3C.

16

FIG. 3C provides cross-sectional views of various different embodiments of switches useful with the time-domain oscillatory apparatus of the invention. The illustrated switch 347 of the first illustrated oscillatory apparatus 346 comprises three layers of tunneling electrodes (the top 314, the middle 315 and the bottom 312), spaced by the same distance.

In yet other embodiments, the oscillatory apparatus 350 comprises a switch 348 with different electrode spacing 347 between the electrodes 312, 314 of the reference electrode assembly (which is mounted on the sensor frame), as compared to the spacing 349 of the sensing electrode assembly (which is mounted on the cantilevered proof mass assembly). In one such implementation, the oscillatory apparatus 356 comprises a switch 353 that uses two reference electrodes and a single sensing electrode. In another such implementation, the apparatus 358 comprises a switch 357 that a single reference electrode and a single sensing electrode, as illustrated in FIG. 3C.

Some of the switch array embodiments shown in FIG. 3B (e.g., the sensors 300, 336, 338, 339) comprise a cantilevered proof mass assembly 304. In another approach, the sensors 340, 342, 344, 345 comprise a proof mass structure 351 that suspended using spring supports 354. As shown in FIG. 3B, the supports 354 can be arranged in a variety of configurations around the perimeter of the oscillating structure 355. FIG. 3C depicts a cross sectional view of the sensor apparatus 352 comprising a proof mass 351 that is suspended via spring support elements 354. Yet other mechanisms or approaches to creating an oscillator (proof-mass based or otherwise) will be appreciated by those of ordinary skill given the present disclosure.

Although only a single set of electrodes is required for operation of the force sensing apparatus (e.g., the apparatus 330 of FIG. 3A), additional electrode sets offer redundancy, thereby increasing sensor resolution, accuracy, and precision by providing additional data and improving sensor reliability. Furthermore, given the very small size of the tunneling tips (1 nm to 50 nm in thickness, and 100 nm to 10 µm in width in one exemplary embodiment), tens or hundreds of tunneling tips per oscillator can easily be fabricated. It will be appreciated by those skilled in the art when provided this disclosure that various other switch configurations may be used, including for instance using switch sets that have different vertical spacing between the electrodes. The additional information provided by these additional sets of tips and/or configurations aids in extending the dynamic range, and to decrease digitization errors, of the force sensing apparatus.

Returning now to FIG. 3A, in the absence of external forcing, the electrode pairs 312, 314 are configured in an aligned position, and form two tunneling trigger junctions 322. Such configuration is referred to as the reference or a zero-force point 330, and it corresponds to the reference trigger point 104 described with respect to FIGS. 1 and 1A.

The proof mass assembly 304 is driven by an oscillating signal, as described in greater detail below, which causes the proof mass to undergo harmonic oscillations relative the reference point 330. When the proof mass 304 is displaced downward from the reference position 330 by the distance  $d_0$  (which corresponds to the vertical spacing 331 between the electrodes 312 and 314), the top electrode 314 of the sensing assembly 320 is aligned with the bottom electrode 312 of the reference assembly 318, thus forming a single tunneling trigger junction 326. Such configuration is referred to as the first known calibration point 332, and it corresponds to the negative trigger point 108 described with respect to FIGS. 1 and  $1\Delta$ 

Similarly, when the proof mass 304 is displaced upward from the reference position 330 by the distance  $d_0$ , the bottom electrode 312 of the sensing assembly 320 is aligned with the top electrode 314 of the reference assembly, thus forming a single tunneling trigger junction 324. Such configuration is referred to as the second known calibration point 328, and it corresponds to the positive trigger point 106 described with respect to FIGS. 1 and 1A. As the proof mass oscillates, the electrodes 312, 314 pass through the three trigger configurations 328, 330,332, thereby causing generation of the triggering events, such as e.g., the trigger events 130, 133,134 described with respect to FIG. 1A.

FIG. 3D shows a cross-sectional view of another embodiment of the time-domain sensing apparatus according to the invention. The sensor 360 of FIG. 3D comprises the frame 302 and a cantilevered proof mass assembly 304. The proof mass assembly comprises a beam structure 328 affixed to the frame element 302\_1 on one end, and a proof mass 378 disposed on the opposing end of the beam 328. The frame 302 20 and the proof mass assembly 304 are sealed between the base wafer 305 and the capping wafer 306 using the intermediate structures 372. It will be appreciated that while a cantilevertype approach is used to "suspend" the proof mass and sustain oscillations thereof in the illustrated embodiment, any num- 25 ber of different approaches or mechanisms can be substituted to provide the desired oscillatory functionality, the cantilever being only one possibility. For example, a proof mass assembly that is suspended using spring supports may be used as well, as described with respect to FIG. 3B and FIG. 3C.

In one variant, the beam 328 is fabricated using conductive material and is electrically connected to the sensor ground pad 382 via a conductive element 380 (that penetrates through the capping wafer 306) and the gold composite bonding layer 372\_2. The beam 328 is electrically isolated from the proof mass 378 and the frame element 302\_1 by a nonconductive layer 376\_2. The conductive beam 328 acts as the proof mass ground plane, and it serves two functions: (i) providing ground to effect the proof mass oscillations; and (ii) providing ground potential for the tunneling discharge.

In another variant, a conductive element 370 is disposed on the top surface of the beam 328. The conductive element 370 is electrically connected to the sensor ground pad 382 via a conductive element 380 (that penetrates through the capping 45 wafer 306) and the gold composite bonding layer 372\_2. In this variant, the insulating layer 376\_2 may be omitted.

The sensing apparatus 360 comprises a digital switch assembly 310 that is disposed proximate the oscillating end of the proof mass assembly 304 as shown in FIG. 3D. The switch 50 310 comprises the sensing electrode assembly 320 and the reference electrode assembly 318, as is described in detail with respect to FIGS. 3-3A. The electrode 312, 314 of the sensing electrode assembly 320 is electrically connected to the proof mass ground plane via conductors 383. The bottom 55 electrode 312 of the reference electrode assembly 318 is electrically connected to the conductive element 390 which, in turn, is connected to the first sensor charge pad 386 via a conductive element 388 (that penetrates through the capping wafer 306) and the gold composite bonding layer 372\_4. The 60 top electrode 314 of the reference electrode assembly 318 is electrically connected to the second sensor charge pad 387 via the conductor 389 (that penetrates through the capping wafer 306) and the conductor portion 389 1. The top and the bottom electrodes 312, 314 are separated by a nonconductive layer 65 316. A nonconductive layer 376 is used to insulate the reference electrode assembly from the sensor frame 302. The

18

charge pads 386, 387 and the ground pad 382 are used to provide the charge voltage and to sense the tunneling current during sensor operations.

The sensor 360 comprises the top 362 and the bottom 363 driving electrodes that are connected to the sensor drive pads 364, 365 via conductive elements 366 that penetrate through the base and the capping wafers, as is shown in FIG. 3D. The driving electrodes in the illustrated embodiment are driven with a harmonic driving signal of  $f_{drv}$  such that the signal applied to the electrode 362 is 90° out of phase from the driving signal applied to the electrode 363, as described in detail elsewhere herein. Because the proof mass is grounded, the capacitive coupling between the ground plane 370 and the electrodes 362, 363 creates electrostatic attractive forces which force the proof mass of the sensor 360 into periodic oscillation at the driving frequency  $f_{drv}$ .

In an alternate embodiment shown in FIG. 3E, only one driving electrode (the top electrode 362) is used for induce oscillations of the proof mass. The sensor 361 comprises the capping wafer and an integral frame/base wafer assembly 302\_1. Although the top driving electrode 362 is shown in FIG. 3E, a bottom mounted driving electrode (e.g., 363, not shown) may be used instead in the single-electrode sensor configuration.

Referring now to FIGS. 3F through 31, various alternate embodiments of the time-domain oscillatory apparatus of the invention are presented. The apparatus 367 shown in FIG. 3F comprises a floating proof mass 351 that is suspended within the frame 302 via spring supports (not shown) and two sets of switches (such as the dual-tip switches 310).

The apparatus 369 shown in FIG. 3G, comprises a dual cantilever proof mass assembly 371 (depicted by the dashed rectangle) comprising the proof mass 378 (that is 'sandwiched' between the two cantilevers 328), and two sets of switches 310.

The apparatus 373 shown in FIG. 3H comprises a floating proof mass 351 that is suspended within the frame 302 via spring supports 354, and multiple sets of switches (such as the dual-tip switches 310).

FIG. 3I illustrates different exemplary embodiments of electrode tips useful with the invention. While the electrode tips of the embodiments of FIGS. 3-3H are shown as having a right prism shape (such as tips 375 in FIG. 3I), the tips can be formed in a variety of shapes that are selected based on the application requirements. Generally, narrowing tips (such as triangular, conical or a trapezoidal) reduce the tip extent proximate to the tunneling gap. Triangular-shaped electrode tips 374 reduce tip vertical extent (that is in the direction of the oscillator motion as referenced by the arrow 311 in FIG. 3I). Such configurations therefore reduce the vertical extent over which the tunneling discharge can occur, thereby increasing repeatability of the proof mass position measurements.

In a different embodiment (denoted by the arrow 377 in FIG. 31), the electrode tips comprise lateral triangular shapes in a direction that is perpendicular to the direction of motion (such as the direction indicated by the arrow 307 in FIG. 3). The lateral triangle tip 377, while still having the same thickness as the rectangular shaped tip 375, reduces the tunneling discharge area, and, therefore, probability that the tunneling location will change. Overall, narrowing tips (such as the triangular-shaped tips 374, 377), whether defined laterally or vertically, tend to aid in localizing the tunneling location.

The triangular shaped tips, however, may in certain cases limit the maximum tunneling current, because the tunneling is confined to a smaller surface area. One approach to increase tunneling current is to extend the tip dimension in a direction that is perpendicular to the direction of motion (that is, along

the dimension indicated by the arrow 307 in FIG. 3). Additionally, higher DC bias voltage and/or higher sensitivity amplifiers may be used to compensate for the reduced surface area of the triangular or similarly shaped tips. While rectangular-shaped tips support larger tunneling current (for the same transverse tip dimension), the tunneling in the rectangular tip can occur at any point across the vertical extent (the height) of the tip. This is potentially undesirable, because the point of tunneling may change with time or other parameters, which may change the stability or accuracy of the switch.

FIGS. 3J and 3K are perspective views of another embodiment of the oscillation apparatus 300. The relationship between the proof mass 304, the frame 302 and the position switch 310 for one embodiment of the oscillation apparatus 1500 is highlighted in these figures.

Referring now to FIG. 4, a functional block diagram of one embodiment of an oscillator and electrode system 400 for use with the time domain inertial sensing apparatus (such as the apparatus 300 or 340) is shown. The system 400 comprises 20 two sets of dual-tip switches (such as, for example, the switch 310 of FIG. 3A). Although only a single set of switches is required for operation of the system 400, additional switches offer, inter alia, redundancy, thereby increasing sensor precision by providing additional data and improving sensor reliability, as previously described with respect to FIG. 3B.

Each dual-tip switch 410 comprises the reference dual-tip electrode assembly 418 disposed on the frame 402, and the sensing dual-tip electrode assembly 420 disposed on the proof mass assembly 404. Each switch assembly 418, 420 30 comprises a pair of electrodes 412, 414 that are separated by a layer of insulating material 416.

The proof mass assembly **404** comprises two conductive layers **406**, **471** (that, similarly to the conductive element **370** shown in FIG. **3**D, act as ground planes) disposed on the top 35 and the bottom sides of the proof mass silicon element **428**. In another embodiment (not shown), the silicon element **428** is conductive and acts as the ground plane. In a different embodiment (shown in FIG. **4**B, below), a single conductive layer **470** is used as the ground plane. The electrodes **412**, **414** 40 of each sensing electrode assembly **420** are electrically connected to the top ground plane **406**, which is connected to the sensor ground **482**. A voltage potential is applied to each of the top **414** and the bottom electrodes **412** of the reference electrode assemblies **320** from a DC source **421**.

A pair of conductive plates 462, 463 is disposed on the sensor base and the capping wafers (not shown), respectively, of the apparatus 400. The plates 462, 463 act as the driving electrodes. During operation of the system 400, a sinusoidal (harmonic) driving signal of frequency  $f_{drv}$ , is generated by 50 the driving circuit 430, and is supplied to the driving plates 462, 463. In the embodiment of FIG. 4, the driving signal that is applied to the plate 463 is shifted by 90° by the phase shift circuit 432, such that the signal that is driving to the bottom plate 463 is 90° out of phase from the signal driving the top 55 plate 462, although other phase shifts/relationships (including time-variant ones) may be used. In one variant, the driving frequency is selected to match the proof mass resonant frequency thereby allowing for a reduced driving duty cycle and reduced power draw of the sensor. In another variant, the 60 proof mass is driven with an off-resonance driving frequency, where  $f_{dry} \neq f_0$ . In yet another variant, the duty cycle and/or the driving frequency is used to dynamically adjust the device (e.g., sensor 400, 470) dynamic range, thereby producing a device (e.g., sensor) with an expanded and selectively tunable 65 dynamic range. Depending on the specific sensor requirements, the driving frequency is in the range from about 100

20

Hz to about 200 kHz. The corresponding maximum amplitude of the proof mass oscillations is between 10 nm and about 50 µm

In another embodiment, (not shown) the oscillation of the proof mass are caused by using a stepped electrostatic force to initiate harmonic oscillation. The electrostatic force is short in duration compared to the resonant frequency of the oscillator thus providing a "pushing" reinforcement that keeps the oscillator in resonance. This force is periodically repeated as necessary to ensure that the amplitude of the oscillator stays above a minimum value at which point another electrostatic pulse or "ping" is applied.

For every cycle of the proof mass oscillation, whenever the electrodes 412, 414 are in any of the three aligned configurations (such as, for example, the configurations 328-332 described with respect to FIG. 3A), tunneling discharge currents (indicated by the arrows 415, 417) are induced across the gaps 423 in one or both electrode pairs. These discharge currents generated by the top and/or the bottom electrodes induce brief current pulses, which are sensed and amplified by the low-noise current amplifiers 422, 424, respectively, as shown and described in further detail with respect to FIG. 4A, below

The width of the tunneling discharge pulse can be of very short duration due to the exponential behavior of the quantum tunneling effect given by Eqn. 11:

$$I=KUe^{-\beta d}$$
 (Eqn. 11)

where:

I is output current;

U is the applied tunneling bias voltage;

d is the tunneling gap width;

K is a constant describing density of available states both source and destination; and)

 $\beta$  is a constant describing the electron work function or the energy that is required to free an electron to vacuum potential.

This very short impulse helps to precisely pinpoint the exact moment in time the oscillating mass passes the reference location, which underscores a salient benefit of the present invention (i.e., the ability to accurately pinpoint the position of the oscillating element as a function of time).

As shown in FIG. 4A, the tunneling discharge pulses 452-456 are generated when the proof mass electrode assembly is 45 at the following positions with respect to the reference electrode:  $-d_0$ ,  $+d_0$ , and at the zero force point (points 328-332, respectively, in FIGS. 3A and 4A). As the pulses 452-456 may differ in amplitude due to, for example, variations in applied tunneling voltage (voltage noise) and/or tunneling distance, the low noise current amplifiers 422, 424 are used to amplify the discharge pulses 452-456 to the rail (that is the maximum current level value of the sensing circuit) so as to produce the amplified pulses 458-462, which exhibit substantially rectangular shapes. Although the amplitude information is lost, the amplified square pulses 458-462 are advantageously well suited for interfacing with digital circuits, such as for example the control logic 434 and the counter 436 in FIG. 4, and/or yet other more sophisticated devices such as digital signal processors.

Furthermore, provided that the amplifier (such as the amplifier 422, 424) is characterized by a constant time delay (which may include zero time delay), the relative timing of the amplified pulses (such as the pulses 458-462 in FIG. 4A) is preserved. The counter 436 is toggled on/off upon detecting the leading edge of the amplified pulse using, in one variant, a comparator circuit, although other solutions will readily be recognized by those of ordinary skill given the present dis-

closure. When the counter **436** is toggled on, it starts a counting sequence, which continues until the next input pulse is received and the counter is read and/or toggled off. During the "on" state, the counter counts timing pulses provided by a reference clock signal generated by a reference timing unit 5 (TU) **438**. The output of the counter is available on channel **440** for use by an external interface, in one implementation of the system **400**.

In the embodiment of FIG. 4, a bipolar driving mechanism is used in order to induce harmonic oscillations of the proof mass. Such configuration allows for more flexible control of driving voltages, as well as reduces the impact of charge buildup on the oscillator. To further reduce the charge build up, the proof mass ground layer 406 is electrically connected to the sensor ground 482.

In another embodiment, shown in FIG. 4B, the sensor system 470 comprises a unipolar driving circuit. That is, one of the driving electrodes (the plates 463) is connected to the ground 465 while the other driving electrode (the plate 462) is driven with the sinusoidal driving signal. The configuration 20 shown in FIG. 4B, simplifies the sensor driving circuit.

Electrically driven oscillators used in the force sensing systems 400, 470 (FIGS. 4, 4B respectively) almost inevitably generate unwanted electromagnetic radiation during operation, due to, for example, noise in the voltage supply, 25 digital pulses being generated by various components (such as the controller 430), etc. In order to prevent coupling of electrical noise into the tunneling current (and hence force) measurements, a pulsed driving mechanism is used.

The proof mass (PM) controller 430 of the force sensing 30 system 400, 470 briefly turns on and off the sinusoidal drive signal thus creating a pulsed train, where each N cycles of sinusoidal oscillations are separated by M cycles of no driving. When the drive signal is briefly turned on, the proof mass oscillations are reinforced. The duty cycle of the drive signal 35 (determined as N/(N+M)) is selected based on the sensor specific design parameters (such as the oscillator damping), and is typically in the range from 0.001 to 0.1. The low damping characteristics of the proof mass oscillator ensure that the oscillation amplitude does not decrease substantially 40 between the driving pulsed events. Furthermore, the use of three triggering points (such as the points 104, 106,108 in FIG. 1A) enable accurate measurements of the proof mass deflection regardless of the oscillation amplitude (provided that the amplitude of oscillations is kept above trigger point 45 106 and below trigger point 108), which is readily attainable with the driving duty cycle of 1 very short pulse every 10-1000 oscillator cycles. Ideally the pulse is an impulse so the narrower the better. The more often we pulse the larger we drive the amplitude of the oscillator. The oscillator position 50 measurements are performed by the force sensor systems 400, 470 when the driving signal to the oscillator is turned off, and therefore no noise is coupled from the electrical drive circuitry to the position sensing circuit of the sensor apparatus. The driver configurations (such as shown and described 55 with respect to FIG. 4 and FIG. 4B) ensure that no feedback force need be applied to the proof mass assembly during the actual measurement of external force.

As those skilled in the art will recognize, the above-described exemplary driving and sensing configurations are 60 provided herein merely to illustrate the broader principles of the invention. Various other sensor driving configurations may be used, such as manually excitation of the resonance by mechanically "pinging", or driving the oscillator with a sinusoidal mechanical driving force. In the case of an electric 65 oscillator system, negative feedback is used to keep the oscillator operational.

22

In the embodiments of FIGS. 4 and 4B, the control logic 434 is configured to differentiate between the incoming tunneling pulses based on whether the incoming pulse arrives on the top, the bottom, or both amplifier channels 422, 424, thus corresponding to the proof mass positions 328-332 of FIG. 3A, respectively. In one variant, the control logic detects incoming pulses using a comparator. FIG. 4C and Table 1 illustrate an exemplary sequence of the tunneling pulse generation, comprising one complete cycle of the proof mass oscillation. The white circles 452 in FIG. 4C on the oscillation profile indicate the tip positions where a conducting path is established for current flow (i.e., the comparator output is a logical "1"). The shaded circles 454 correspond to positions where there is no conducting current (i.e., the comparator output is a logical "0").

When the proof mass is in the zero force position 330 (denoted with the designators 1, 7, 13), both electrodes of the electrode assemblies 418 and 420 are aligned, hence causing current pulses on both amplifier channels 422, 424 as indicated by numeral 1 in columns labeled  $I_T$  and  $I_B$ , respectively, in Table 1. When the proof mass is in the negative displacement position 332 (denoted with the designators 3, 5), the bottom electrode 412 of the switch 410 reference electrode assembly 418 causes the current pulse on the bottom amplifier channel 424, as indicated by numeral 1 in columns labeled I<sub>B</sub>, in Table 1 below. Similarly, when the proof mass is in the positive displacement position 328 (denoted with the designators 9, 11), the top electrode 412 of the switch 410 reference electrode assembly 418 causes the current pulse on the top amplifier channel 422, as indicated by numeral 1 in columns labeled  $I_T$ , in Table 1. When the proof mass in the positions denoted with the designators 2, 4, 6, 8, 10, and 12, no current pulses are generated by the electrodes 412, 414.

TABLE 1

Proof mass position in FIG. 4C	Proof mass position in FIG. 3A	Triggering Event of FIG. 1	I <sub>T</sub> channel 422	I <sub>B</sub> channel 424
1	330	110	1	1
2	222	114	0	0
3 4	332	114	0	0
5	332	114	Ö	1
6			0	0
7	330	110	1	1
8	228	112	0	0
10	328	112	0	0
11	328	112	1	0
12			0	0
13	330	110	1	1

The proof mass positions 5, 7, 9 correspond to the triggering events 114, 110, 112, respectively, described with respect to FIGS. 1-1A. Whenever triggering events 110, 112,114 occur (that is, whenever pulses 452-456 toggle the counter 434), the counter begins counting pulses of the reference clock signal.

As shown in FIG. 4A, the periods  $T_1$ - $T_4$  are computed as follows:

- T<sub>1</sub> is the counter value at the second reference trigger point event (proof mass position 7) minus the counter value at the first reference trigger point event (proof mass position 1):
- T<sub>2</sub> is the counter value at the second negative trigger point event (proof mass position 5) minus the counter value at the first negative point trigger event (proof mass position 3):

T<sub>3</sub> is the counter value at the second positive trigger point event (proof mass position 11) minus the counter value at the first positive point trigger event (proof mass position 9); and

T<sub>4</sub> is the counter value at the third reference trigger point 5 event (proof mass position 13) minus the counter value at the second reference point trigger event (proof mass position 7).

As seen from FIG. 4C and Eqns. 3 and 4 above, the dual tip switch (such as the switch 410 of FIG. 4, comprising 4 electrodes) provides three predetermined trigger points (110, 112, 114), thus enabling the sensing system 400 to obtain two estimates of the oscillator deflection (and hence the force) every period (or twice per cycle). Such switch configuration can be used to increase sensor system frequency response, or 15 to improve sensor system precision by averaging successive measurements and reducing measurement uncertainly. A switch comprising two trigger points (such as, for example, the three electrode switch 348 of FIG. 3C) enables one measurement of the oscillator deflection every period. Both above 20 measurement configurations (e.g., using switches 310, 348) are advantageously insensitive to the oscillator amplitude.

Assuming that the oscillator amplitude is known (by for example using a factory calibration table relating oscillator displacement to the supplied drive voltage), a switch com- 25 prising a single electrode pair may be used to estimate oscillator deflection. While this approach relies on the accurate knowledge the proof mass amplitude, under most practical conditions it provides measurement performance that is well in excess of the presently available sensor implementations. 30 Furthermore, similarly to the dual electrode switch configuration (e.g., the switch 410 in FIG. 4, the single electrode pair sensor utilizes the width 464 (that is the time between the leading edge and the falling edge, as shown in FIG. 4A) of the amplified pulses 458-462, in combination with the electrode 35 thickness, thus obtaining additional timing information required to obtain oscillator displacement measurements independently from the oscillation amplitude. In this instance, the pulse width is serving effectively the same purpose as the electrode spacing  $d_0$  of the dual-electrode switch 40 embodiment shown, for example, in FIGS. 3, 3A, 3D. That is, it provides a fixed distance between two events that are used to toggle a counter on/off.

In one embodiment of the system, four separate counters are used to measure the periods  $T_1$  through  $T_4$ , as shown and 45 described with respect to FIG. 5. The time-domain inertial sensor control block 500 comprises a programmable logic apparatus 502 (depicted by a polygon filled with a dotted pattern in FIG. 5) such as field programmable gate array FPGA, programmable logic device (PLD), microcontroller, 50 or any other computerized apparatus configured to execute machine readable code. In one variant, the control logic is implemented within an FPGA that supports an embedded microprocessor or digital processor 504. The apparatus 502 comprises a drive sub-block 510, a sensing sub-block 530, 55 and a reference clock 512. The drive sub-block 510 comprises a delay lock loop/phase lock loop (DLL/PLL) module 514 configured to generate a drive clock signal 516. The direct digital synthesizer/power supply (DDS/PS) module 518 generates drive waveforms (such as the waveform 202 in FIG. 2), 60 which are amplified by the amplifier 520. The amplifier 520 provides the harmonic oscillation signal 522 to the driving electrodes (such as the electrodes 462, 463 of FIG. 4).

As described with respect to FIG. 4A discussed, in order to minimize potential noise cross-coupling from the driving signal into tunneling current measurements, the driving sinusoidal signal 522 is pulsed—that is, briefly turned on and off.

24

When the signal 522 is briefly turned on, the proof mass is oscillations are reinforced. The drive pulsing is controlled by the control logic module 504 via the control signal path 524 in this embodiment. The waveform generation by the DDS/PS module 518 is controlled by the control logic module 504 via the path 526. The gain control module 528 controls the amplifier gain in order to adjust the amplitude of the oscillator.

The sensing sub-block 530 is configured to determine positions of the oscillating proof mass. The sensing sub-block 530 comprises the comparator bank 532 coupled to the output channels 534, 536 of the top 422 and the bottom 424 current amplifiers. The logic states of the comparator 532 are fed to the counter finite state machine (FSM) 538, the latter which controls operation of four period counters 542-548, corresponding to the periods  $T_1$  through  $T_4$ , respectively, of FIGS. 1A and 4C. The counter outputs are coupled to the four registers 552-558, configured to store period duration counts T<sub>1</sub> through T<sub>4</sub>, respectively. Without any external force acting on the proof mass, the mass oscillates with a zero deflection bias. When there is external force acting on the proof mass. the oscillating trajectory of the mass changes due to a nonzero deflection bias (as illustrated in FIG. 1A). The sensing sub-block is configured to detect the proof mass deflection using different trigger point events (such as the events 110-112 in FIG. 1), and determine the force using Eqns. 3-6 described above.

As described above with respect to FIG. 4A, the comparators of the comparator bank 532 are used to detect the presence of the tunneling current pulses. The truth table for the relationship of the comparator 532 logic states to the tunneling electrode tip positions is given in Table 1. Note that the numeral '1' denotes tunneling current being generated, and numeral '0' corresponds to no current.

An exemplary counting sequence, corresponding to the mass oscillation depicted in FIG. 4A and used in the exemplary force sensor of the embodiment shown in FIG. 5 is presented in FIG. 6. The comparator bank 532 detects current pulses 630 on both channels 534, 536, corresponding to the reference trigger position of the proof mass (point 1 in FIG. 4C). At this instant, the counter state machine 538 starts the counter 542 by setting the enable signal EN1 high (edge 612) on channel 600. When the tunneling current pulse 632 is received on the bottom channel 536 by the comparator bank 532 corresponding to the negative trigger point event (for example, the proof mass position 3 in FIG. 4A), the counter 544 is started by setting the enable signal EN2 high (edge 614) on channel 602. When the next negative trigger point event is detected by the comparator 532 (i.e., the pulse 634 is received on channel 536), for example corresponding to the proof mass position 5 in FIG. 4A), the enable signal 602 is set low (edge 616) and the counter 544 is stopped. The content of the counter 544 (corresponding to the period  $T_2$ ) is then stored in the register 554, and the counter 544 is reset.

When the second reference point trigger event is detected by the comparator bank by sensing the current pulses 636 on both channels 534, 536, (for example, the event corresponding to the proof mass position 7 in FIG. 4A), the counter 542 is stopped by setting the EN1 signal 600 low (edge 618) and the counter 546 is started by setting the EN3 signal 604 high (edge 620). The content of the counter 542 (corresponding to the period  $T_1$ ) is stored in the register 552, and the counter 542 is reset.

When the tunneling current pulse 638 is received on the top channel 534 by the comparator 532 (corresponding to the positive trigger event, for example corresponding to the proof mass position 9 in FIG. 4A), the counter 548 is started by setting the EN4 signal 606 high (edge 622).

When the next positive trigger point event is detected by the comparator 532 receiving the pulse 640 on channel 534, (for example, corresponding to the proof mass position 11 in FIG. 4A), the counter 548 is stopped by setting the EN4 signal 606 low (edge 624), the content of the counter 548 (corresponding to the period  $T_4$ ) is stored in the register 558, and the counter 548 is reset.

When the next reference trigger point event is detected when the comparator receives current pulses 642 on both channels 534, 536 (for example the event corresponding to 10 the proof mass position 13 in FIG. 4A), the counter 546 is stopped by setting the EN3 signal 604 low (edge 626), the content of the counter (corresponding to the period T<sub>3</sub>) is stored in the register 556, and the counter 546 is reset. If the next counting sequence is scheduled to commence, the 15 counter 542 is started. The timing operation of the system 500 is controlled by the clock 516 and reset signal 508 is used to initiate (or reset) the counting sequence of FIG. 6.

In another embodiment (not shown), a single counter instance (for example, the counter 542) is used for all of the 20 counting operations, and is combined with several registers that serve as memory buffers. In this implementation, by way of example, the counting sequence begins with the receipt of the reference trigger point event by the counter 542. When the first negative trigger event is received (for example corre- 25 sponding to the proof mass position 3 in FIG. 4A), the current value of the sequence count is stored in the negative trigger event\_start register. When the second negative trigger event is received (for example the event corresponding to the proof mass position 5 in FIG. 4A), the current value of the counter 30 542 sequence count is stored in the negative trigger event end register. When the second zero reference level trigger event is received (for example corresponding to the proof mass position 7 in FIG. 4A), the current value of the sequence count is stored in the reference trigger event\_end register. Similarly, 35 the counter sequence values corresponding to the proof mass positions 9, 11 are stored in the respective registers. Other variations are possible, such as stopping and starting the counting sequence for each incoming pulse.

Referring now to FIG. **6** a timing diagram illustrating an 40 exemplary operational sequence for the time-domain force sensing system of FIG. **5** is shown. The accuracy of the force measurements produced by the sensing system **400**, or **470** is largely determined by accuracy of the clock rate. The more accurately that the periods  $T_1$  through  $T_4$  are resolved, the 45 more accurately the deflection d, and, therefore, the quasistatic force acting on the harmonic oscillator, are determined.

Because the periods  $T_1$  through  $T_4$  are measured using a digital counter which keeps track of the clock cycles between the trigger events, the accuracy, stability and precision of the 50 sensor are substantially dependent upon the input clock rate to the counter, and the long-term stability of the clock source. By an analogy with other digital sensing devices, the sensor system 400 resolution and dynamic range may be described by a number of bits which is related to the total number of the 55 effective clock cycles contained within one period of the harmonic oscillator.

Some trigger events may occur between clock cycles, thereby potentially impacting precision of the measured time periods. These timing errors may result in a quantization 60 noise which limits the resolution and precision of the sensor, but not the stability or accuracy. Several techniques may be used consistent with the invention in order to improve resolution of the sensor. In one approach, time quantization noise is reduced through the use of Vernier interpolators of the type 65 known in the art. In another approach, dithering techniques are applied that introduce an intentional jitter into the refer-

ence clock (e.g., on the order of a half clock cycle) such that low frequency inertial forces applied to the sensor can be averaged over time. Given that the periods  $T_1$  through  $T_4$  are computed using differences between successive counter values, as described with respect to FIG. 4C, the absolute accuracy (drift) of the reference clock is cancelled, hence making the sensing apparatus of the embodiment of FIG. 4 less susceptible to long term clock drift errors.

26

Bias instability, on the other hand, is ultimately determined by the instability of the clock source. This is true because any other mechanical instability can be accounted for based on the fact that a harmonic oscillator will always have a zero mean in the absence of an applied external force. Electrical drift, due to e.g., charging of the proof mass, can be eliminated or at least significantly mitigated by alternating positive and negative "pings" to the oscillator, thus providing a net zero charge. In addition, any measurement of the position can be performed during a period when there is no applied electrical force.

Sensing Apparatus Calibration

A dual set of tunneling tips (such as, for example, the electrodes 314, 312 of the electrode assemblies 318, 320 in FIG. 3A), separated by a predefined physical gap, d<sub>0</sub>, provides a convenient configuration for in situ calibration of the inertial sensing apparatus (such as for, example, the apparatus 300 in FIG. 3). In this case,  $d_0$  is the physical spacing between the tunneling tips, and is precisely defined during the fabrication process. The final measurement of the electrode spacing is performed during device factory calibration. The spacing  $d_0$  advantageously does not change over time, since it is based on a physical device configuration (layer deposition), and not on dynamic properties of the oscillator. Thus, the calibration is effectively "built-in" into the operation of the sensor, and no subsequent calibration need be performed. All parameters required to measure acceleration are either fixed (e.g. d<sub>0</sub>), or are measured every oscillation period (e.g., T<sub>1</sub> through T<sub>4</sub> and P). Therefore, there are no parameters that can drift, and there is no need for recalibration. The parameters that could drift are measured every period. This is yet another salient advantage over the prior art provided by the present invention.

The time-domain oscillatory (TDO) apparatus and methods described herein advantageously provide a digital time-based output, compared to analog signal output typically provided by prior art MEMS devices. The accuracy of TDO devices of the invention is, therefore, dependent only on the consistency of the trigger events, the oscillation properties (e.g., harmonic oscillation of the proof mass), and timing measurement accuracy of the trigger events. Since the time separation between the triggering events is based on the physical dimensions established during fabrication, the sensing apparatus of the embodiments of the invention does not require continuing calibration, as discussed above.

Furthermore, the sensing employed by the various exemplary embodiments described herein is based on non-contact triggering events, which are generated without any physical contact between the oscillator and the sensor frame. This approach advantageously reduces oscillator damping and wear, increases sensor longevity and long-term accuracy, and reduces power consumption (as the oscillator may be driven with lower power due to reduced damping). Measurement of external force is performed without any electrostatic or feedback force applied to the proof mass element, thereby improving measurement accuracy while reducing sensor complexity.

Auto-Ranging Method

Most existing inertial MEMS sensors rely on the dynamic characteristics of the sensing apparatus (such as, the oscillating frequency  $f_0$ , or amplitude A, for example) in order to measure effects of external forcing. These dynamic properties are dependent on the sensor parameters (such as the elastic constant k) which change in time due to sensor aging, 'annealing' of the cantilever, etc. Such changes result in reduced sensor accuracy with time, and necessitate periodic calibrations.

On the contrary, the accuracy of the time-domain apparatus 10 constructed in accordance with the principles described herein only depends on the physical spacing of the sensing elements (which is defined by the sensor manufacturing process), thus dramatically improving sensor long term stability accuracy, and obviating the need for recalibrations. As a 15 result, the accuracy and stability of the oscillatory apparatus described herein significantly exceeds accuracy of any available device (MEMS or otherwise), for a given device size, manufacturing precision, sensor operating bandwidth, and sensor cost target. Moreover, by changing the amplitude of 20 the oscillations, the dynamic range of the oscillatory apparatus of the invention is dynamically adjusted and may even be made user- or controller-selectable.

Because prior art tunneling-based accelerometers measure the proof mass deflection using the relationship between the 25 tunneling current and the tip-to-surface distance, their dynamic range is limited. In contrast, an exemplary force sensing apparatus constructed in accordance with the principles of the present invention uses tunneling discharge only to generate triggering events. It, therefore, advantageously offers a greatly increased dynamic range of measurements (e.g., from  $1\times10^{-4}$  g<sub>0</sub> to 2 g<sub>0</sub> in one fixed amplitude oscillator implementation), compared to the previously available force sensing tunneling devices. Furthermore, dynamic oscillation amplitude adjustment allows for a further increase of the 35 dynamic range as previously indicated.

For a given dynamic range the error can be optimized by adjusting the amplitude and resonant frequency. The amplitude is easily adjusted by varying the capacitively forced pulse magnitude used to initiate harmonic oscillation. As 40 expressed in equation (2), in order to change the resonant frequency, the spring constant or the mass needs to be adjustable. The proof mass and the silicon spring are fixed. However, if the same bias is applied to the capacitive plates above and below the proof mass the linearly approximated capacitive force is proportional to the mass displacement, in effect reducing the spring constant.

$$F_{capacitive} = \frac{\epsilon_0 A}{2D^2} (V_t^2 - V_b^2) + \frac{\epsilon_0 A}{D^3} (V_t^2 + V_b^2) x$$
 (Eqn. 12) 50

 $V_t$  and  $V_b$  are the applied voltages on the top and bottom plate respectively, A is the proof mass surface area, D is distance between the surface of the proof mass and each capacitive plate when the proof mass is in the rest position, and x is the displacement of the proof mass from the rest position. When  $V_t = V_b = V$ , the effective spring constant becomes:

$$k_{effective} = k - \frac{2\epsilon_0 A V^2}{D^3} \tag{Eqn. 13}$$

FIG. 7 shows the effective spring constant and resulting 65 tunable resonant frequency based on equation (13). Since the period of the harmonic oscillation is continuously measured,

28

the resonant frequency can be set using feedback. The resonant frequency and oscillation amplitude can be continuously adjusted in order to prevent the measured forces from going out of range of the current settings.

As referenced above, certain sensor embodiments described herein measure force based on a ratio of clock frequency to proof mass oscillation frequency, thereby making the sensor accuracy insensitive to clock drift (to the first order). Additionally, measurements averaged over multiple oscillation cycles enable the filtering out of unwanted noise.

While primarily discussed in the context of the electron tunneling sensing tip elements, the present invention is not so limited. In fact, many other physical switching mechanisms are useful with the sensor apparatus and methodologies described herein, including but not limited to: optical (based on an alignment between a light source, such as a light emitting diode (LED) and a light detector (such as a photo detector), magnetic (based on an alignment between two ferrous elements, such as in a reed switch), piezoelectric, thermal, capacitive, chemical, biological, etc.

It will be recognized that while certain aspects of the invention are described in terms of a specific sequence of steps of a method, these descriptions are only illustrative of the broader methods of the invention, and may be modified as required by the particular application. Certain steps may be rendered unnecessary or optional under certain circumstances. Additionally, certain steps or functionality may be added to the disclosed embodiments, or the order of performance of two or more steps permuted. All such variations are considered to be encompassed within the invention disclosed and claimed herein.

While the above detailed description has shown, described, and pointed out novel features of the invention as applied to various embodiments, it will be understood that various omissions, substitutions, and changes in the form and details of the device or process illustrated may be made by those skilled in the art without departing from the invention. The foregoing description is of the best mode presently contemplated of carrying out the invention. This description is in no way meant to be limiting, but rather should be taken as illustrative of the general principles of the invention. The scope of the invention should be determined with reference to the claims.

What is claimed is:

1. A method for adjusting the accuracy and dynamic range of a time-domain inertial sensor comprising the following steps:

operatively positioning a harmonic oscillator of the timedomain inertial sensor between two capacitive plates;

initiating harmonic oscillation of the oscillator in a first plane by creating with the capacitive plates a capacitively forced pulse;

monitoring the harmonic oscillation of the oscillator; and electrostatically biasing both of the two capacitive plates such that a spring constant of the oscillator is effectively altered.

- 2. The method of claim 1 further comprising the step of setting a resonant frequency of the oscillator to a desired frequency by using feedback.
- 3. The method of claim 2 further comprising altering the bias of the capacitive plates based on an applied acceleration that the time-domain inertial sensor is experiencing by adjusting the effective resonant frequency of the oscillator such that the performance of the time-domain inertial sensor is tailored to the range of measured acceleration.
- **4**. The method of claim **3**, wherein the oscillator is a proof mass coupled to a frame via a cantilever spring.

- 5. The method of claim 4, wherein the time-domain inertial sensor comprises a plurality of electron tunneling electrodes positioned on the oscillator and the frame such that a tunneling current pulse is generated when a free end of the oscillator is at a zero force position with respect to the frame and when the free end of the oscillator is displaced from the zero force position in the first plane by a distance of  $\pm d_0$ .
- **6**. The method of claim **5**, wherein the time-domain inertial sensor is a micro-electro-mechanical system (MEMS).
- 7. The method of claim 6, wherein the time-domain inertial  $^{10}$  sensor is sealed under vacuum.
- **8**. The method of claim **3** further comprising the step of adjusting the bias in response to monitoring the harmonic oscillation to ensure that an effective measurement range of the time-domain inertial sensor is sufficient to measure any <sup>15</sup> applied acceleration.
- 9. The method of claim 6, wherein the plurality of electron tunneling electrodes comprises;
  - a first electrode disposed on the oscillator;
  - a second electrode stacked on top of the first electrode in 20 the first plane and separated from the first electrode by a dielectric layer:
  - a third electrode disposed on the frame;
  - a fourth electrode stacked on top of the third electrode in the first plane and separated from the third electrode by <sup>25</sup> a dielectric layer; and
  - wherein the plurality of electron tunneling electrodes are arranged with respect to each other such that when the oscillator is at the zero force position a current pulse tunnels between the first and third electrodes and between the second and fourth electrodes, and wherein when the oscillator is displaced from the zero force position in the first plane by a distance of +d<sub>0</sub> a current pulse tunnels between the first and fourth electrodes, and wherein when the oscillator is displaced from the zero force position in the first plane by a distance of -d<sub>0</sub> a current pulse tunnels between the second and third electrodes
- 10. The method of claim 9, wherein the step of monitoring the harmonic oscillation of the oscillator further comprises the step of monitoring a first time difference between successive  $-d_0$  current pulses and a second time difference between  $+d_0$  current pulses.
- 11. The method of claim 10, further comprising the step of adjusting the bias to the capacitive plates if the first or second  $^{45}$  time difference drops below a threshold value such that  $^{+}$ do current pulses and  $^{-}$ do current pulses occur during every oscillation of the oscillator.
- 12. A method for adjusting the accuracy of a time-domain inertial sensor in real time comprising the following steps: initiating harmonic oscillation of an oscillator in a first plane with respect to a frame by creating a capacitively forced pulse with capacitive plates, which are operatively coupled above and below the oscillator;

30

- monitoring trigger event signals generated by a position switch, wherein the position switch comprises:
  - a first electrode disposed on the oscillator,
  - a second electrode disposed above the first electrode in the first plane by a distance of  $d_0$ ,
  - a third electrode disposed on the frame,
  - a fourth electrode disposed above the third electrode in the first plane by a distance of d<sub>0</sub>, and
  - wherein the first, second, third, and fourth electrodes are arranged with respect to each other such that when the oscillator is at a zero force position first and second trigger event signals are generated by the first and third electrodes and by the second and fourth electrodes respectively, and wherein when the oscillator is displaced from the zero force position in the first plane by a distance of +d<sub>0</sub> a third trigger event signal is generated by the first and fourth electrodes, and wherein when the oscillator is displaced from the zero force position in the first plane by a distance of -d<sub>0</sub> a fourth trigger event signal is generated by the second and third electrodes; and
- electrostatically biasing both of the two capacitive plates such that a spring constant of the oscillator is effectively altered.
- 13. The method of claim 12, wherein the trigger event signals are electron tunneling current pulses.
- 14. The method of claim 13, further comprising the step of adjusting the bias to both capacitive plates if a first time difference between successive third trigger event signals or a second time difference between successive fourth trigger event signals drops below a threshold value such that the spring constant of the oscillator is altered in real time to ensure that two third trigger event signals and two fourth trigger event signals are generated during each oscillation of the oscillator.
- **15**. A method for adjusting the accuracy and dynamic range of a time-domain inertial sensor comprising the following steps:
  - operatively positioning a harmonic oscillator of the timedomain inertial sensor above or below at least one capacitive plate;
  - initiating harmonic oscillation of the oscillator in a first plane by creating with the capacitive plate a capacitively forced pulse;
  - monitoring the harmonic oscillation of the oscillator; and electrostatically biasing the at least one capacitive plate such that the harmonic oscillation amplitude is effectively altered.
- **16**. The method of claim **15**, further comprising the step of setting an oscillation amplitude of the oscillator to a desired magnitude by using feedback.
- 17. The method of claim 15, wherein the harmonic oscillator is a sine-wave generator.

\* \* \* \* \*